ERDC/GSL TR-18-7

Geotechnical and Structures Laboratory

US Army Corps
of Engineers®
Engineer Research and
Development Center

ERDC
INNOVATIVE SOLUTIONS
for a safer, better world

Rapid Airfield Damage Repair (RADR)

Evaluation of AM2 2-1 Lay Pattern Over a 25 CBR Subgrade

Nolan R. Hoffman, Lyan Garcia, and Timothy W. Rushing

April 2018

The U.S. Army Engineer Research and Development Center (ERDC) solves the nation's toughest engineering and environmental challenges. ERDC develops innovative solutions in civil and military engineering, geospatial sciences, water resources, and environmental sciences for the Army, the Department of Defense, civilian agencies, and our nation's public good. Find out more at www.erdc.usace.army.mil.

To search for other technical reports published by ERDC, visit the ERDC online library at http://acwc.sdp.sirsi.net/client/default.

ERDC/GSL TR-18-7
April 2018

Evaluation of AM2 2-1 Lay Pattern over a 25 CBR Subgrade

Nolan R. Hoffman, Lyan I. Garcia, and Timothy W. Rushing

Geotechnical and Structures Laboratory
U.S. Army Engineer Research and Development Center
3909 Halls Ferry Road
Vicksburg, MS 39180-6199

Final report

Prepared for Headquarters, Air Force Civil Engineer Center
Tyndall Air Force Base, FL 32403-5319

Under Project Number 470802

Abstract

AM2 matting has a long history of successful performance as an expeditionary airfield surfacing system. Previous evaluations determined the number of passes to failure of AM2 when installed in a brickwork pattern over a wide range of soil strengths and alternate 2-1 and 3-4 lay patterns installed over soft soils. To determine the reliability of AM2 when installed in alternate patterns over stronger soils, the U.S. Air Force Civil Engineer Center (AFCEC) sponsored the evaluation of AM2 over a soil with a CBR of 25 installed in a 2-1 lay pattern. A CBR of 25 is considered by the U.S. Navy Naval Air Systems Command (NAVAIR EAF) to be the minimum threshold at which no subgrade maintenance is required during expeditionary operations. Recent investigations showed that the 2-1 configuration significantly reduces the operating life of AM2 over subgrades with a CBR of 6. In contrast, the results of the 25 CBR, 2-1 lay evaluation showed that both F-15E traffic and C-17 traffic surpassed the 1,500 pass requirement. The evaluation validated the NAVAIR EAF requirement for a minimum CBR of 25 to minimize maintenance requirements for F-15E and C-17 operations.

Contents

Figures and Tables

Figures

Tables

Preface

This study was conducted for the Air Force Civil Engineer Center (AFCEC) under the Rapid Airfield Damage Repair (RADR) Program. The technical monitor was Mr. Jeb S. Tingle.

The work was performed by the Airfields and Pavements Branch (GMA) of the Engineering Systems and Materials Division (GM), U.S. Army Engineer Research and Development Center, Geotechnical and Structures Laboratory (ERDC-GSL). At the time of publication, Dr. Timothy W. Rushing was Chief, CEERD-GMA; Dr. Gordon W. McMahon was Chief, CEERD-GM; and Mr. Nicholas Boone, CEERD-GVT was the Technical Director for Force Projection and Maneuver Support. The Deputy Director of ERDC-GSL was Dr. William P. Grogan, and the Director was Mr. Bartley P. Durst.

COL Bryan S. Green was the Commander of ERDC, and Dr. David Pittman was the Director.

Unit Conversion Factors

Multiply	By	To Obtain
feet	0.3048	meters
inches	0.0254	meters
inch-pounds (force)	0.1129848	newton meters
pounds (force)	4.448222	newtons
pounds (force) per square foot	47.88026	pascals
pounds (force) per square inch	6.894757	kilopascals
pounds (mass)	0.45359237	kilograms
square feet	0.09290304	square meters
square inches	6.4516 E-04	square meters

1 Introduction

1.1 Background

The U.S. military's force projection requirements include the need to rapidly construct new and expand existing airfield facilities in support of increased throughput at intermediate staging bases and forward airfields. The fast pace of contingency operations rules out the construction of additional permanent pavements to support the increased numbers of aircraft during contingency operations. Currently, the primary expeditionary airfield surfacing for the U.S. military is AM2 matting, which has been used for temporary runway, taxiway, and parking apron surfaces since the 1960s.

AM2 has a long history of satisfactory performance, but its dimensions and weight are limiting factors for deployment. Thus, the U.S. Air Force initiated the Rapid Parking Ramp Expansion program, now the AMX program, to develop a lightweight replacement for AM2. The AMX program calls for a new mat system that is as durable as AM2 in terms of passes to failure, yet weighing less than 4.0 lb/ft^2 and having a maximum thickness of 1.0-in.

In order to develop a new lightweight system and establish performance parameters, there was a need to understand the performance of AM2 under today's controlling aircraft over various subgrade strengths to quantify the sensitivity of the mats' performance to changes in subgrade strength. Subgrade sensitivity tests were conducted with simulated F-15E and C-17 traffic over CBRs of 6, 10, 15, 25, and 100. A summary of the results of the AM2 subgrade sensitivity tests is shown in Table 1.1. Based on the results of the full-scale testing performed by the ERDC, researchers determined the significance of subgrade improvement on the life expectancy extension of an AM2 installation.

Table 1.1. AM2 subgrade sensitivity results.

Subgrade Strength (CBR)	Sustained Traffic Passes		Reference
	F-15E	C-17	
6	1,500	1,500	Rushing and Tingle (2007)
10	3,000	6,000	Rushing et al. (2008)
15	4,100	7,000	Rushing and Mason (2008)
25	6,300	10,000*	Garcia et al. (2014a)
100	23,000	-	Garcia et al. (2014b)

* Failure was not achieved. Trafficking was stopped because of time constraints.

1.2 AM2 certified configuration lay patterns

The Naval Air Systems Command developed a Dynamic Interface model (DIM) to analyze aircraft landings and takeoffs on AM2. The model was validated through laboratory subscale tests, but additional development ad validation was required to accurately model the matting-soil interaction for various installation patterns. Therefore, NAVAIR partnered with the Air Force Civil Engineer Center to sponsor the evaluations listed in Table 1.2. Descriptions of the placement, or lay, patterns shown in Table 1.2 (brickwork, 2-1, and 3-4) are provided in *Expeditionary Airfield AM2 Mat Certification Requirements* (NAWCADLKE 2006).

Table 1.2. AM2 testing configuration summary.

Test sequence	Test name	AM2 lay pattern	Condition of AM2 mats	F-15E traffic	C-17 traffic
1	In-plane bow on asphalt surface	Brickwork	New	N/A	N/A
2	Vehicle braking test on asphalt surface	Brickwork	New	N/A	N/A
3	Brickwork on voided subgrade (CBR of 6)	Brickwork	New and refurbished	Yes	No
4	Brickwork on CBR of 6	Brickwork	New and refurbished	Yes	Yes
5	In-plane bow on CBR of 6	Brickwork	New	N/A	N/A
6	Opposite lay on CBR of 6*	Brickwork	New	Yes	Yes
7	3-4 lay on CBR of 6	3-4	New	Yes	Yes
8	2-1 lay on CBR of 6	2-1	New	Yes	Yes
9	Brickwork on voided subgrade (CBR of 6)	Brickwork	New	Yes	No
10	Brickwork on CBR of 6	Brickwork	New	Yes	Yes

*traffic applied parallel to long dimension of AM2 panels

The individual lay patterns were established as part of an initiative to optimize the use of 6-ft half panels. The original AM2 shipping package, F44, contained 16 12-ft panels and four 6-ft panels. Each package was designed to allow assembly of two 108-ft-wide rows or four 54-ft-wide rows in a brickwork configuration with no continuous longitudinal joints. The brickwork pattern assures excellent load-carrying capability of the system. Since 6-ft panels are used only for the row ends, more 12-ft panels are required for assembly. However, ship transportation of the mats across the globe led to a need for the mats to be shipped on an International Organization for Standardization (ISO) flat rack for compatibility with other containerized goods. A decision was made by the U.S. Navy to repackage AM2 into new shipping packages, resulting in the development of the F71 and F72 shipping configurations.

The F71 contains 18 12-ft mats, and the F72 contains 18 6-ft mats. The new configurations allow one F71 and one F72 to be placed end-to-end on a 20-ft ISO flat rack to optimize the use of the available space. The new package configuration also reduces confusion when designing a mat surface. In some instances, F44 packages were being re-bundled with different numbers of 6-ft panels inside the 12-ft mat packages. Separating the panels into the F71 and F72 packages eliminated the need to include mixed sizes in packages and improved the accuracy of panel inventories.

The optimization of packaging and shipping of AM2 required equal numbers of 12-ft and 6-ft mat panels to be delivered with each AM2 order. Since only a fraction of the available 6-ft panels were needed to assemble a brickwork pattern, many 6-ft panels were unused. To optimize mat use, NAVAIR EAF created an allowance for two alternate lay patterns, the 2-1 and the 3-4 lay patterns.

The 2-1 lay pattern was designed for use on all aircraft operating surfaces, including runways and high-speed taxiways. The pattern consists of installing AM2 in a brickwork configuration for two rows. The third row is started with a single, 12-ft panel and the remainder is then filled entirely with 6-ft panels to complete the desired width. The 2-1 lay pattern results in sections with two continuous 2-ft end (longitudinal) joints (Figure 1.1). The 3-4 lay pattern was designed only for parking or slow-speed secondary taxi areas and is not allowed for use on runways or high-speed primary taxiways. The 3-4 pattern consists of installing three rows of a brickwork pattern and then four rows of any matting that is available. Under worst-case conditions, the 3-4 pattern can result in as many as six continuous 2-ft end (longitudinal) joints.

Figure 1.1. Sketch of 2-1 lay pattern configuration.

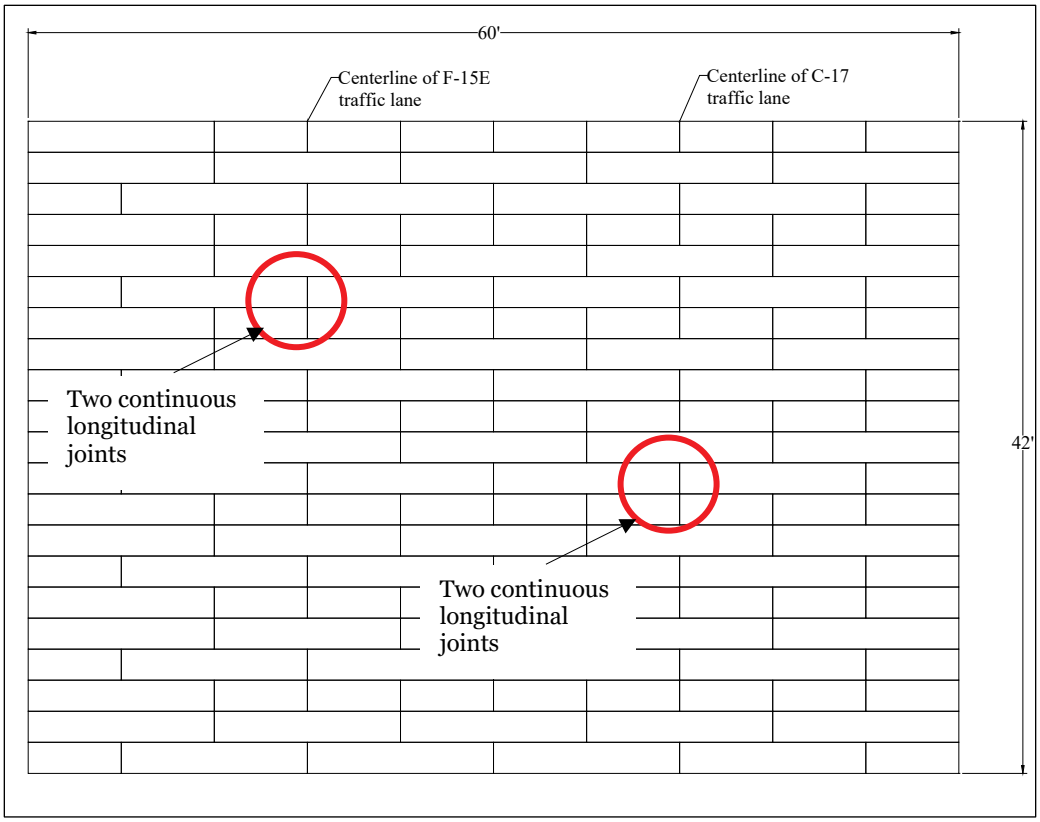

Although the two patterns were approved by NAVAIR EAF, they had not been evaluated under simulated aircraft loading conditions to determine whether any reduction in the number of allowable passes was caused by the allowance of continuous longitudinal joints. Therefore, they were included in the test program (Table 1.2). Results for the 3-4 lay pattern are reported in ERDC/GSL TR-14-38 (Rushing et al. 2014).

The report for the 2-1 lay pattern results is currently in development, but initial analyses showed that a reduction in performance in terms of sustainable aircraft passes of at least 30% occurred when compared to the brickwork pattern for an AM2 surface placed on a CBR of 6. This was largely attributed to the sections that consisted of two continuous end joints (Figure 1.1), where premature, consecutive rail failures occurred due to reduced support on each 2-ft end. The brickwork pattern, in comparison, provided better load transfer and improved end connector performance because it had an unsupported length of only one panel.

NAVAIR EAF requires that a minimum CBR of 25 be used for construction of AM2 airfields that will allow C-17 aircraft operations, but typically uses

this criterion for construction of all aircraft operating surfaces to reduce maintenance and repair activities. Due to this requirement, AFCEC funded the AM2 25 CBR, 2-1 lay pattern test in order to quantify its actual performance.

1.3 Objective and scope

The objective of the evaluation was to determine the reduction in performance of AM2 in terms of passes to failure when installed in the 2-1 lay pattern over a 25 CBR subgrade. A full-scale test section measuring 60-ft-wide by 42-ft-long and 36-in.-deep was constructed out of a high-plasticity clay (CH) obtained from a source local to Vicksburg, MS. Subsequently, the test section was divided into two adjacent test items. One measured 24-ft-wide by 42-ft-long and the other measured 36-ft-wide by 42-ft-long. The 24-ft-wide section was subjected to simulated, fully-loaded F-15E aircraft traffic, while the 36-ft-wide section was subjected to simulated, fully-loaded C-17 traffic. Trafficking was performed using a normally distributed wander pattern.

2 Materials

2.1 AM2 airfield mat

AM2 airfield matting was developed in the 1960s under a program sponsored by the Naval Air Engineering Center, Philadelphia, PA. Various versions of AM2 were tested under simulated aircraft loads at the U.S. Army Engineer Waterways Experiment Station in Vicksburg, MS, from 1961 through 1971, with major procurements beginning in 1965. The original AM2 mat has been modified through the years to address limiting structural concerns. A limited number of new AM2 panels were provided for the test section by NAVAIR. The other panels of the current production version of AM2 used in this test, modification version 5, were obtained from ALFAB, Inc., Enterprise, AL. The panels were coated with an antiskid material to increase the surface friction and were received at the ERDC in bundles.

Pertinent properties of the AM2 mat used are shown in Table 2.1. Each full panel was 24-in. by 144-in. by 1.5-in. and fabricated from a single 6061-T6 aluminum alloy extrusion with end connectors welded to the 24-in. ends to form a complete panel. The core of the extruded panels was comprised of vertical stiffeners spaced 1.75 in. apart in the 12-ft direction. The mat was also made in half-panels, which were 72-in.-long but otherwise identical, to allow a staggered "brickwork" configuration. The panels were joined along the two transverse edges by a hinge-type male/female connection. The adjacent 24-in. ends were joined by an overlap/underlap connection secured by an aluminum locking bar. The AM2 panels used in this test section were visually inspected to ensure that they had not been damaged prior to testing and to make certain they met the procurement specifications for AM2 matting. More specifically, the radii in the locking bar channel measured within specification.

Table 2.1. AM2 specifications.

Property	Full-panel	Half-panel
Length (ft)	12	6
Width (ft)	2	2
Thickness (in.)	1.5	1.5
Panel Weight (lbf)	145.5	74.4
Unit Weight (lbf/ft^2)	6.1	6.3

2.2 High-plasticity clay (CH) subgrade

The CH material used for subgrade construction was procured from a local source in Vicksburg, MS, and was subjected to laboratory tests including a grain-size analysis (hydrometer), Atterberg limits, modified-Proctor compaction, and unsoaked CBR testing, which are also listed in Table 2.2. Classification data for the subgrade soil are shown in Figure 2.1. Moisture-density and CBR-moisture content relationships are shown in Figures 2.2 and 2.3, respectively. These data were used to determine the target moisture content and dry density required to obtain the target CBR of 25. Laboratory testing was conducted by the Materials Testing Center (MTC) at ERDC. Based on the lab data, the maximum achievable dry density for the CH material was 103.9 pcf at an optimum moisture content of 21%; however, the target moisture content to achieve a 25 CBR strength was 24% with a target dry density of 100 pcf for construction.

Table 2.2. Laboratory tests conducted on soil.

Test Name	ASTM
Standard Practice for Classification of Soils for Engineering Purposes (USCS)	D 2487
Standard Test Method for Particle Size Analysis of Soils	D 422
Standard Test Method for Laboratory Compaction Characteristics of Soil Using Modified Effort	D 1557
Standard Test Method for CBR of Laboratory Compacted Soils	D 1883
Standard Test Methods for Liquid Limit, Plastic Limit, and Plasticity Index of Soils	D 4318

Figure 2.1. Classification data for the subgrade soil.

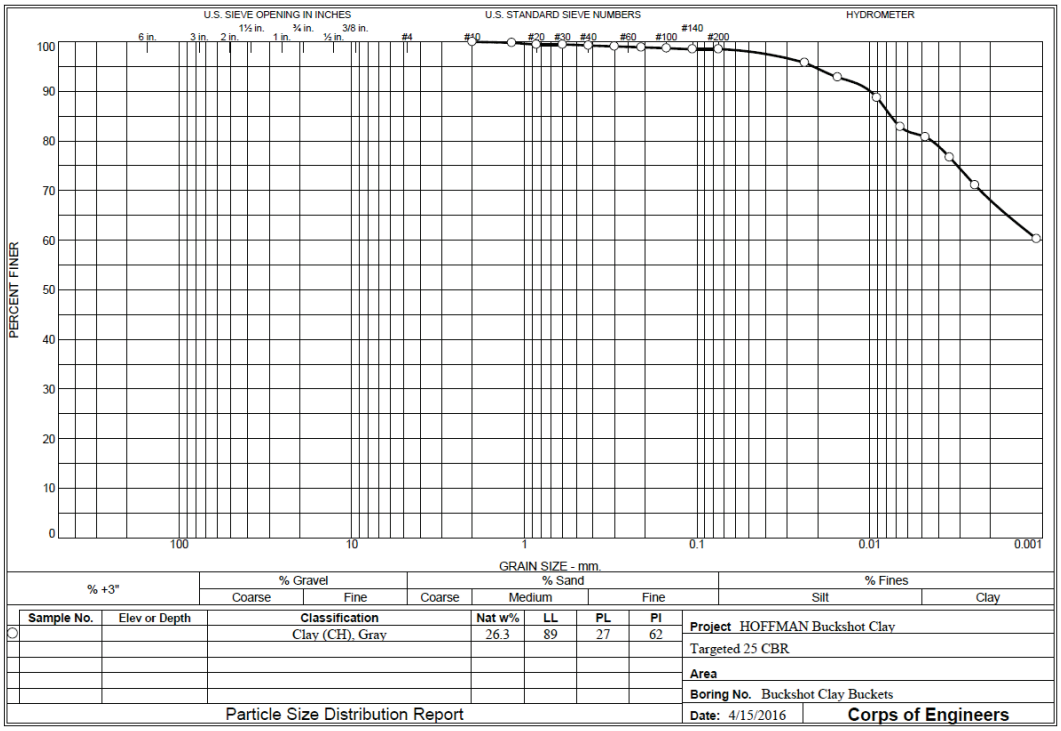

Figure 2.2. Density versus moisture for subgrade soil.

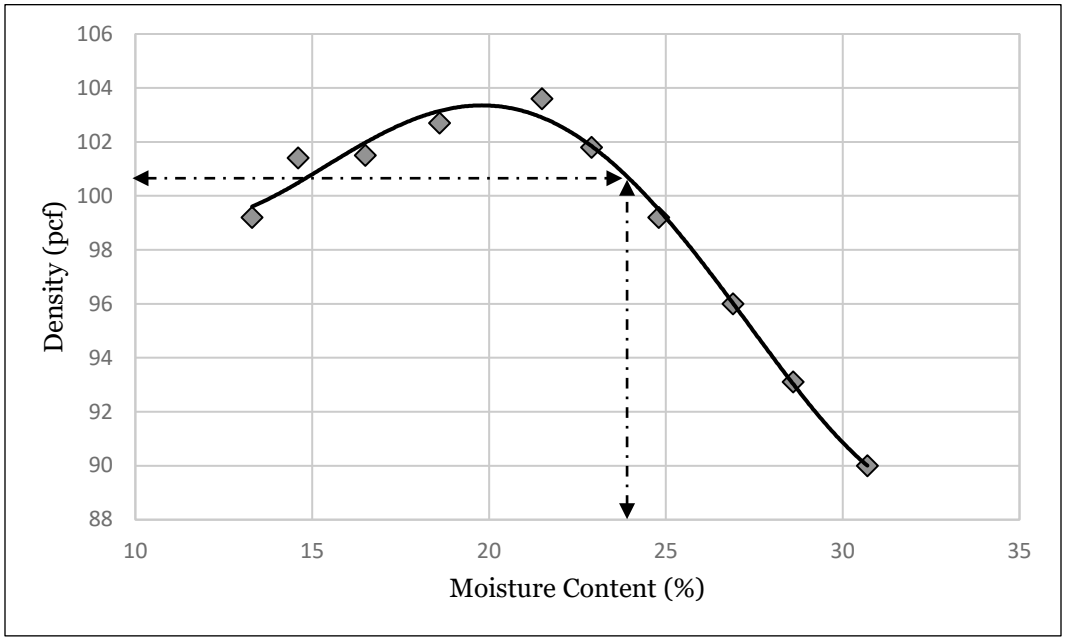

Figure 2.3. CBR versus moisture content for subgrade soil.

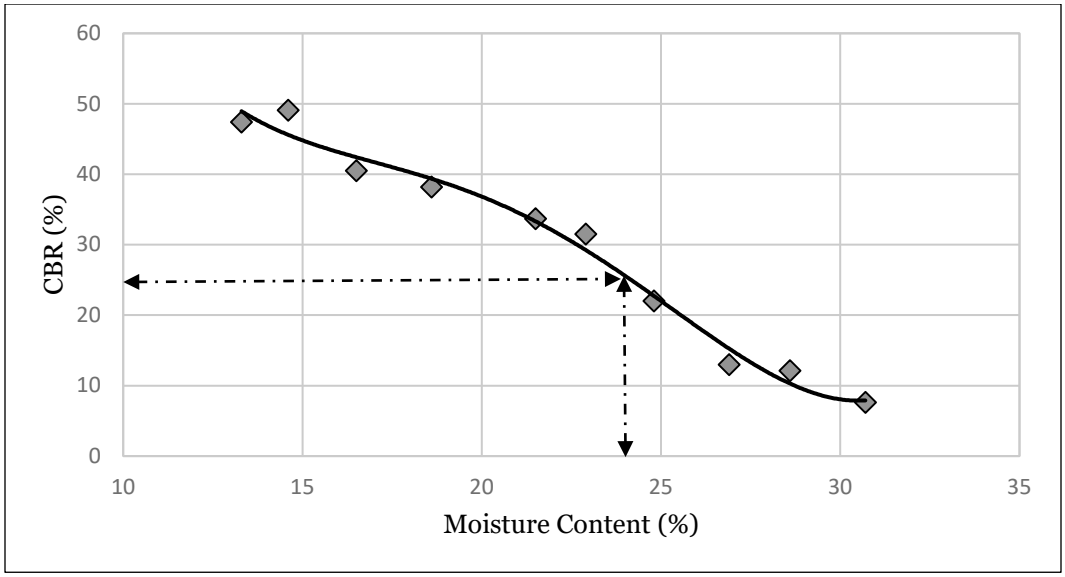

2.3 Low plasticity silt (ML)

The material used to backfill the excavated test pit to the required subgrade depth was a low-plasticity silt (ML), according to ASTM D 2487 (2011). This material was used to provide a uniform foundation for the test subgrade. It was procured from a local aggregate supplier (Vinco, Inc., Vicksburg, MS). Classification data are shown in Figure 2.4

Figure 2.4. Classification data for low plasticity silt (ML).

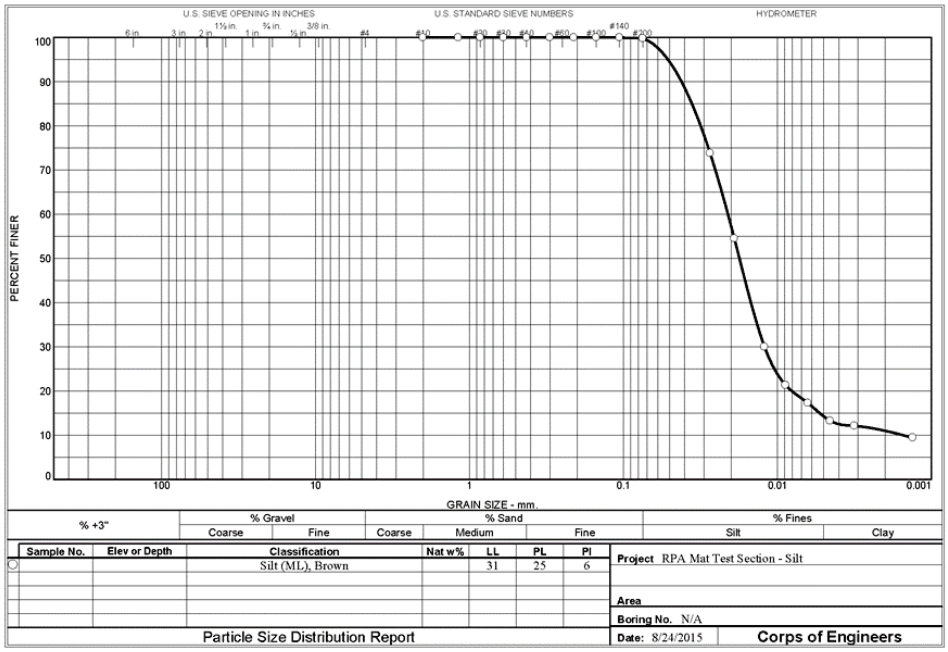

3 Test Section

3.1 General description

A full-scale test section was constructed and trafficked under shelter in the Hangar 2 Pavement Test Facility located at the ERDC. AM2 mat panels were installed over a 36-in.-thick CH subgrade prepared and constructed to a CBR of 25 over a silt (ML) foundation, as shown in Figure 3.1. Polyethylene sheeting was placed between the silt foundation and the CH along the bottom and sides of the excavation to prevent moisture migration to or from the CH soil. A general layout of the test section, along with panel designations, is shown in Figure 3.2.

Each panel was identified with a unique number to facilitate observation and recording of damage during trafficking. The matting surface was 60-ft-wide by 42-ft-long. The test had a 3.75-ft-wide lane designated for simulated F-15E traffic and a 12-ft.-wide lane designated for simulated C-17 traffic. Traffic was applied in normally distributed wander patterns associated with the F-15E and C-17.

Figure 3.1. Test section subgrade specifications.

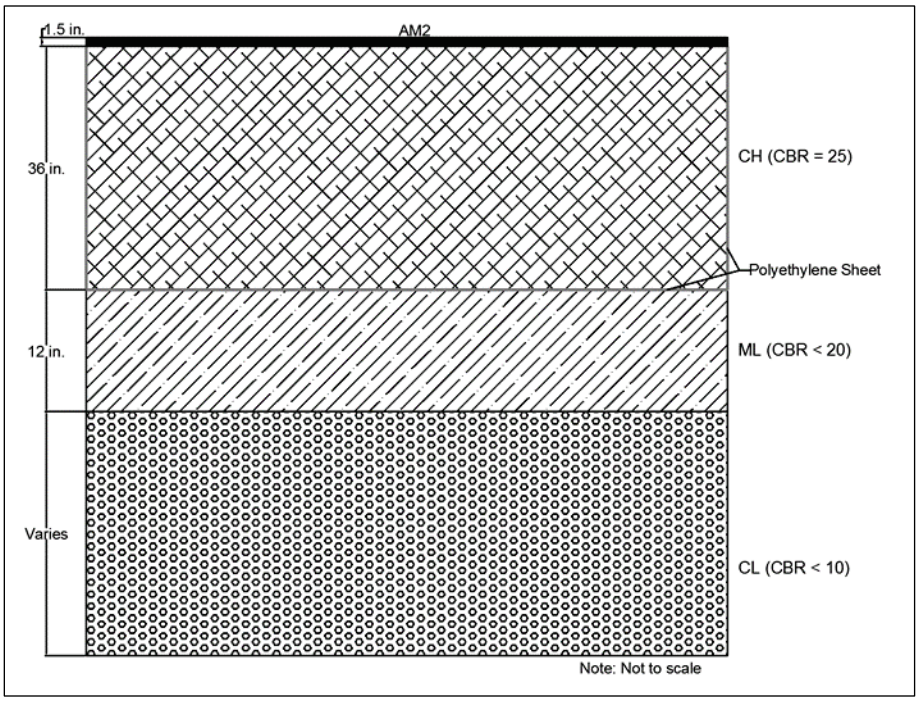

Figure 3.2. Test section overall layout.

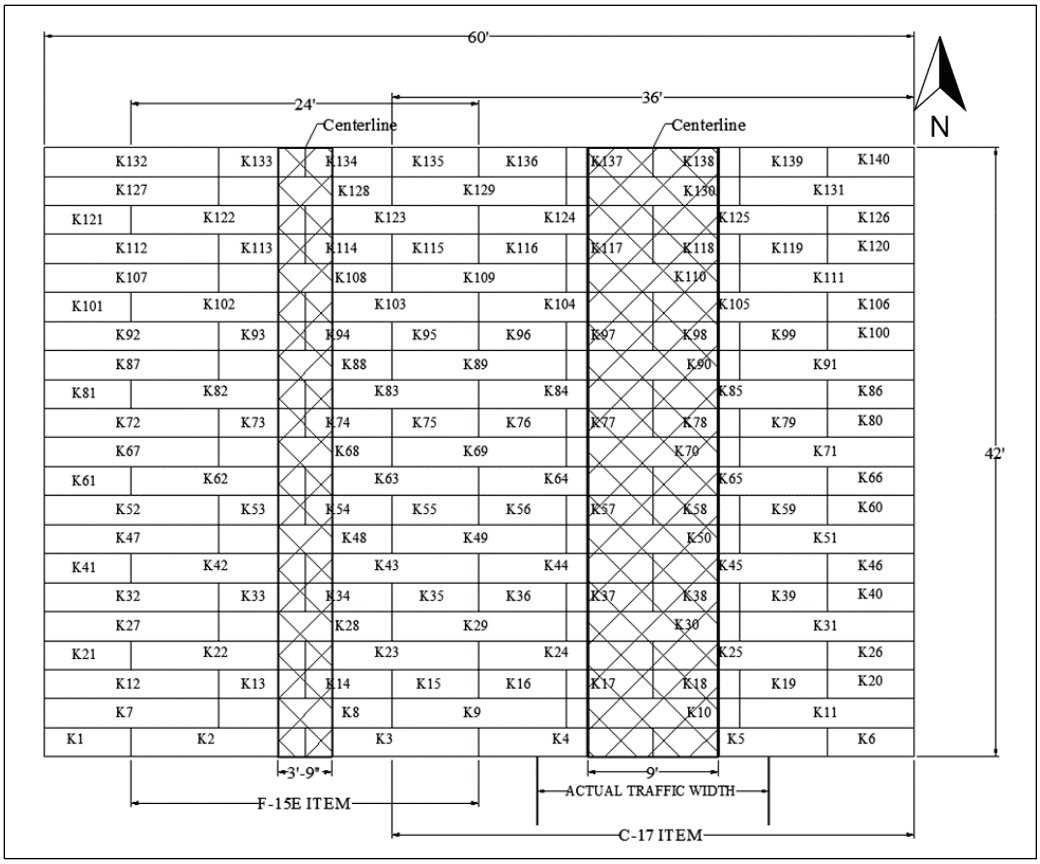

3.2 Test section construction

The subgrade was constructed by excavating a 60-ft-wide by 42-ft-long pit to a depth of 48-in. below the existing finished grade in Hangar 2. The lowest 12-in. of the pit was filled with a silt (ML) material having a CBR less than 20. The ML material was leveled with a bulldozer and compacted with a pneumatic roller and a vibratory steel-wheel compactor to ensure that the test section was constructed over a stable foundation. Then, the bottom and sides of the test pit were lined with 6-mil polyethylene sheeting to minimize moisture migration to and from the 36-in. of prepared CH soil.

The CH was processed at a nearby preparatory site by spreading the material to a uniform 12-in. depth, pulverizing the material with a rotary mixer, adjusting the moisture content, pulverizing the material again, and stockpiling it as shown in Figure 3.3. This was an iterative process necessary to achieve a uniform distribution of moisture throughout the material. Once the CH had been processed to the target moisture content, it was placed in the test section, spread by a bulldozer in 8-in. lifts, and

compacted with a pneumatic roller to a depth of approximately 6-in., as shown in Figure 3.4. Each compacted lift was subjected to a variety of tests, listed in Table 3.1, to ensure proper construction.

In situ CBR tests (CRD-C654-95), as shown in Figure 3.5, were conducted at the north and south quarter point locations of each test item on every 6-in. compacted lift to verify that the target 25 CBR value had been reasonably achieved. If the average pre-test CBR of a lift had differed from the target value by more than a CBR of 5, the lift would have been reconstituted. As shown in Figure 2.3, when the moisture of the CH is less than approximately 30%, the strength of the CH is more susceptible to change with a change in moisture. Therefore, the error margins for the strength of the subgrade were increased from what were typically allowed for lower CBR values, which were 0.5 CBR from the target value when a lower CBR was expected.

Figure 3.3. Laying out and pulverizing CH to improve moisture consistency.

Figure 3.4. Spreading and compacting CH material to create a lift.

Figure 3.5. In situ CBR test.

In addition to the soil characterization tests listed in Table 3.1, each compacted lift was surveyed to obtain an average elevation for determining lift thickness. After data collection, each lift was scarified to an average depth of 1 in. with a rotary mixer (Figure 3.6) prior to placing an additional lift to facilitate bonding between lifts.

Table 3.1. Field tests on each constructed lift.

Test Name	Test Number
Standard Test Method for Density of Soil in Place by the Drive Cylinder	ASTM D 2937
Standard Test Methods for In-Place Density and water content of Soil and Soil Aggregate by Nuclear Methods	ASTM D 6938
Standard Test Method for Density and Unit Weight of Soil in Place by the Sand Cone Method	ASTM D 1556
Standard Test Method for Laboratory Determination of Water Content of Soil and Rock Mass	ASTM D 2216
Standard Test Method for Use of the Dynamic Cone Penetrometer in Shallow Pavement Applications	ASTM D 6951
Standard Test Method for Determining the California Bearing Ratio of Soils	CRD-C654-95

Figure 3.6. Scarifying a lift after installation.

After the mat testing had been completed, posttest in situ CBR, moisture, and density measurements were used to determine the depth of subgrade that might have undergone gradual drying and possible densification under traffic. If the change in strength from pre-test to posttest was a CBR of 5 or less, the change was considered to be within acceptable limits. Typically, when the change in CBR is within acceptable limits, posttest measurements are not required in layers beneath the surface. The results of the pre- and posttest density, moisture, and in situ CBR measurements are reported in Table 3.2.

According to Figure 2.3, small changes in moisture content produce large changes in the bearing capacity as the target CBR increases above a CBR of 10, corresponding to a moisture content of 30%. Additionally, it can be determined from Figure 2.3 that in order for the CH to produce a CBR value of 25, an overall moisture content of 23.7% is desired. The field data backed these findings by producing consistent CBRs within the range specified earlier.

For the F-15E test item, posttest CBR measurements at the surface showed an increase from a CBR of 22.5 to a CBR of 26.8, which was most likely a result of minor densification under traffic and a decrease in moisture content from being exposed to the environment. The dry density of the material increased from 94.7 lbf/ft^3 before traffic was applied to 95.6 lbf/ft^3 after traffic ceased, also supporting the idea of densification. For the C-17 test item, posttest CBR measurements at the surface showed an increase from a CBR of 25.4 to a CBR of 26.5, also likely due to densification of the subgrade and a decrease in moisture content. The dry density of the material increased from 92.1 lbf/ft^3 before traffic commenced to 97.7 lbf/ft^3 after traffic was completed, again supporting minor densification.

Table 3.2. Average in situ subgrade properties.

Pretest						
		Nuclear Gage Test			CBR Test	
Item	Lift	Wet Density (pcf)	Dry Density (pcf)	Moisture (%)	Oven Moisture (%)	CBR
F-15	7	115.8	94.7	22.2	23.7	22.5
	6	109.2	90.5	20.7	20.8	26.2
	5	113.9	91.8	24.0	22.8	24.8
	4	111.4	89.7	24.1	22.6	25.4
	3	111.7	90.1	24.0	23.2	23.8
	2	106.5	88.2	20.7	23.5	22.2
	1	113.7	90.9	25.1	24.6	25.0
	Average	*111.1*	*90.2*	*23.1*	*22.9*	*24.6*
C-17	7	114.7	92.1	24.5	21.1	25.4
	6	105.5	86.9	21.5	20.6	24.7
	5	112.4	90.3	24.3	22.9	23.9
	4	114.0	91.5	24.5	23.2	25.5
	3	113.4	92.2	23.0	22.8	25.9
	2	107.6	87.5	22.7	23.2	24.4
	1	116.0	94.0	23.3	24.9	23.1
	Average	*111.5*	*90.4*	*23.2*	*23.0*	*24.6*
Posttest						
		Nuclear Gage Test			CBR	
Item	Lift	Wet Density (pcf)	Dry Density (pcf)	Moisture (%)	Oven Moisture (%)	CBR
F-15	7	116.3	95.6	21.6	21.5	26.8
	5	104.2	85.1	22.6	21.8	25.3
	Average	*110.2*	*90.3*	*22.1*	*21.7*	*26.1*
C-17	7	117.9	97.7	20.7	19.8	26.5
	5	105.3	87.0	21.2	21.4	24.8
	Average	*111.6*	*92.4*	*21.0*	*20.6*	*25.6*

Test pits were excavated to a depth of 12-in. at the same locations for both F-15E and C-17 test items to determine posttest properties below the surface. The change in CBR at this depth for either test item was less than 5; therefore, the bearing capacity was within acceptable limits. Since there was no evidence of drying, in situ CBR tests were not conducted below the 12-in. depth.

3.3 Subgrade instrumentation

The subgrade was instrumented with 12 9-in.-diameter Geokon earth pressure cells (EPCs). The gauges were installed at specific locations within the subgrade for both of the test items in order to monitor the stress distribution below the mat system. Data points were collected at a rate of 250 Hz with a Campbell Scientific CR5000 measurement and the data logger system was operated by an experienced instrumentation technician. EPCs were installed at depths of 6 in., 12 in., and 24 in. below the surface of the subgrade along the centerline of the two test items. The pressure range for gauges installed at 6 in. and 12 in. below the subgrade was 360 psi, while the range for the gauges installed at a depth of 24 in. was 145 psi. Figure 3.7 shows the instrumentation locations relative to mat placement. During subgrade construction, the EPCs were placed as shown in Figure 3.8 and surveyed for elevation to ensure placement at the proper depths.

Figure 3.7. Instrumentation layout.

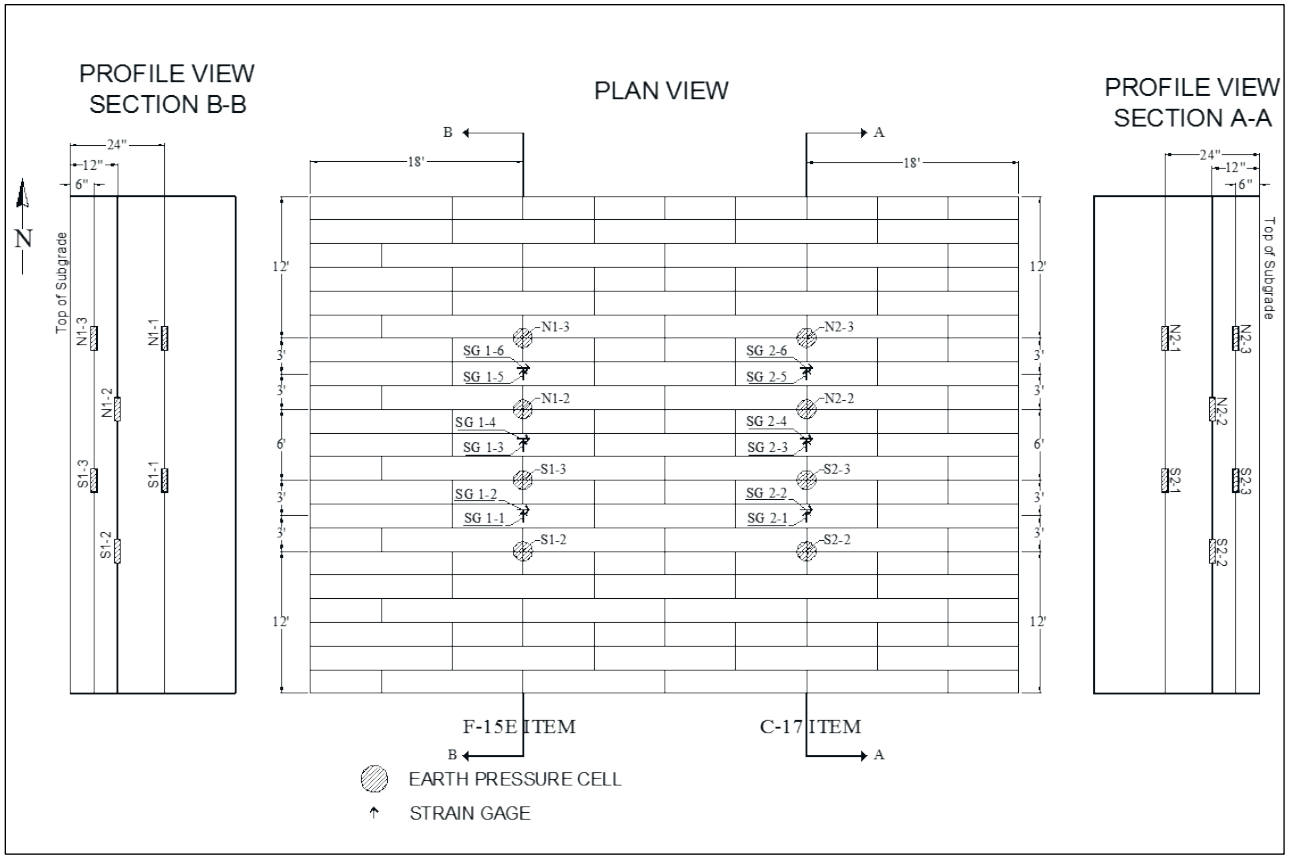

Figure 3.8. Installation of EPC in the 25 CBR subgrade.

3.4 AM2 mat instrumentation

Prior to installation, six individual mat panels were instrumented with foil strain gauges on the bottom surface of the mat. The strain gauges were covered with a thick gauge coat in an attempt to protect them from damage. Three instrumented panels were placed in the center of both the F-15E and C-17 traffic lanes to measure transverse and longitudinal strains induced in the mats under aircraft traffic loads. Data points were collected at a rate of 250 Hz with the Campbell Scientific CR5000 measurement and data logger system operated by an experienced instrumentation technician. A layout of the position of the strain-gauged mat panels is shown in Figure 3.7 and a photo of an instrumented panel is shown in Figure 3.9.

Figure 3.9. Strain gauge installed on AM2 panel.

3.5 AM2 mat installation

The AM2 airfield mat system was placed on the surface of the prepared test section by an experienced labor crew. The mat bundles were placed on the edge of the test section with a forklift while each of the individual panels was carried and installed by two men.

The first panel was placed flat on the ground in the southeast corner of the test section with the long dimensions perpendicular to the direction of traffic and with the male hinge connector facing north. The second panel was positioned adjacent to the 2-ft end of the first, allowing the overlapping end connector of the second panel to drop onto the underlapping end connector of the first panel. A rectangular slot was formed between the two end connector rails, allowing an aluminum locking bar to be inserted into the slot. This locking bar prevented the 2-ft ends of the panels from separating. This process was repeated until the first row was finished. For the second row, the female hinge connector was attached to the male hinge connector of panels from the first row, and the panel was pivoted into place, as shown in Figure 3.10. The next panel was installed by attaching the female hinge connector to the male hinge connector of panels in the first row and allowing the overlapping end connector rail to pivot over and connect to the underlapping end connector rail of the adjacent panel. An aluminum locking bar was inserted into the space provided to keep the panels from separating.

Figure 3.10. Hinging AM2 panel into place.

The same process was repeated until the assembly was complete. Panels were installed in compliance with the 2-1 lay pattern. Towing tubes, mandrels, and end caps available at the ERDC from older U.S. Air Force Airfield Damage Repair kits were installed on the eastern edge of the test section to avoid shifting of the rows during traffic.

Once assembly was complete, full panels of AM2 on hand at the ERDC from previous testing were installed along the ends of the traffic lanes to allow for the ingress and egress of the test vehicles. To facilitate the installation of these panels, male keylocks were attached to the female hinge connector of the panels in the first row. Photos of the final assembled test sections for the F-15E and C-17 are shown in Figures 3.11 and 3.12, respectively. Once the mats had been installed, 1,000-lb steel weights were placed along the east and west edges of the section (approximately 10 ft apart) to anchor the mats and simulate the resistance to movement provided by a large expanse of matting, representative of an airfield parking apron.

Figure 3.11. Assembled F-15E test item.

Figure 3.12. Assembled C-17 test item.

3.6 Traffic application

3.6.1 F-15E load cart

A specially designed single-wheel load cart simulated F-15E aircraft traffic. The load cart was equipped with a 36-in. by 11-in., 30-ply tire inflated to 325 psi and loaded such that the test wheel was supporting 35,235 lb. The F-15E load cart was equipped with an outrigger wheel to prevent overturning and was powered by the prime mover of a case vibratory steel-wheel roller, as shown in Figure 3.13.

Figure 3.13. Photograph of the F-15E load cart.

A normally distributed pattern of simulated traffic was applied in a 3.75-ft-wide traffic area for the F-15E test item, as shown in Figure 3.14. The traffic area was broken into five lanes that were designed to simulate the traffic distribution pattern, or wander width, of the main landing gear wheel on a mat surface when taxiing to and from an active runway. The width of each lane corresponded to the measured contact width, 9-in., of the F-15E tire when fully loaded and not to the overall published tire width of 11 in. The normally distributed traffic patterns were simplified for ease-of-use by the load cart operator. Traffic was applied by driving the load cart forward and backward over the length of the test item and then shifting the path of the load cart laterally approximately one tire width on each forward path. Tracking guides were attached to assist the driver in shifting the load cart the proper amount for each forward path. This procedure was continued until one pattern of traffic was completed. One pattern resulted in 16 passes, or 4 coverages. Traffic was continued in this manner until failure of either the mat or the subgrade in the test item occurred.

Figure 3.14. F-15E normally distributed wander pattern.

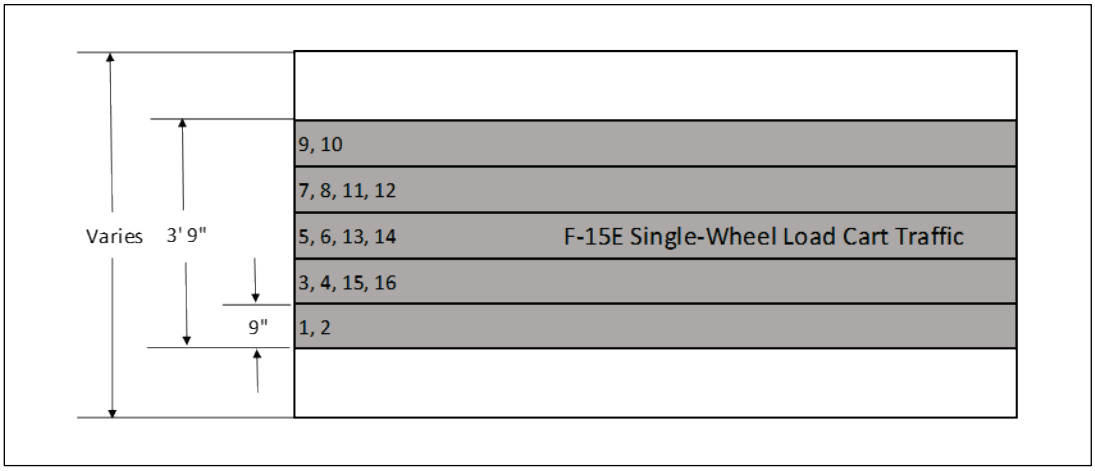

3.6.2 C-17 load cart

The multiple-wheel C-17 load cart was designed to exactly match one full main gear of a C-17. The multiple-wheel C-17 load cart was equipped with six 50-in. by 21-in., 20-ply tires inflated to 142 psi and loaded such that the test gear was supporting 269,560 lb, with estimated individual wheel loads of 44,930 lb. The test cart was powered by the front half of a Fiat scraper, as shown in Figure 3.15

Figure 3.15. Photograph of the C-17 load cart.

A simulated normally distributed traffic pattern was applied in a 9-ft-wide traffic lane for the C-17 test item, as shown in Figure 3.16. These lanes were designed to simulate the traffic distribution pattern, or wander width, of the main landing gear wheels on a mat surface when taxiing to and from an active runway. The width of each lane corresponded to the measured contact width, 18-in., of the C-17 tires when fully loaded and not the overall published tire width of 21-in. The normally distributed traffic patterns were simplified for ease-of-use by the load cart operator. Traffic was applied by driving the load cart forward and backward over the length of the C-17 test item and then shifting the path of the load cart laterally approximately one tire width on each forward pass. Tracking guides were attached to assist the driver in shifting the load cart the proper amount for each forward pass. This procedure was continued until one pattern of traffic was completed. For the C-17 test item, one pattern resulted in 28 passes, or 25 coverages. Traffic was continued in this manner until failure, either of the mat or the subgrade, occurred in the test item.

Figure 3.16. C-17 normally distributed wander pattern.

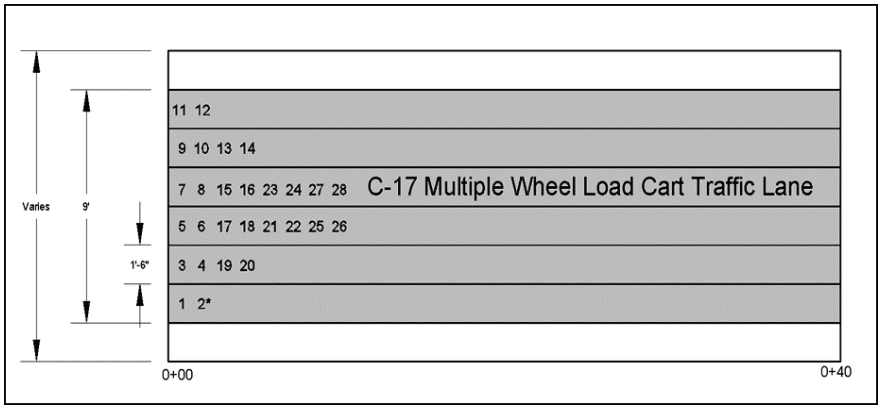

3.7 Data collection

Data collection during trafficking included the following tasks:

- Robotic total station measurements of cross sections
- Robotic total station measurements of centerline profiles
- Robotic total station measurements of dynamic elastic deflections
- Visual inspection of mat surface
- Dynamic instrumentation readings

These data were collected after every data collection interval. The data collection intervals for the F-15E and C-17 tests are shown in Tables 3.3 and 3.4, respectively. Pass levels for the F-15E are all factors of 16 in order to record deflection measurements in the same locations.

Table 3.3. F-15E scheduled data collection intervals.

Total Passes	Centerline Profile	Unloaded Cross Sections	Unloaded Rut Depth (in.)	Loaded Cross Sections w/ 6,000- lb Forklift	Loaded Rut Depth w/ 6,000-lb Forklift	Static Elastic Deflection	EPCs - and Strain Gauges
Subgrade							Baseline data
0							
10							
16*							
32							
48							
112							
240							
496							
1008							
1520							
2032							
Subgrade							

*Pattern will not be restarted on outer lane. The pattern will continue, starting Pass 11 in lane adjacent to centerline.

Table 3.4. C-17 scheduled data collection intervals.

Total Passes	Centerline Profile	Unloaded Cross Sections	Unloaded Rut Depth (in.) (w/ Straightedge)	Loaded Cross Sections w/ 6,000 lb Forklift	Loaded Rut Depth (w/ Straightedge) w/ 6,000 lb Forklift	EPCs, Strain Gauges
Subgrade						Baseline data
0						
12						
28*						
56						
84						
168						
308						
504						
784						
1008						
1512						
Subgrade						

*Pattern will not be restarted on outer lane. The pattern will continue, starting Pass 13 on second lane.

The data collected before, during, and after trafficking were collected at the locations labeled A1, A2, and A3, as well as along the centerlines of each traffic lane, as shown in Figure 3.17. The locations of perpendicular lines A1, A2, and A3 were selected at the approximate quarter-points of the test items to characterize the average performance while avoiding potential effects associated with boundary conditions at the ends of the test sections. Robotic total station elevation data collected at specified intervals along these lines are called “cross sections” in this report.

In an attempt to measure the permanent deformation of the subgrade underneath the mat surface, a forklift carrying two 2,000-lb lead weights was parked adjacent to each cross section, and elevation data were once again recorded. These data are noted as “loaded cross sections” in this report. The loaded forklift applied a 6,000-lb load at each cross section. The goal of the load application was to deflect the mat enough to contact the subgrade, but not so much as to induce elastic deflections in the subgrade; however, since the panels’ surfaces contained no visual access points, the extent of deflecting and the location of the subgrade surface were unknown.

Figure 3.17. Prescribed data collection locations.

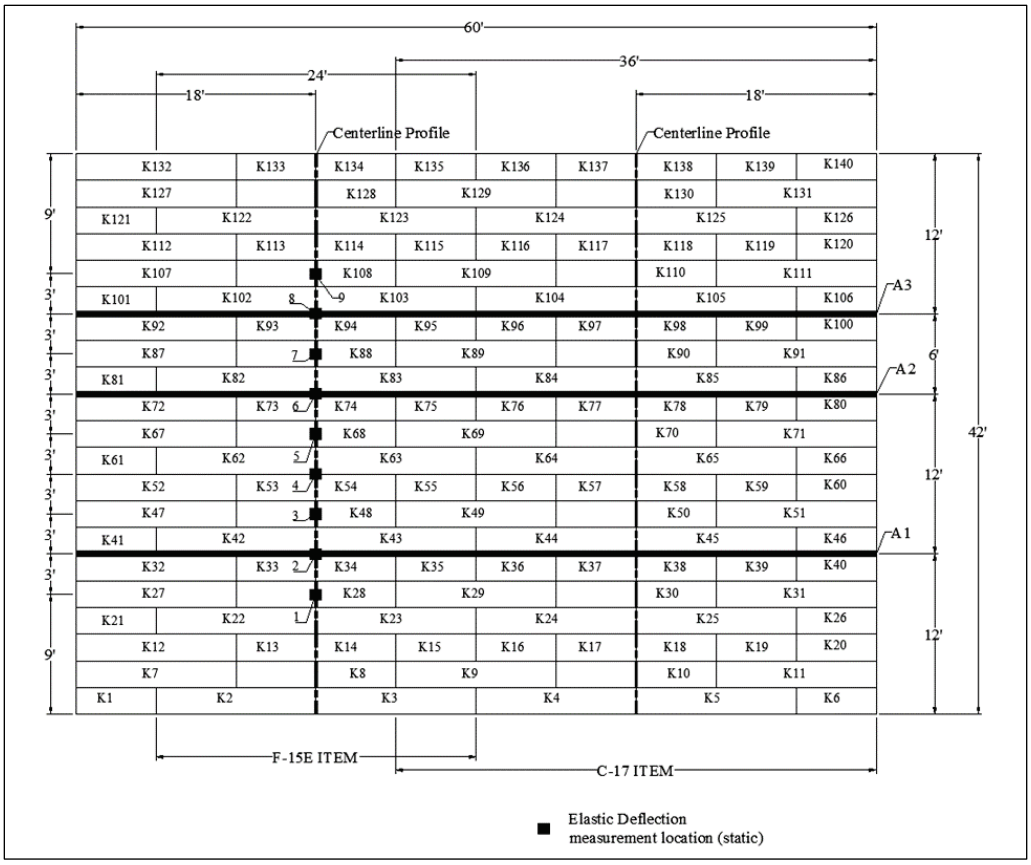

Robotic total station elevation data collected at 1-ft intervals along the traffic centerline are labeled “centerline profiles” in this report. Dynamic elastic deflection data were collected by placing a survey prism next to the load wheel on the F-15E load cart, as shown in Figure 3.18, at the specified locations on the last pass of each pass interval. Data were then collected at the same locations on the unloaded mat surface. The amount of mat damage and the mode of failure were recorded during the traffic phase. Figures 3.19 through 3.21 show typical data collection activities for each test item.

Figure 3.18. Elastic deflection measurement during trafficking.

Figure 3.19. Surveying centerline profile.

Figure 3.20. Loaded rut depth measurements.

Figure 3.21. Surveying designated cross section.

3.8 Failure criteria

The failure criteria established included (1) 10% mat breakage or (2) the development of 1.25-in. of permanent surface deformation for the F-15E or 3.0-in. of permanent surface deformation for the C-17. These failure criteria were developed based upon the maximum amount of mat damage deemed to be repairable in a contingency environment. Failure criteria values were recorded and monitored for compliance.

3.8.1 Mat breakage

Mat breakage percentages were calculated by dividing the area of the failed panel (or half-panel) by the total area of the assembled test item. For example, the total area of the F-15E item was 1,008 ft^2 (24-ft by 42-ft). Ten percent of this area is 100.8 ft^2, which is slightly over the area of 4 full panels, 8 half panels, or a combination of the two. Individual panels were considered failed if damage posed a significant tire hazard or caused instability of the load cart. Tire hazards were defined as damage that could not be reasonably maintained by simple field maintenance procedures. A typical example was top skin tears in excess of 10- to 12-in., representing significant structural damage to the surface skin with sharp edges that might endanger an aircraft tire.

3.8.2 Permanent deformation

The permanent surface deformation limits of 1.25-in. and 3.0-in. are based on roughness limitations for the F-15E and C-17 aircrafts, respectively. An abrupt change in elevation or the development of a rut in the wheel path greater than the allowable values may exceed roughness limits. The rut depth limit is required, since many connecting taxiways and aprons intersect at 90 deg and crossing perpendicular to a pre-formed rut may cause an abrupt change in elevation, exceeding aircraft limits. Failure by permanent surface deformation was determined from robotic total station elevation measurements of cross sections and centerline profiles. Each of the following data collection categories was analyzed for compliance with the failure criterion:

1. Centerline profile deformation,
2. Loaded surface deformation, and
3. Unloaded surface deformation.

3.8.2.1 Centerline profile deformation

Centerline profile deformation was measured by robotic total station elevation recordings along the traffic centerline. The difference in elevation one or two stations apart (1-ft or 2-ft apart) was analyzed from plots of the data to determine whether an abrupt change in elevation reached failure limits for each interval during trafficking.

3.8.2.2 Unloaded surface deformation

Unloaded surface deformation values were determined using collected data according to section 3.7. The maximum deformation at each location was determined as the difference in elevation from the average height of the elevated material on each side of the trough to the deepest point in the bottom of the trough. Measurements were averaged to obtain a single value for comparison to the failure criterion. The deformation measurements determined by this method are noted as “unloaded cross sections” in this report.

3.8.2.3 Loaded surface deformation

Loaded deformation was determined from data collected according to section 3.7. The maximum deformation at each location was determined as the difference in elevation from the average height of the elevated material on each side of the trough to the deepest point in the bottom of the trough. Measurements were averaged to obtain a single value for comparison to the failure criterion. The deformation measurements determined by this method are noted as “loaded cross sections” in this report.

4 Test Results

4.1 Behavior of mat under traffic (visual observations)

The following sections describe all mat breakage and the behavior of the AM2 airfield mat under simulated F-15E and C-17 traffic. General views of each item prior to trafficking are shown in Figures 3.11 and 3.12.

4.1.1 F-15E test item

Trafficking on the F-15E test item began 6 July 2016. The first damage noted on the AM2 surface was after 1,008 passes. A slight corner curl developed in panels 2, 3, 33, and 34 on their south edge. Panels 13 and 74 acquired a hairline crack along the weld between the female hinge connector and the overlap connector at the top skin, as can be seen in Figure 4.1.

Figure 4.1. Hairline crack in panel 74 observed after pass 1,008.

After 1,520 passes, panel 53 also developed a hairline crack in the weld between the female hinge connector and the overlap/underlap joint at the top skin. At 2,032 passes, panel 14 acquired a hairline crack in the same spot as the others. Panels 73, 74, 113, 114, 133, and 134 all displayed small corner curls on the south edges. At pass level 3,552, panels 93 and 94 developed small weld cracks similar to the others.

Inspection at pass level 4,576 revealed that the corner curls on panels 2 and 3 had cracked at the base of the curl and started to propagate along the top skin of the female hinge connectors, shown in Figure 4.2. At pass 5,600, panels 73 and 74 cracked at the base of the corner curls and the crack also propagated down the top skin of the female hinge connectors, similar to panels 2 and 3.

Figure 4.2. Corner curl cracks in panels 2 and 3 at 4,576 passes.

By pass 6,100, a skin tear that measured approximately 10 in. appeared in panel 8, shown in Figure 4.3. Panels 2 and 3 continued to crack along the female hinge connector (Figure 4.4). Additionally, panel 33 developed a new crack with a length of 1 in. between the male hinge connector and the overlap connector along the top rail. A photograph of panel 33 is shown in Figure 4.5. Panels 53, 133, and 134 each displayed a new crack at the top skin along the female hinge connector, most likely due to the corner curls.

At pass 6,700, panels 2, 3, and 8 were all considered failed (Figures 4.6 and 4.7). The damaged panels brought the number of total failed panels to three. Panels 2 and 3 had become tire hazards, and the skin tear in panel 8 measured over 12-in. At pass 6,900, it was noted that panel 128 acquired a skin tear approximately 10 in. in length. Additionally, a large steel plate was placed over panels 2, 3, and 8 to prevent damage to the load cart.

Figure 4.3. Top skin tear on panel 8 at 6,100 passes.

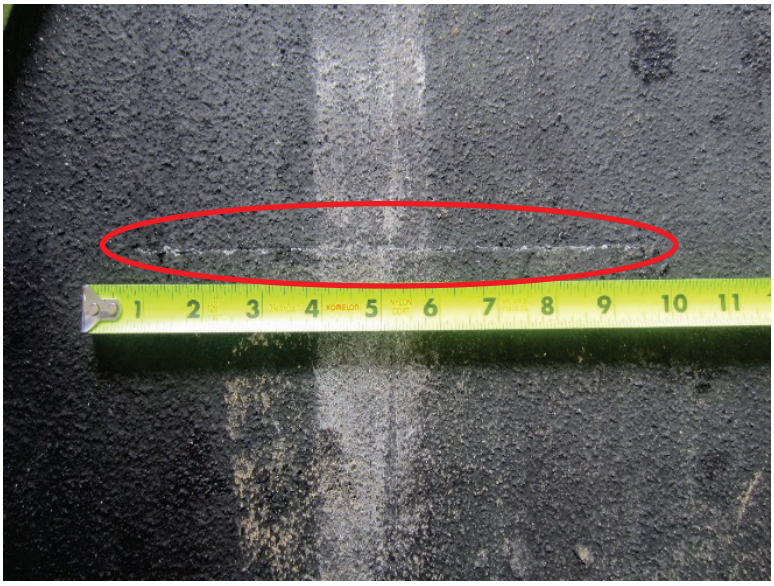

Figure 4.4. Cracks propagating in panels 2 and 3 at pass 6,100.

Figure 4.5. Crack in top rail of overlap joint in panel 33 at pass 6,100.

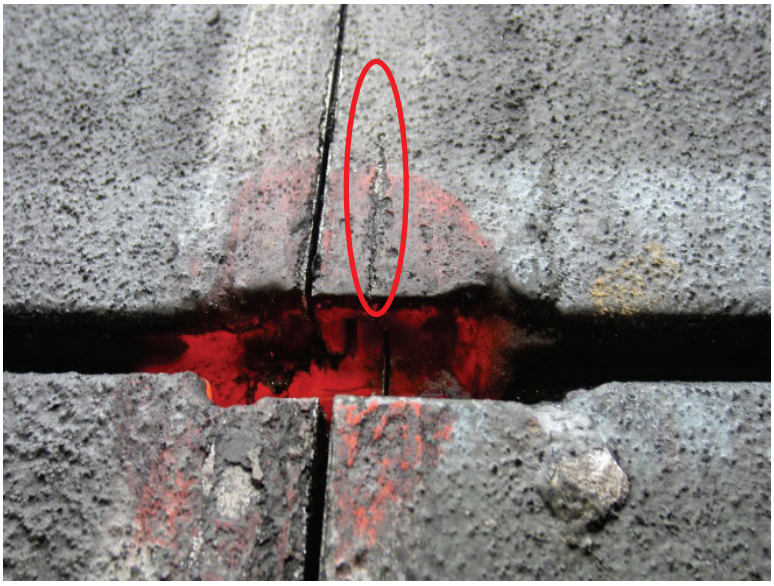

Figure 4.6. Tire hazards on panels 2 and 3 at pass 6,700.

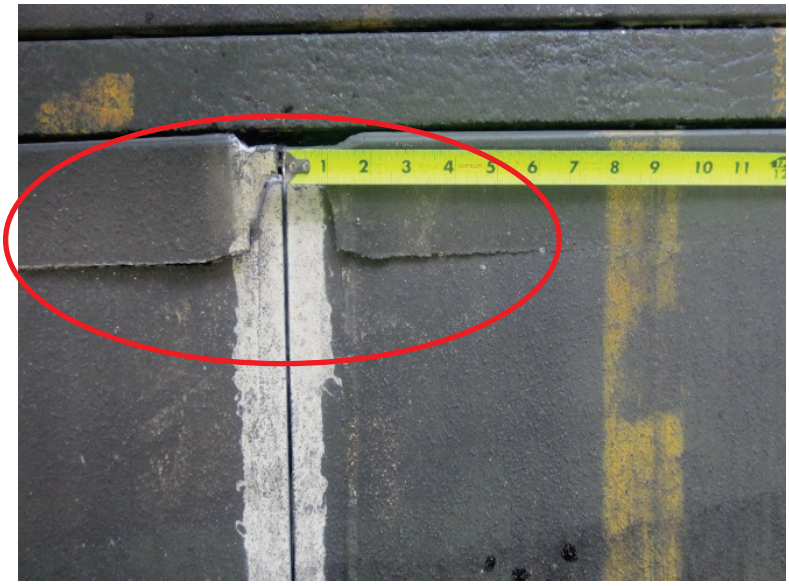

Figure 4.7. Panel 8 failure at pass 6,700.

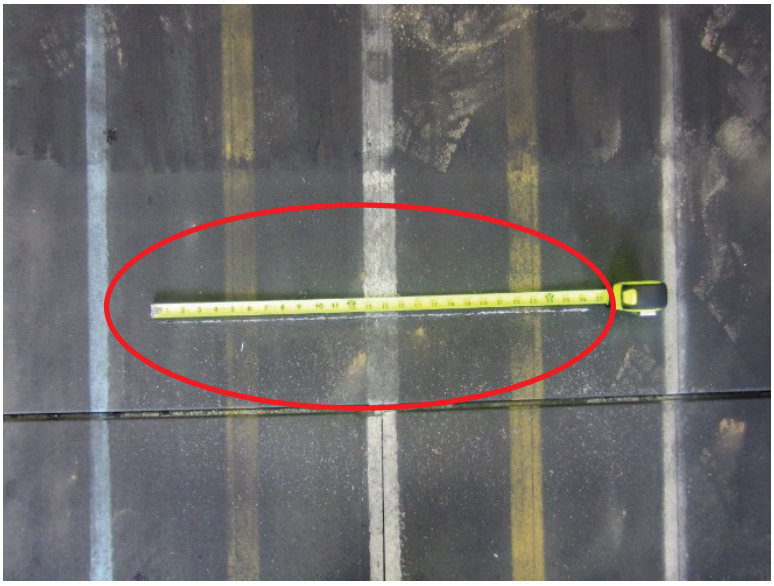

After 7,120 passes, panel 128 was considered failed, with its skin tear measuring well over 13-in., increasing the number of failed panels to four. Also, panel 53 developed a hairline crack on the top skin along the underlap/overlap joint weld. Panels 33 and 34 began to crack at the base of the present corner curls. At pass level 8,440 a skin tear appeared in panel 68 that measured 7-in. in length.

By pass 9,152, the skin tear in panel 68 propagated to 15-in., surpassing the failing threshold. Additionally, panels 73 and 74 were considered failed by tire hazard due to the corner curls cracking and the skin tearing greater than 10 in. Panels 73 and 74 counted as one equivalent panel, since they were both half panels, while panel 68 was a full panel. These damaged panels brought the total number of failed panels to six, which surpassed the 10% mat breakage failure criteria, officially failing the test item. Even so, traffic continued for an additional 300 passes, bringing the final pass total to 9,452. At this pass level, panel 48 developed a 9-in. skin tear along one of the vertical stiffeners, but this was the only new damage recorded. Table 4.1 is a summary of the F-15E test item damage.

Table 4.1. Damage summary from F-15E test item.

F-15E Passes	Failure Type	Damage Description	Cumulative Failed Panels	Cumulative % Mat Failure	Panel Number
6402	Skin Tear > 10"	18” skin tear	1	2.4%	K8
6700		26” skin tear			K8
	Skin Tear > 10"	11” skin tear	2	4.8%	K3
		9.5” skin tear			K2
6900		10" skin tear			K128
	Skin Tear > 10"	10” skin tear	3	7.1%	K2
7120	Skin Tear > 10"	13” skin tear	4	9.5%	K128
8440		7" skin tear			K68
		8" skin Tear			K73, K74
9152	Skin Tear > 10"	15” skin tear	5	11.9%	K68
		Test item failed by mat breakage			
	Tire hazard + >10" skin tear	18" skin tear	6	14.3%	K73, K74
9250		5" skin tear			K48
9452		9" skin tear			K48

4.1.2 C-17 test item

Trafficking of the C-17 test item began 22 August 2016. A total of 10,080 passes were completed on the test section without incurring damage to the panels. These data indicated that the mat system should not require maintenance before the life expectancy of an expeditionary airfield when utilizing AM2 in the 2-1 lay pattern over a CBR of 25 or higher; therefore, trafficking was ceased.

4.2 Permanent deformation

Permanent deformation was measured in each test item on the subgrade as well as the mat surface. For the subgrade, measurements were taken before and after the test. For the mat surface, measurements were recorded before trafficking, at specific intervals during trafficking (Tables 3.19 and 3.20), and after trafficking was complete. In order to show the changes due to trafficking, the pre-traffic data were subtracted from all subsequent data to normalize the data. The discussions that follow are based on the normalized data.

Plots of the centerline profile data, as determined from robotic total station recordings, for the F-15E and C-17 test items are shown in Figures 4.8 through 4.11. Cross-section elevations collected along lines A1, A2, and A3, as seen in Figure 3.21, were averaged and used in Figures 4.12 through 4.17. Maximum deformation values for the unloaded, loaded, and subgrade cross sections were determined as the difference in elevation between the average heights of the elevated material on each side of the trough to the deepest point in the bottom of the trough.

Figure 4.8. F-15E centerline profile on mat surface.

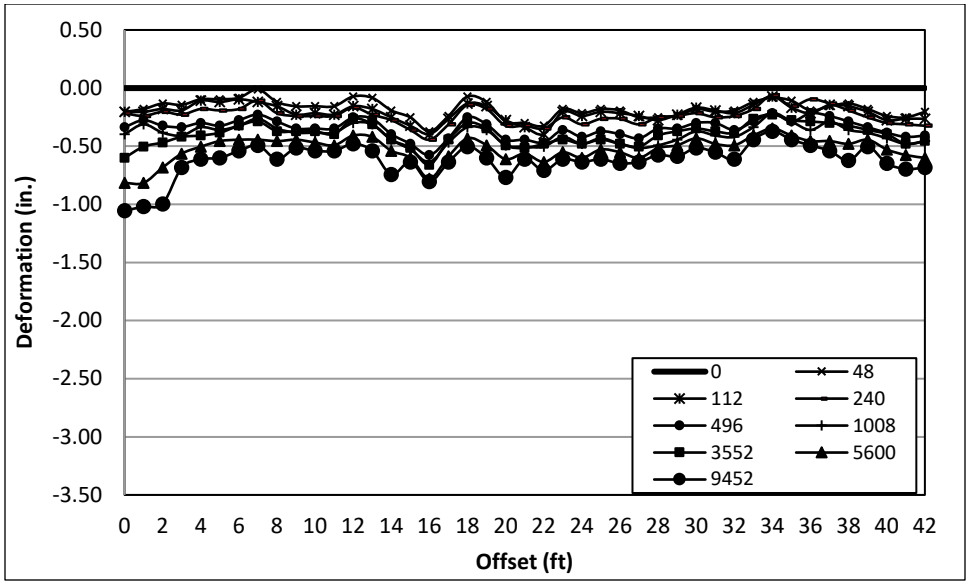

Figure 4.9. F-15E subgrade centerline profile.

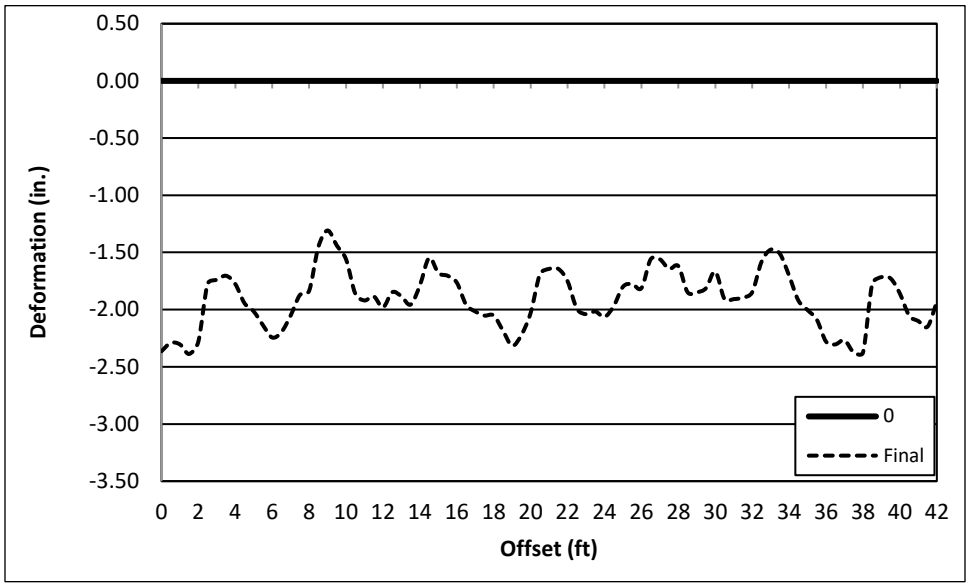

Figure 4.10. C-17 centerline profile on mat surface.

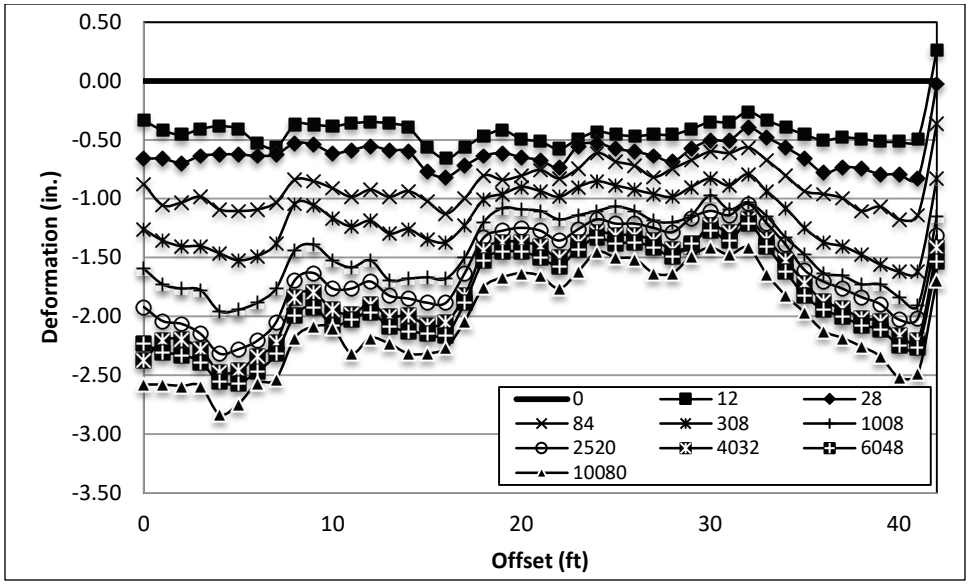

Figure 4.11. C-17 subgrade centerline profile.

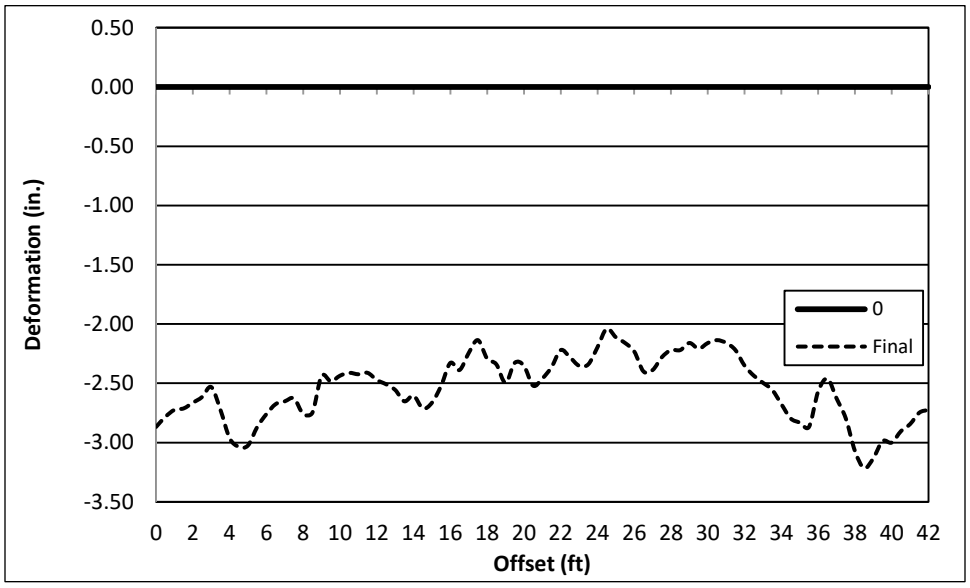

Figure 4.12. Average unloaded deformation across F-15E cross sections.

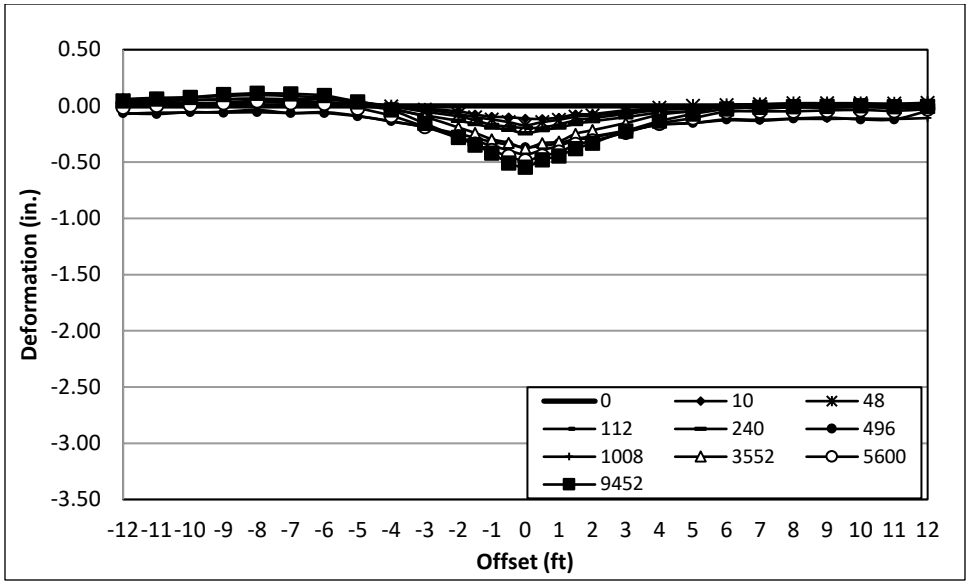

Figure 4.13. Average loaded deformation across F-15E cross sections.

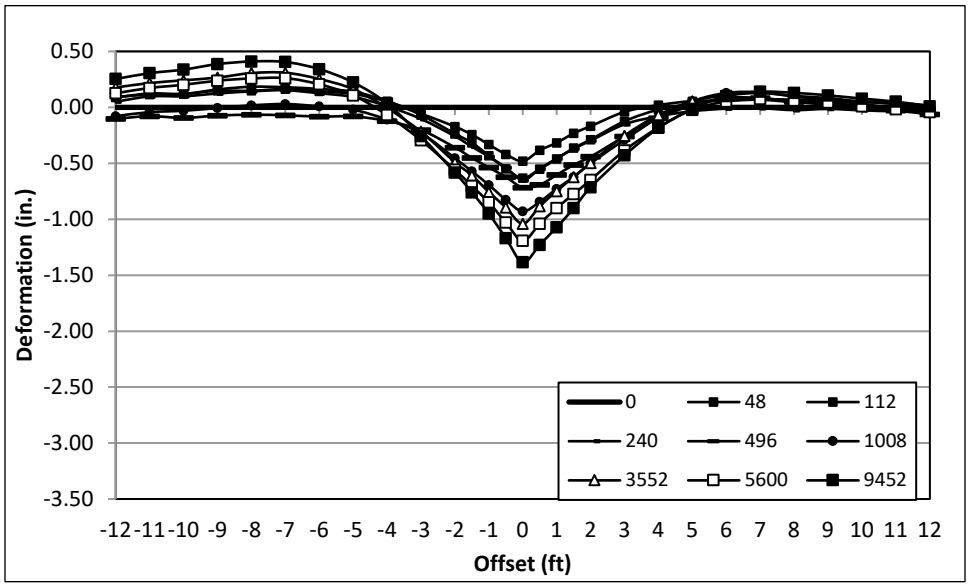

Figure 4.14. F-15E subgrade deformation.

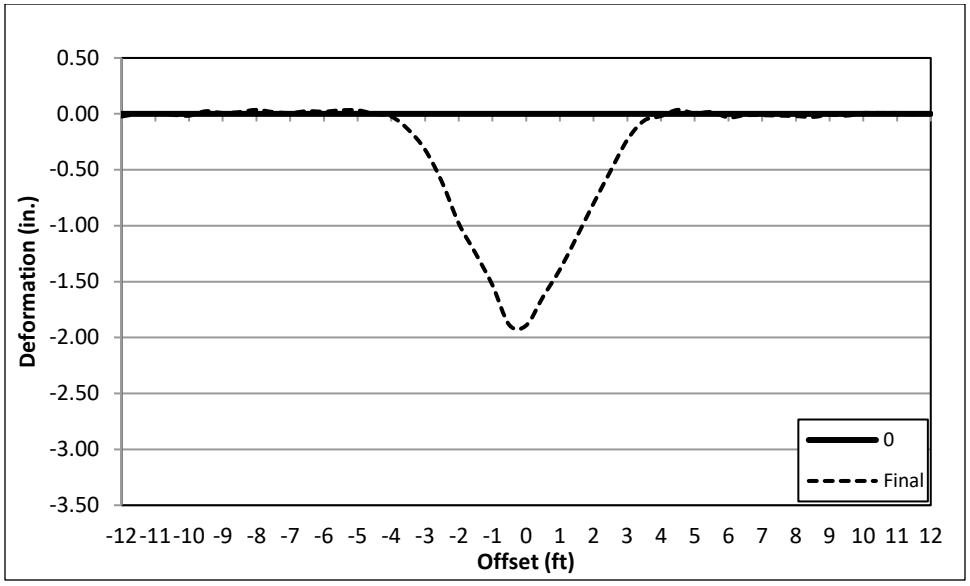

Figure 4.15. Average unloaded deformation across C-17 cross sections.

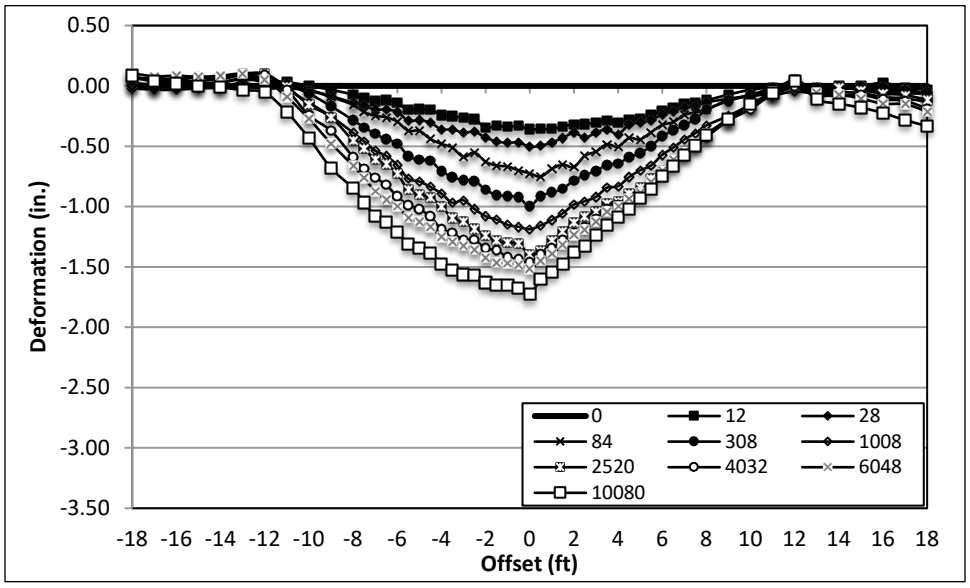

Figure 4.16. Average loaded deformation across C-17 cross sections.

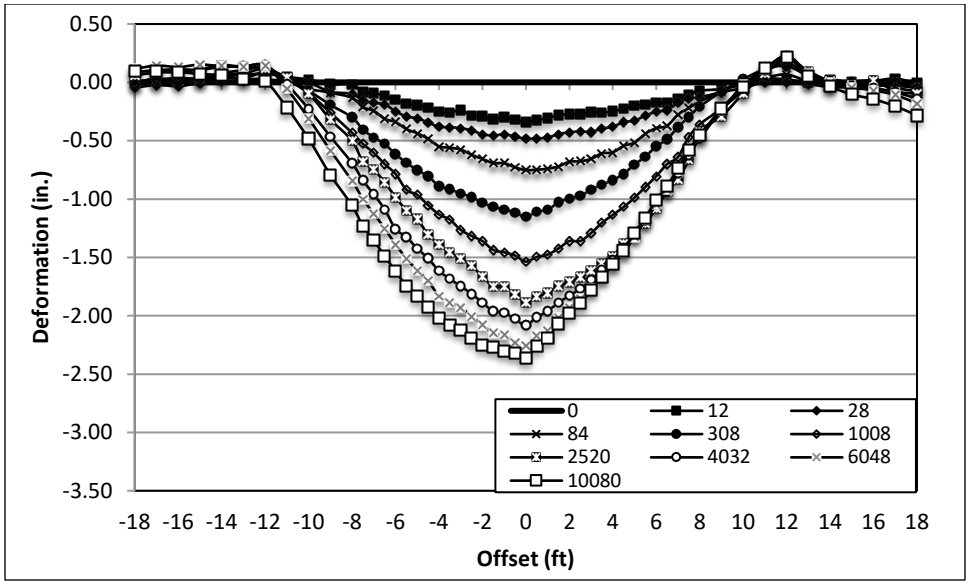

Figure 4.17. C-17 subgrade deformation.

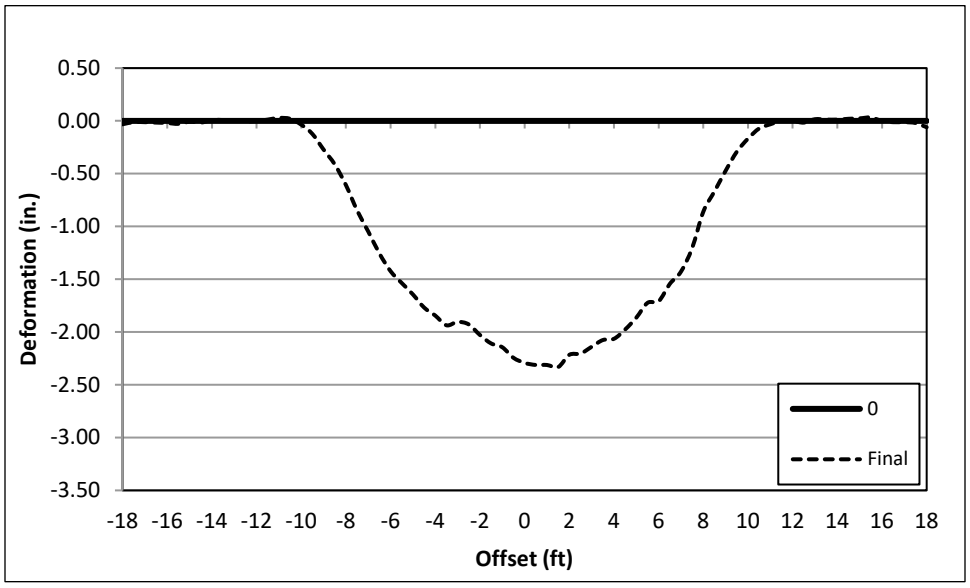

4.3 Elastic deflection

Elastic deflection was measured on the F-15E item at the scheduled pass intervals. Elastic deflection was not measured on the C-17 item due to safety concerns for mounting the survey prism. A plot of these data is shown in Figure 4.18. These data indicate the elastic deflection, or rebound, of the mat and subgrade as the test wheel moved across the surface.

Figure 4.18. F-15E elastic deflection on mat surface.

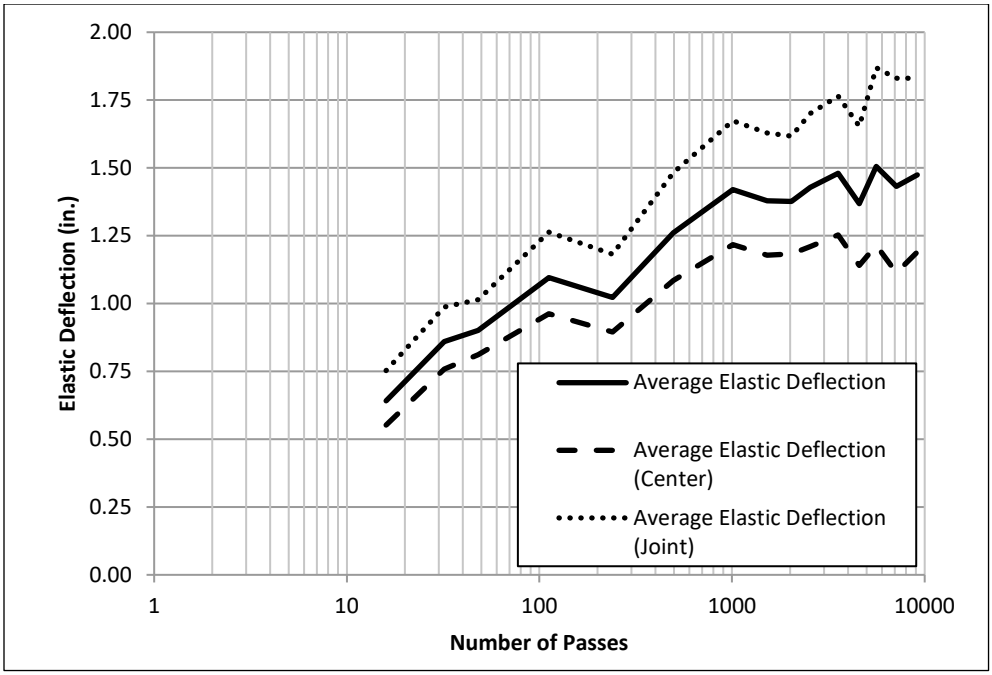

Elastic deflection was determined by mounting a survey prism on the F-15E load cart just above the center of the load wheel, as shown in Figure 3.22. A continuous survey mode was used with the robotic total station so that elevations were recorded each time the load cart moved 3-ft from the previous measurement.

4.4 Earth pressure cells

EPCs were installed in the subgrade underneath both the F-15E and C-17 test items. Figures 4.19 and 4.20 show the maximum recorded pressure values for the F-15E and C-17 test item, respectively. These data have been normalized to show the effect of only the load cart on the subgrade by removing the effects of the soil pressure. Plots of entire data sets can be seen in Appendix A and Appendix B for the F-15E and C-17 test items, respectively.

For the F-15E item, pressure values remained fairly constant throughout the trafficking. As can be seen, most of the gauges showed a slight increase in pressure as traffic increased. The maximum normalized pressure values ranged from 80 psi to 104 psi, 40 psi to 56 psi, and 13 psi to 18 psi for depths of 6-in., 12-in., and 24-in., respectively.

Figure 4.19. F-15E maximum recorded pressure values.

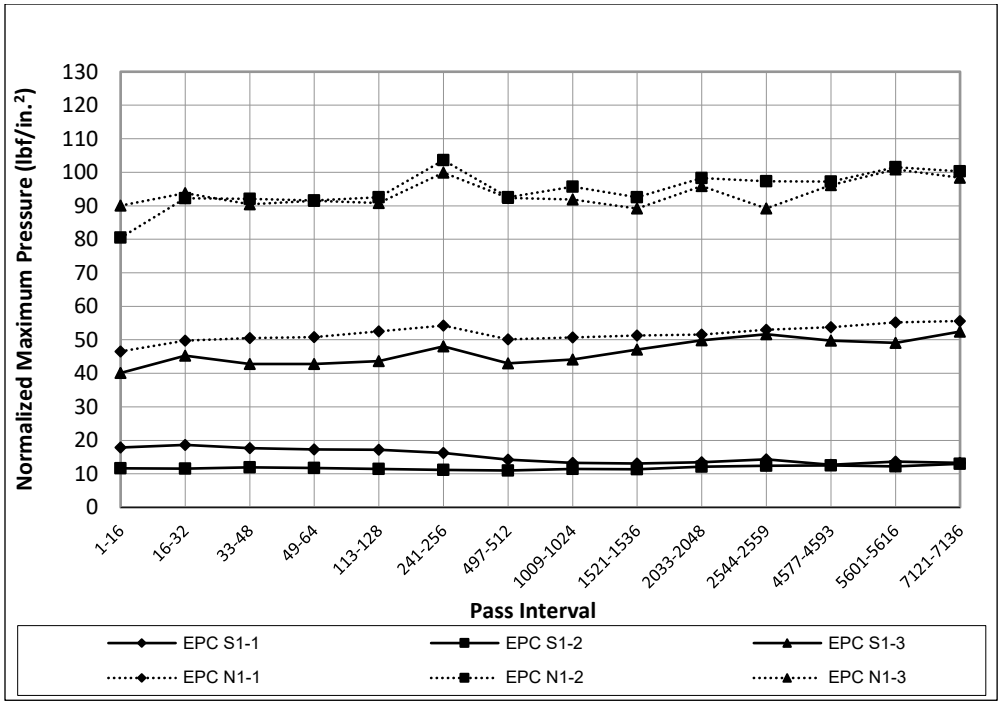

Figure 4.20. C-17 maximum recorded pressure values.

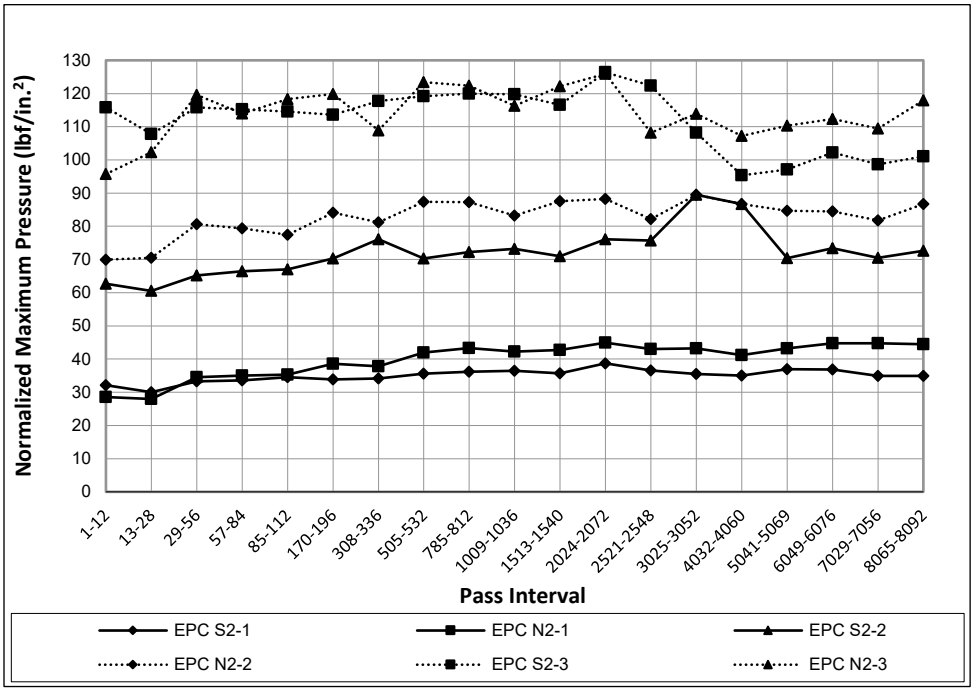

For the C-17 item, the pressure values also remained nearly constant throughout the application of traffic. As can be seen, most of the gauges showed a slight increase in pressure throughout the test. The maximum

normalized pressure values ranged from 96 psi to 126 psi, 63 psi to 89 psi, and 28 psi to 45 psi for depths of 6-in., 12-in., and 24-in., respectively.

4.5 Strain gauges

Strain gauge data were recorded at a rate of 250 Hz at regular intervals throughout trafficking for both the F-15E and C-17 test items. The gauges were installed on the bottom surface of mat panels to monitor their performance and to assist in future modeling efforts. A layout of the instrumentation is shown in Figure 3.9. As can be seen in Figure 3.9, each test item had three sets of strain gauges installed along the centerline, with one gauge in each set installed in the longitudinal direction and the other one in the transverse direction.

The strain gauges in previous tests proved to be relatively fragile and were typically unable to function throughout the entire test. Gauges used in this test also failed at different stages during testing. Gauges 2-1, 2-3, and 2-5 failed before traffic initiated. Strain gauge data recorded for the F-15E and C-17 items are presented in Appendix C and Appendix D, respectively.

5 Analysis of Results

5.1 F-15E test item

5.1.1 Mat breakage

The F-15E test item sustained a total of 9,152 passes (2,288 coverages) of simulated F-15E aircraft traffic before failure by mat breakage. Three panels failed as the result of top skin tears along a vertical stiffener and three other panels failed as a result of skin tears along the female hinge connector. The mat breakage at 9,152 passes was 14.3% of the F-15E traffic area. Based on the results from this experiment, it is now evident that the maintenance of the subgrade or panel replacement should not be required before the expected operating life of an expeditionary airfield when the mat system is placed in the 2-1 lay configuration over a CBR of 25 or higher and subjected to F-15E traffic.

Photographs of the various damage types can be seen in Figures 5.1 through 5.7. All of the failed panels received damage in one of two modes. The most common mode was top skin tears along a vertical stiffener resulting from core damage. Similar damage was documented in previous AM2 tests using the same F-15E loads; however, the top skin did not always crack (Rushing and Tingle 2007, Garcia et al. 2014a). The second damage mode was the top skin tearing along the female hinge connector. This damage resulted from the flexibility of the joints due to the 2-1 lay pattern. The flexibility caused corner curls on the top skin where the overlap/underlap connectors met the female hinge connector. These corner curls cracked at their base and traveled toward the center of the mats along the female hinge connector.

Other types of damage noted were bottom skin tears, female hinge connector cracks, and overlap/underlap connector rail cracks. The bottom skin tears were always located directly underneath a top skin tear; most likely the result of a vertical stiffener buckling. The female hinge connector cracks noted here were located directly in the center of full panels and were typically found on panels with top and bottom skin tears. The female hinge connector failures were most likely associated with the buckling of vertical stiffeners as well. Finally, the underlap/overlap rail cracks were assumed to be caused by fatigue due to the stress concentration in the corners on the underside of the rails. All damage associated with underlap/overlap connector rails occurred in topmost rails only, regardless of whether it was the underlapping or overlapping joint.

Figure 5.1. 17 in. female hinge crack on panel 2.

Figure 5.2. Female hinge crack in panel 3.

Figure 5.3. 54 in. female hinge connector crack on panel 8.

Figure 5.4. Two large bottom skin tears on panel 8.

Figure 5.5. Top skin tear in upper rail of overlap connector on panel 53.

Figure 5.6. 4 in. crack in upper rail of underlap connector on panel 54.

Figure 5.7. 1 in. crack on upper rail of underlap connector on panel 102.

Additionally, it is interesting to note that the first five panels to fail were all full panels. One possible cause for these failures may have been due to proximity to the ends of the test section. The north and south ends of the test section were connected to AM2 ramps via male and female keylocks. The keylocks were only about 4-in. wide, allowing more rotation than the normal panels would and potentially causing premature failures.

5.1.2 Permanent deformation

5.1.2.1 Centerline profile

The centerline profiles for the mat surface and the subgrade at various traffic intervals are shown in Figures 4.11 and 4.12, respectively. Both profiles were analyzed to determine whether the roughness criterion was exceeded. Measuring approximately 0.51-in. at 1,520 passes, the maximum change in elevation was below the 1.25-in. maximum depth established for the F-15E aircraft. Therefore, the system performed adequately to prevent excessive roughness from occurring along the profile.

5.1.2.2 Cross sections

The permanent deformations on the unloaded mat surface, the loaded mat surface, and the subgrade are shown in Figures 4.15, 4.16, and 4.17, respectively. For the F-15E test item, the maximum average permanent deformation for the loaded cross sections measured 1.07-in. at 1,520 passes, which did not exceeded the 1.25-in. limit for the aircraft. However, at pass level 2,544, the deformation measured 1.25-in., satisfying the failure

criteria. Therefore, the system was considered failed due to rutting at this pass level. Even so, the test was continued in order to further monitor the deformation and panel performance. At the end of the test, the loaded deformation on the mat surface measured 1.83-in.

5.1.3 Elastic deflection

The elastic deflection measurements shown in Figure 4.21 were the sum of (1) the gap between the bottom surface of the mat and the top surface of the subgrade when the mat was unloaded (elastic deflection of the mat) and (2) the elastic deflection of the subgrade. The elastic deflection generally increased throughout the traffic test to approximately 1.5-in. Assuming that the elastic deflection of the subgrade remained nearly constant throughout the test, the increase in the total elastic deflection of the mat and the subgrade indicates that the air gap underneath the mat increased as deformation occurred in the subgrade surface.

5.1.4 Earth pressure cells

The EPC data obtained during trafficking show the stresses measured in the subgrade at 6-in., 12-in., and 24-in. below the surface along the centerline. The average maximum pressures recorded were 94 psi, 49 psi, and 14 psi for 6-in., 12-in., and 24-in. depths, respectively. The data showed that the most critical area underneath the mat is just under the surface. Any improvements to the upper layers of the subgrade directly under the mat would increase the mat system's performance even if the underlying layers remained much weaker.

An additional point to note is that recorded pressure values were higher when the load cart was on the right side of the centerline compared to when the load cart was the same distance to the left of the centerline. The authors concur that these findings were different due to the direction of the underlap/overlap connectors. When the load cart was on the right side of the centerline, the panels that were taking the direct load connected to the centerline via the underlapping connector; therefore, whatever load was transferred through this joint must have traveled through the locking bar, which is not as effective as the opposite condition in which the overlapping connector fully contacts the underlapping connector when loaded.

One common trend from Figure 4.22 is that most of the gauges recorded a slight increase in pressure from the beginning to the end of the test. EPC S1-1 was the only gauge that recorded a net decrease in pressure throughout

the test. A decrease in pressure was unexpected since EPC S1-3 was positioned directly above EPC S1-1 and did not show the same trend. Overall, increasing pressures were expected since the load cart densified the subgrade within the traffic lane throughout the test. The decreasing values recorded by EPC S1-1 might have been attributed to improper installation technique or, more specifically, incomplete compaction of the lift directly above the gauge. Incomplete compaction would have caused the subgrade material at this location to have a large number of voids, inhibiting proper distribution of the load applied at the surface throughout the material.

5.1.5 Strain gauges

Strain data (Appendix C) were collected beneath the F-15E item in order to determine the response of the mat from the applied aircraft load. The positive peaks indicate tensile strains, while the negative peaks represent compressive strains. Figure 5.8 shows the maximum recorded tensile strain values for each gauge at the designated pass intervals, and Figure 5.9 shows the maximum recorded compressive strains values from each of the pass intervals. The average maximum tensile strain was almost 3,200 micro-strain, while the average maximum compressive strain was approximately -1,650 micro-strain. Gauges 1, 3, and 5 recorded average max compressive strains around -2,800 micro-strain, while gauges 2, 4, and 6 recorded average max compressive strains around 500 micro-strain. The significant difference between compressive strain values was most likely due to permanent deformation in the mats, since gauges 2, 4, and 6 were all mounted transverse to the direction of traffic. Strain data collected for this test item were very similar to those reported in Garcia et al. (2014a).

Figure 5.8. F-15E test item maximum tensile strains.

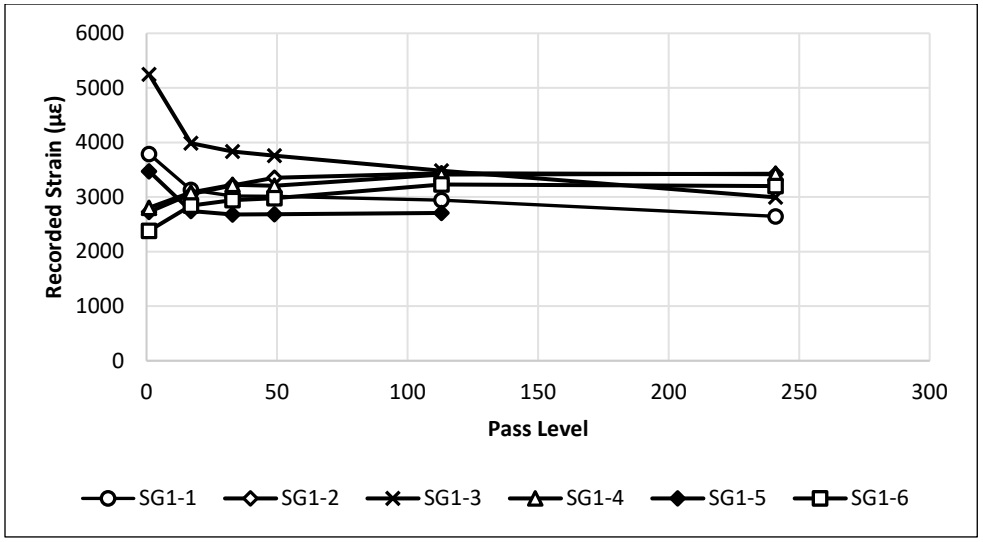

Figure 5.9. F-15E test item maximum compressive strains.

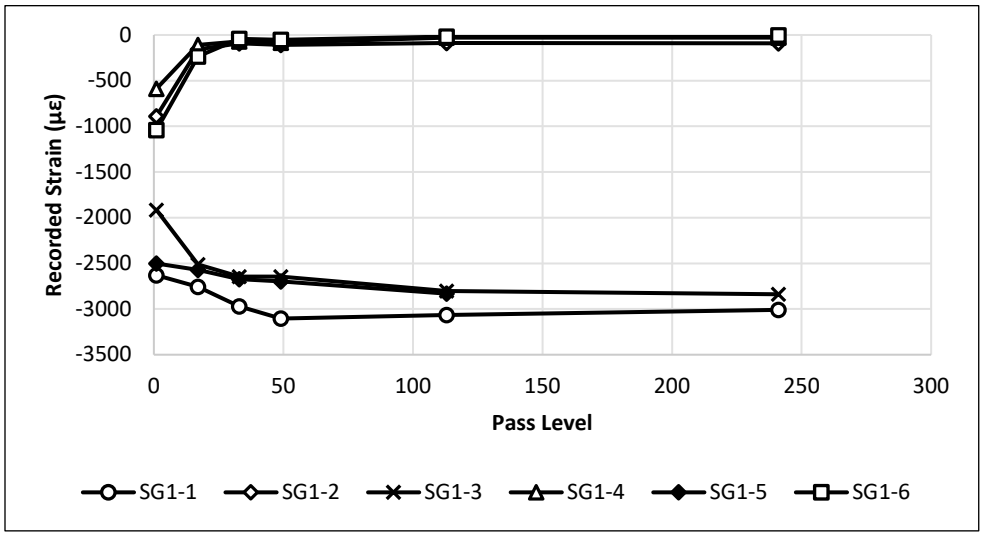

5.2 C-17 test item

5.2.1 Mat breakage

The C-17 test item was trafficked until 10,080 passes (9,000 coverages) were completed. No mat breakage occurred in the test item. Researchers expected the mat system to sustain approximately 7,000 passes before failing by either permanent deformation or mat breakage, based on previous test results. Based on the results from this experiment, it is now evident that the maintenance of the subgrade or panel replacement should not be required before the expected operating life of an expeditionary airfield when the mat system is placed in the 2-1 lay configuration over a

CBR of 25 or higher and subjected to C-17 operations. The increased capacity of the AM2 mat system to sustain C-17 traffic compared to F-15E traffic can be attributed to the broader load distribution from the C-17 landing gear configuration and lower tire pressures.

5.2.2 Permanent deformation

5.2.2.1 Centerline profile

The centerline profiles for the post-traffic mat surface and subgrade at various traffic intervals are depicted in Figures 4.13 and 4.14. Both profiles were analyzed to determine whether the roughness criterion was exceeded. The maximum change in elevation measured about 1.1-in., which was below the 3.0-in. deep threshold established for the C-17 aircraft. Therefore, the system performed adequately to prevent excessive roughness from occurring along the profile.

5.2.2.2 Cross sections

The permanent deformation on the unloaded mat surface, the loaded mat surface, and the subgrade are shown in Figures 4.18 through 4.20, respectively. For the C-17 test item, the maximum value for permanent deformation after 10,080 passes was recorded at 2.5-in. on the loaded mat surface. As stated previously, the failure criteria state that the permanent deformation on the mat surface must not exceed 3.0-in. for C-17 traffic. None of the deformation values exceeded the limit; therefore, the system performed adequately to prevent excessive roughness from occurring in the transverse direction.

5.2.3 Earth pressure cells

The EPC data collected during trafficking show that the average maximum stresses measured in the subgrade at 6-in., 12-in., and 24-in. under the traffic centerline were approximately 113 psi, 77 psi, and 37 psi, respectively. The 2-1 lay pattern data showed that the most critical area underneath the mat is just under the surface. Any improvements to the upper layers of the subgrade directly under the mat would increase the mat system performance even if the underlying layers remained much weaker.

An additional point to note is that recorded pressure values were higher when the load cart was on the right side of the centerline compared to when the load cart was the same distance to the left of the centerline. The

authors concur that these findings were different due to the direction of the underlap/overlap connector. When the load cart was on the right side of the centerline, the panels that were taking the direct load connected to the centerline via the underlapping connector; therefore, whatever load was transferred through this joint must travel through the locking bar, which is not as effective as the opposite condition in which the overlapping connector fully contacts the underlapping connector when loaded.

A common trend from Figure 4.23 is that most of the gauges recorded a slight increase in pressure from the beginning to the end of the test. EPC S2-3 was the only gauge that recorded a net decrease in pressure throughout the test. A decrease in pressure was unexpected since the gauge was positioned directly above EPC S2-1, which did not show the same trend. Overall, increasing pressures were expected since the load cart basically compacted throughout the test. The decreasing values recorded by EPC S2-3 may have been attributed to improper installation technique or, more specifically, incomplete compaction of the lift directly above the gauge. Incomplete compaction would have caused the subgrade material at this location to have a large number of voids, which inhibited proper distribution of the load applied at the surface throughout the material.

5.2.4 Strain gauges

Strain data (Appendix D) were collected beneath the C-17 item in order to determine the response of the mat from the applied aircraft load. The positive peaks indicate tensile strains, while the negative peaks represent compressive strains. Figure 5.10 shows the maximum recorded tensile strains from the working gauges at the designated pass intervals while Figure 5.11 shows the maximum recorded compressive strains at each of the pass intervals. The maximum tensile strains averaged to be approximately 1,500 micro-strain while the maximum compressive strains averaged just over -800 micro-strain. Similar to the F-15E test item, the compressive strains in gauges 2, 4, and 6 reduced as the pass level increased, indicating plastic deformation within the mats. Strain data collected for this test item were very similar to those collected in Garcia et al. (2014a).

Figure 5.10. C-17 test item maximum tensile strains.

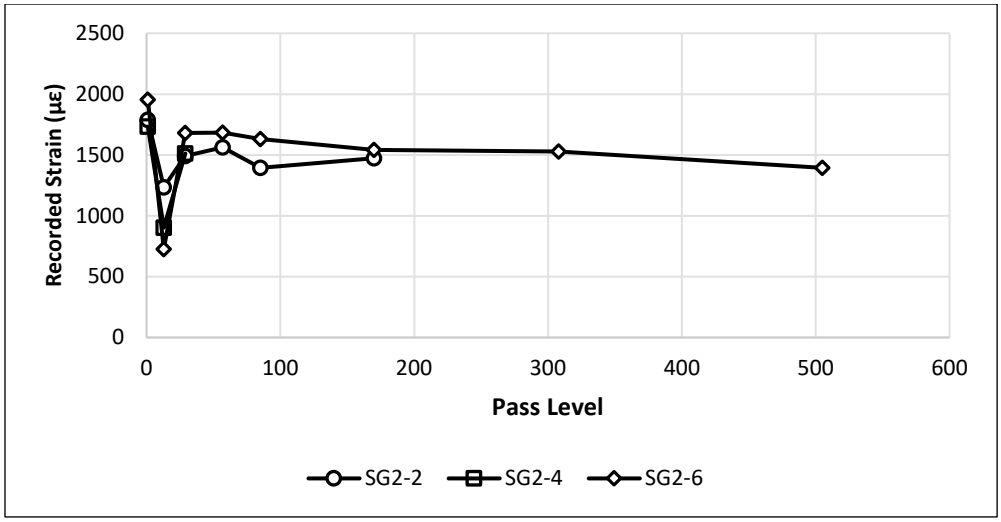

Figure 5.11. C-17 test item maximum compressive strains.

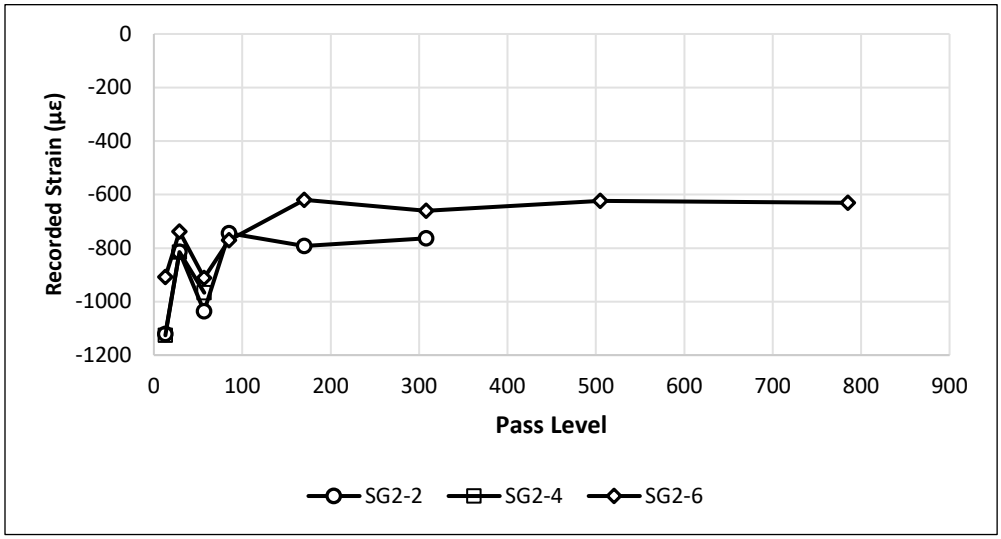

6 Comparison of 25 CBR 2-1 and Brickwork Pattern Results

For comparative purposes, the results of the 2-1 lay pattern presented in this study were compared to a previously performed brickwork evaluation over the same 25 CBR subgrade condition. The results of the comparisons are presented in this chapter.

6.1 F-15E

6.1.1 Mat breakage

According to the results of the F-15E evaluations, the 2-1 lay pattern test achieved 9,152 passes, surpassing the 6,294 passes sustained by the brickwork pattern documented by Garcia et al. (2014a). Interestingly, the increased number of passes to failure was achieved, even though more rutting occurred during the 2-1 lay evaluation than in the brickwork evaluation (this was unexpected since increased rutting typically causes earlier failure). The authors infer the difference in performance between the brickwork and the 2-1 lay evaluations may have been caused by manufacturing discrepancies in the mat's 2-ft end connector extrusions. Although actual dimensional discrepancies cannot be verified, there is a strong possibility that the mat panels used in the brickwork evaluation lacked the proper fillets in the locking bar channel. Without proper fillet radii, large stress concentrations occur during trafficking, causing premature failure of the end connector. Garcia et al. (2015) showed a significant reduction in performance of panels that did not have the proper fillet radius in the locking bar channel. Therefore, if the mats tested in Garcia et al. (2014a) had been manufactured with the proper fillet radii, the system would likely have sustained more passes than the 2-1 lay pattern. Panels used in the 2-1 lay pattern evaluation underwent verification for proper fillet dimensions prior to placement; however, mats trafficked in the brickwork evaluation were not measured for compliance.

Another significant factor that directly affected the performance comparison was the total area of the evaluation surface. The total area for the 2-1 pattern measured 1,008 ft^2 versus 960 ft^2 for the brickwork pattern. While 48 ft^2 may seem like a small difference, it does make a difference for the percent damage calculation. Based on the calculations described in section 3.8.1, 5 mats were required to fail to reach 10% mat

damage for the 2-1 evaluation, while only 4 mat failures caused 10% in the brickwork evaluation. During the 2-1 lay evaluation, the fourth mat panel failed at pass 7,120, which is much closer to the 6,294 passes from the brickwork test. Even so, the 2-1 lay pattern still performed better than the brickwork pattern, which was unexpected.

An additional factor that had potential to affect the performance comparison between the 2-1 pattern and the brickwork pattern is the use of half panels in the traffic lane. Since the half panels are exactly one half the area of a full panel, two half panels would have been required to fail in order to have the same effect on damage percentage as one full panel. Considering only full panels failed before the 10% breakage requirement, this did not affect the evaluation.

6.1.2 Permanent deformation

Deformation values were also compared to see if any insight could be gained. Test results showed greater deformation values for the 2-1 lay pattern F-15E test item than for the brickwork pattern. A comparison between the average maximum deformations for both patterns can be seen in Figure 6.1. The deformation from the 2-1 lay pattern evaluation was greater than the brickwork pattern evaluation at virtually every pass level. The increased deformation was a direct result of the additional flexibility in the mat system caused by additional joint alignment associated with the rows of half panels that were included in the pattern.

Figure 6.1. F-15E deformation versus number of passes for 25 CBR brickwork and 2-1 lay patterns.

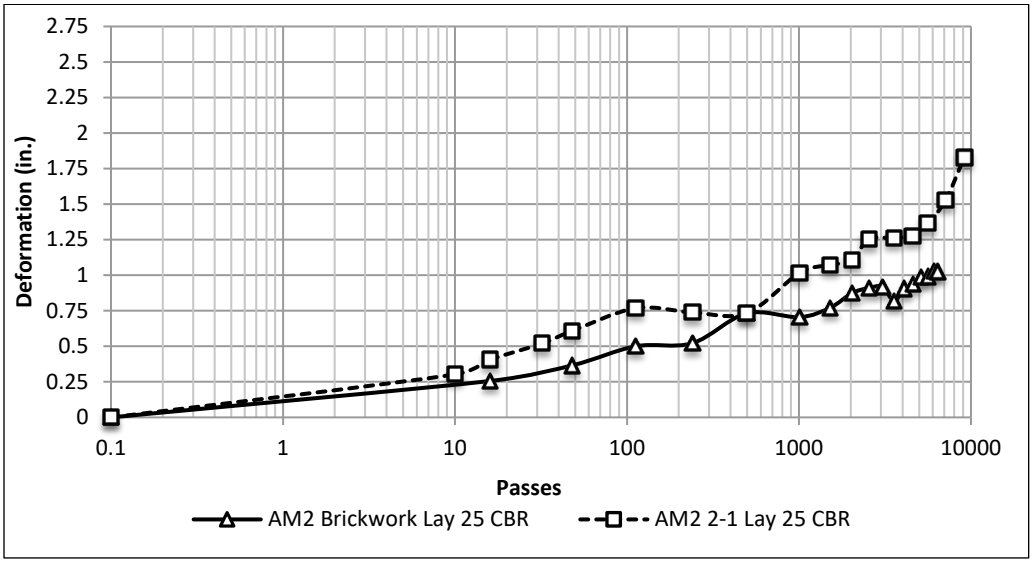

6.1.3 Earth pressure cells

In the previous 25 CBR brickwork analysis (Garcia et al. 2014a), the average maximum pressure values for EPCs located at 6-in., 12-in., and 24-in. beneath the centerline were 57 psi, 33 psi, and 17 psi, respectively. In comparison, the average maximum pressures recorded for the 2-1 lay evaluation were 94 psi, 49 psi, and 14 psi for 6-in., 12-in., and 24-in. depths, respectively. Both sets of values showed that the most critical area underneath the mat is just under the surface. Any improvements to the upper layers of the subgrade directly under the mat would increase the mat system's performance even if the underlying layers remained much weaker. Additionally, the vertical stress on the subgrade was higher when the panels were arranged in the 2-1 lay pattern. At 6-in. in depth, the pressure value recorded for the 2-1 lay pattern was 60% greater than that of the brickwork pattern. Additionally, at 12-in., the pressure value was almost 50% greater for the 2-1 lay pattern than the brickwork pattern. At 24-in., the pressure values were nearly equal for both patterns. According to these data, the 2-1 lay pattern has a lower global stiffness than the brickwork pattern, which would account for the large rut formation since the subgrade absorbed more of the load on each pass.

6.2 C-17

6.2.1 Mat breakage

The results of the 2-1 lay evaluation confirmed the benefits for AM2 when placed over a strong foundation. The correlation between AM2 performance and subgrade strength has been portrayed for the brickwork pattern by Garcia et al. (2014a), which resulted in the same number of passes before testing was ceased. Neither evaluation had any damaged panels.

Similarly as described in the F-15E comparison above, a significant factor that could have directly affected the performance comparison was the total area of the evaluation surface. The total area for the 2-1 pattern measured 1,512 ft^2 versus 1,440 ft^2 for the brickwork pattern. Based on the calculations described in section 3.8.1, 7 mats were required to fail to reach 10% mat damage for the 2-1 evaluation, while only 6 mat failures caused 10% in the brickwork evaluation. Considering that no panels failed in either evaluation, the total area did not affect the results.

An additional factor that had potential to affect the performance comparison between the 2-1 lay pattern and the brickwork pattern is the use of half panels in the traffic lane. Since the half panels are exactly one half the area of a full panel, two half panels would have been required to fail in order to have the same effect on damage percentage as one full panel. Even so, the C-17 test item was not affected by this since no panels failed during testing.

6.2.2 Permanent deformation

Deformation values were also compared for the C-17 items to see if any insight could be gained. Similarly as seen for the F-15E items, test results showed greater deformation values for the 2-1 lay pattern C-17 test item than for the brickwork pattern. A comparison between the average maximum deformations for both patterns can be seen in Figure 6.2. The deformation from the 2-1 lay pattern evaluation was greater than the brickwork pattern evaluation at nearly every pass level. The increased deformation was a direct result of the additional flexibility in the mat system caused by additional joint alignment associated with the rows of half panels that were included in the pattern.

Figure 6.2. C-17 deformation versus number of passes for 25 CBR brickwork and 2-1 lay patterns.

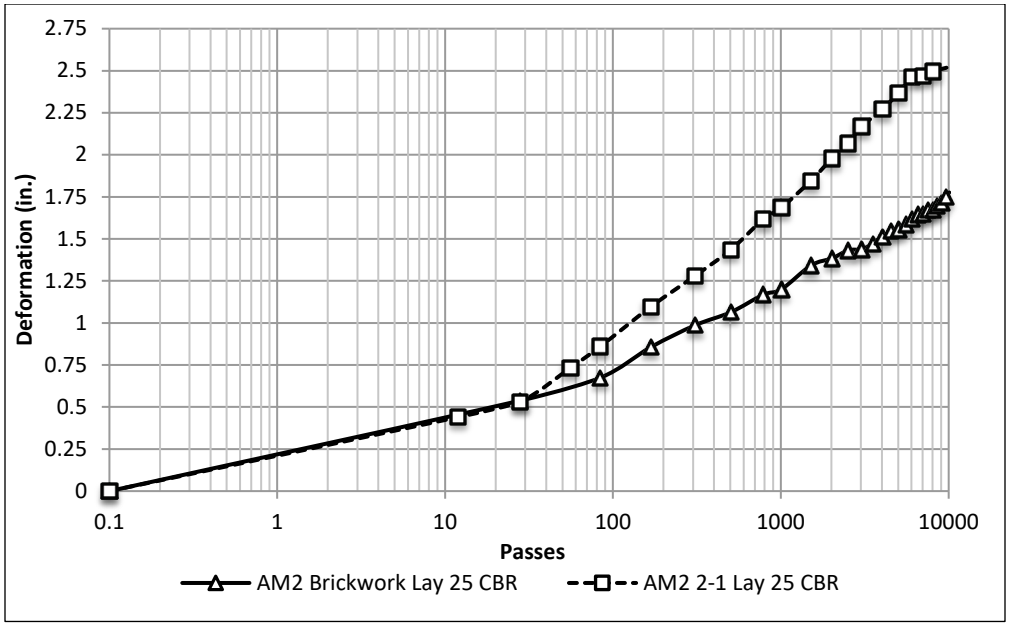

6.2.3 Earth pressure cells

In the 25 CBR brickwork evaluation performed previously by Garcia et al. (2014a), the average maximum stresses were 75 psi and 52 psi for depths of 6-in. and 12-in., respectively. In comparison, the EPC data collected during the 2-1 evaluation showed that the average maximum stresses measured in the subgrade at 6-in., 12-in., and 24-in. under the traffic centerline were approximately 113 psi, 77 psi, and 37 psi, respectively. Similar to the F-15E comparison, both the 6-in. and 12-in. pressure measurements recorded were approximately 50% greater for the 2-1 lay pattern than for the brickwork pattern. According to these data, the 2-1 lay pattern has a lower global stiffness than the brickwork pattern, which would account for the large rut formation since the subgrade absorbed more of the load on each pass. Additionally, both sets of measured values showed that the most critical area underneath the mat is just under the surface. Any improvements to the upper layers of the subgrade directly under the mat would increase the mat system performance even if the underlying layers remained much weaker.

7 Conclusion and Recommendations

7.1 Conclusions

The purpose of this investigation was to evaluate the ability of the AM2 airfield mat to sustain simulated F-15E and C-17 aircraft traffic when placed in the 2-1 lay pattern over a CH subgrade with a CBR of 25. Permanent deformation and mat breakage were monitored to determine the number of passes in regards to pre-determined failure criteria.

The following conclusions were derived from accelerated traffic testing of AM2 airfield matting conducted from July 2016 through October 2016:

- The F-15E test item sustained 2,544 passes (636 coverages) of simulated F-15E aircraft traffic on AM2 installed in the 2-1 lay pattern on a CH subgrade with a CBR of 25 prior to failure by permanent deformation.
- The F-15E test item sustained 9,152 passes (2,288 coverages) of simulated F-15E aircraft traffic on AM2 placed in the 2-1 lay pattern on a CH subgrade with a CBR of 25 before failure by mat breakage.
- Two failure modes were present during testing of the F-15E test item. The first was corner curls cracking along the female hinge connector. The second was top skin tears along vertical stiffeners.
- Four panels had cracked overlap/underlap connector rails; however, none of the cracks reached failure criteria during testing of the F-15E test item. Researchers verified proper locking bar channel fillets in the connectors prior to testing.
- The 25 CBR 2-1 lay pattern acquired less damage than the 25 CBR brickwork pattern for the F-15E test item. Researchers concluded that the difference in performance was caused by improper fillet radii in the locking bar channel on the mats used in the 25 CBR brickwork evaluation, since the 2-1 lay pattern sustained more passes while sustaining larger measured deformations.
- The C-17 test item sustained 10,080 passes (9,000 coverages) of simulated C-17 aircraft traffic on AM2 installed in the 2-1 lay pattern on a CH subgrade with a CBR of 25 before testing was ceased. The test item did not fail from permanent deformation nor mat breakage.

7.2 Recommendations

Based on the airfield mat evaluations described herein, the following recommendations are provided:

- Only install AM2 panels in the 2-1 lay configuration if a subgrade with a CBR of 25 or greater is present for equivalent performance to the more stable brickwork pattern.
- The results of this evaluation confirm that a 25 CBR requirement will greatly reduce the underlying subgrade deformation whether using the traditional brickwork or the 2-1 lay patterns for AM2 mat installations. If a mixture of aircraft were to operate on an AM2 surface placed over a soil with a CBR of 25 or greater, the life of the system can be assumed indefinite. However, even with a relatively high number of allowable operations, routine inspections and maintenance activities should not be reduced to ensure the system remains safe and functional.

References

ASTM International. 2007. *Standard test method for CBR of laboratory compacted soils*. Designation: D 1883. West Conshohocken, PA: ASTM International.

_____. 2007. *Standard test method for density and unit weight of soil in place by the sand cone method*. Designation: D 1556. West Conshohocken, PA: ASTM International.

_____. 2007. *Standard test methods for liquid limit, plastic limit, and plasticity index of soils*. Designation: D 4318. West Conshohocken, PA: ASTM International.

_____. 2007. *Standard test method for particle size analysis of soils*. Designation: D 422. West Conshohocken, PA: ASTM International.

_____. 2009. *Standard test method for use of the dynamic cone penetrometer in shallow pavement applications*. Designation: D 6951. West Conshohocken, PA: ASTM International.

_____. 2010. *Standard test method for density of soil in place by the drive cylinder*. Designation: D 2937. West Conshohocken, PA: ASTM International.

_____. 2010. *Standard test methods for laboratory determination of water (moisture) content of soil and rock by mass*. Designation: D 2216. West Conshohocken, PA: ASTM International.

_____. 2011. *Standard practice for classification of soils for engineering purposes (USCS)*. Designation: D 2487. West Conshohocken, PA: ASTM International.

_____. 2012. *Standard test method for laboratory compaction characteristics of soil using modified effort*. Designation: D 1557. West Conshohocken, PA: ASTM International.

_____. 2015. *Standard test methods for in-place density and water content of soils and soil aggregate by nuclear methods (shallow depth)*. Designation D 6938. West Conshohocken, PA: ASTM International.

Garcia, L., T. W. Rushing, and Q. S. Mason. 2014a. *AM2 25 CBR subgrade sensitivity test*. ERDC/GSL TR-14-7. Vicksburg, MS: U.S. Army Engineer Research and Development Center.

Garcia, L., T. W. Rushing, B. A. Williams, and C. A. Rutland. 2014b. *AM2 100 CBR subgrade sensitivity test*. ERDC/GSL TR-14-37. Vicksburg, MS: U.S. Army Engineer Research and Development Center.

Garcia, L., T. W. Rushing, Q. Mason, J. S. Tingle, and C. A. Rutland. 2015. *AM2 mat end connector modeling and performance validation*. ERDC TR-15-28. Vicksburg, MS: U.S. Army Engineer Research and Development Center.

NAWCADLKE. 2006. *Expeditionary airfield AM2 mat certification requirements*. NAWCADLKE-MISC-48J200-0011. Lakehurst, NJ: Naval Air Warfare Center, Aircraft Division.

Rushing, T. W., and J. S. Tingle. 2007. *AM2 and M19 airfield mat evaluation for the rapid parking ramp expansion program*. ERDC/GSL TR-07-5. Vicksburg, MS: U.S. Army Engineer Research and Development Center.

Rushing, T. W., L. Garcia, J. S. Tingle, P. G. Allison, and C. A. Rutland. 2014. *AM2 3-4 alternate lay pattern evaluation*. ERDC/GSL TR-14-38. Vicksburg, MS: U.S. Army Engineer Research and Development Center.

Rushing, T. W., N. Torres, and Q. S. Mason. 2008. *AM2 10 CBR subgrade sensitivity test for the rapid parking ramp expansion program*. ERDC/GSL TR-08-13. Vicksburg, MS: U.S. Army Engineer Research and Development Center.

Rushing T. W., and Q. S. Mason. 2008. *AM2 15 CBR subgrade sensitivity test for the rapid parking ramp expansion program*. ERDC/GSL TR-08-25. Vicksburg, MS: U.S. Army Engineer Research and Development Center.

U.S. Army Engineer Research and Development Center. 1995. *Standard test method for California Bearing Ratio of Soils in place*. Designation: CRD-C654-95. Vicksburg, MS.

Appendix A: Earth Pressure Cell Data for the F-15E Test Item

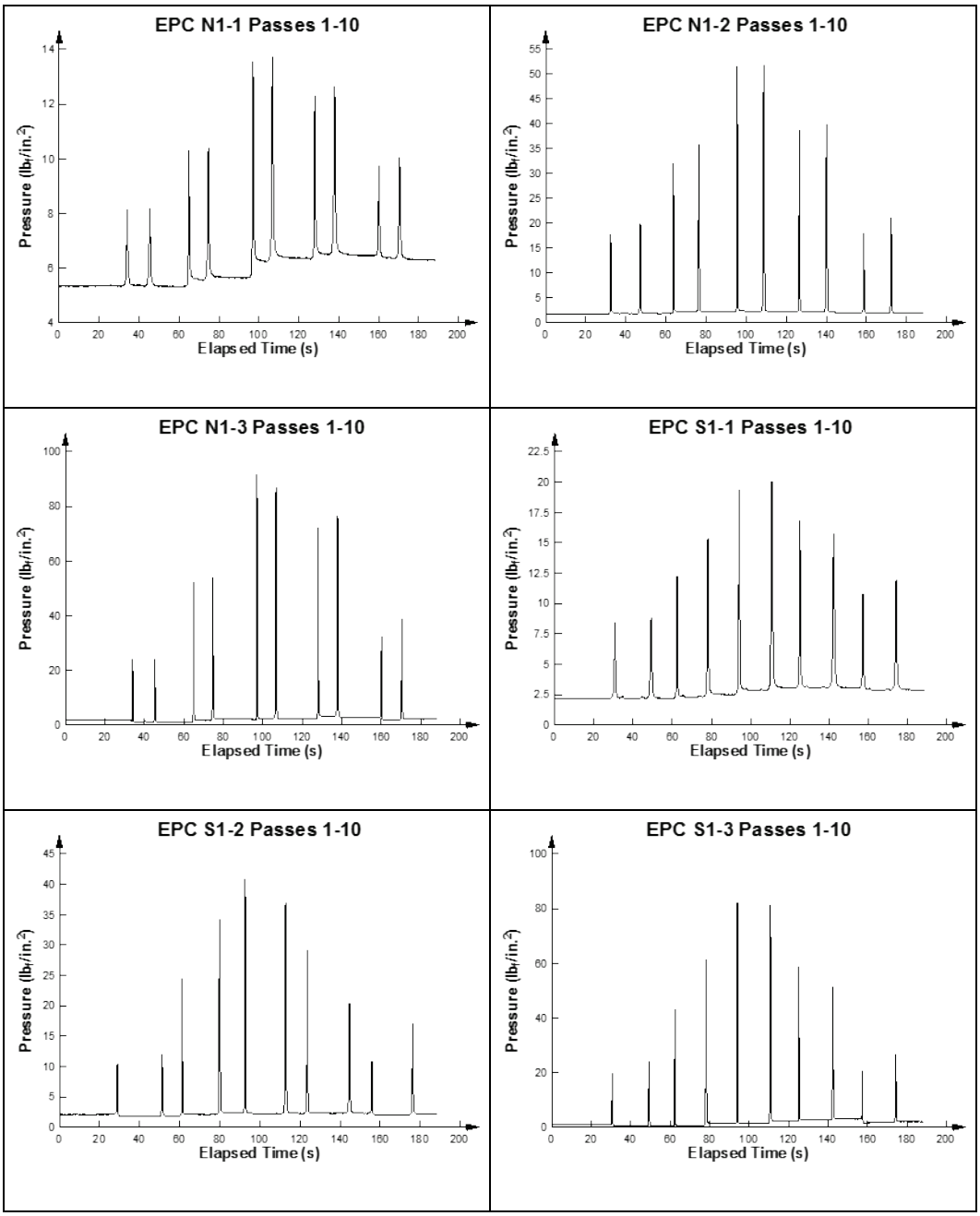

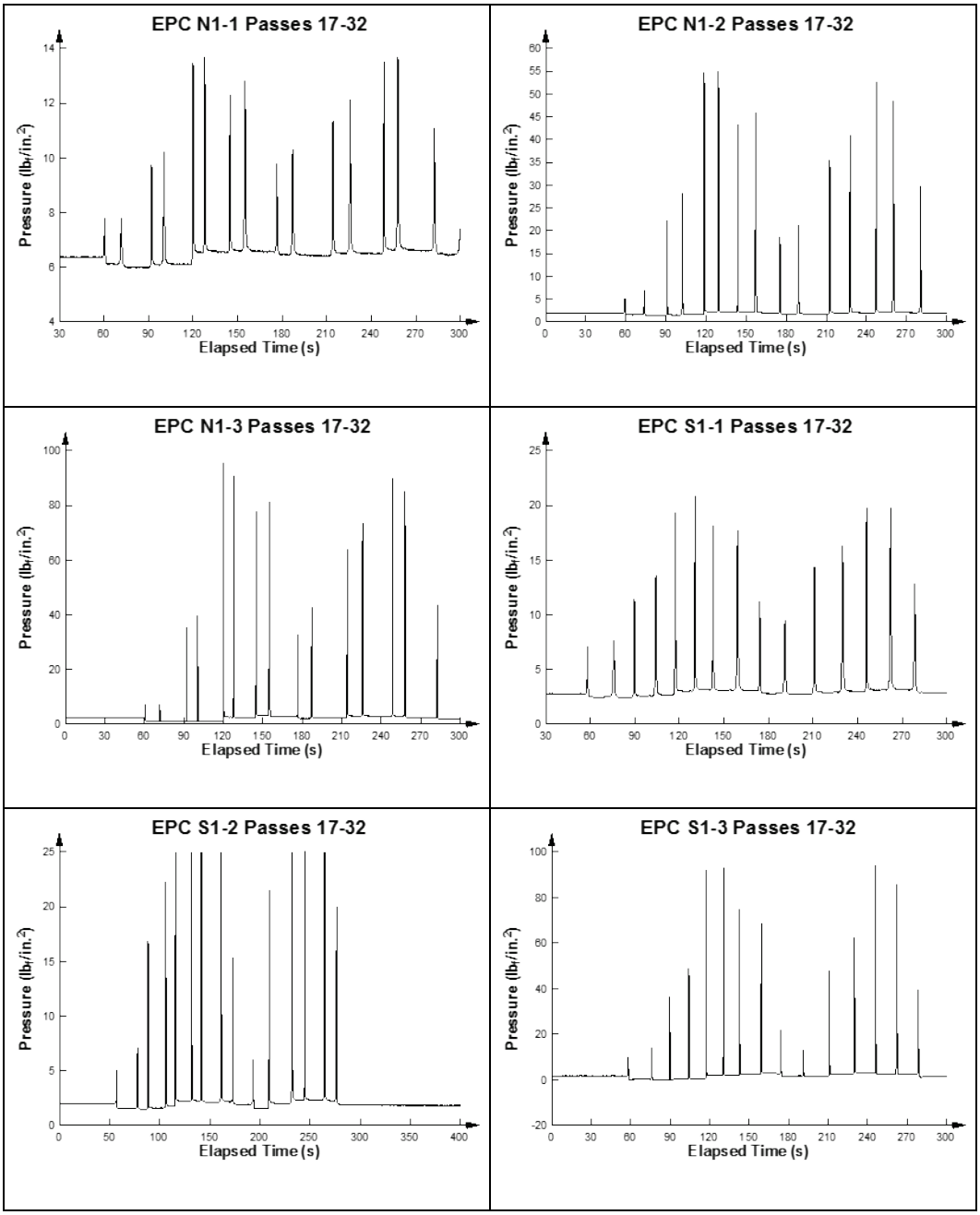
EPC N1-1 Passes 17-32
Pressure (lbf/in.2)
Elapsed Time (s)
EPC N1-2 Passes 17-32
Pressure (lbf/in.2)
Elapsed Time (s)
EPC N1-3 Passes 17-32
Pressure (lbf/in.2)
Elapsed Time (s)
EPC S1-1 Passes 17-32
Pressure (lbf/in.2)
Elapsed Time (s)
EPC S1-2 Passes 17-32
Pressure (lbf/in.2)
Elapsed Time (s)
EPC S1-3 Passes 17-32
Pressure (lbf/in.2)
Elapsed Time (s)

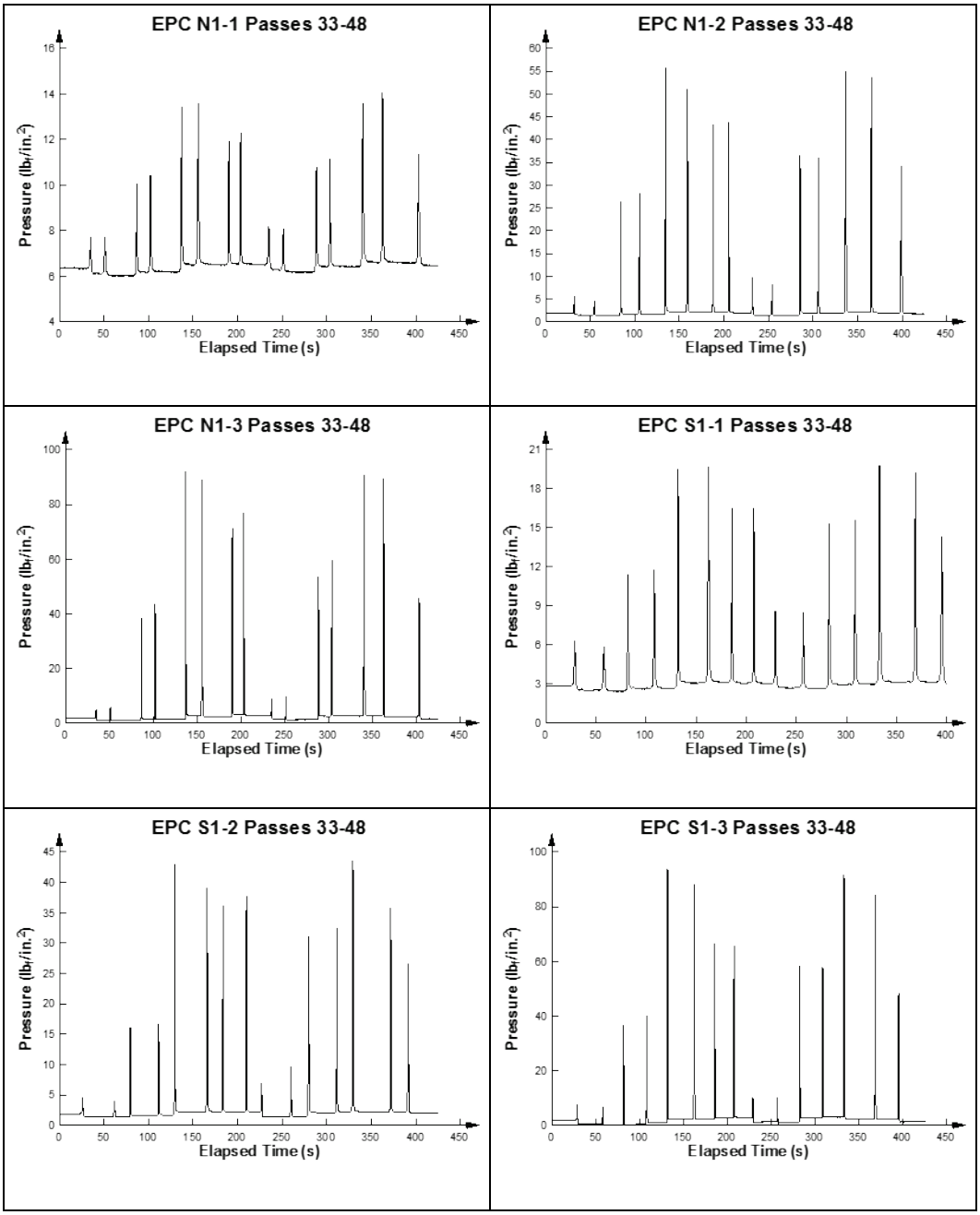
EPC N1-1 Passes 33-48
EPC N1-2 Passes 33-48
EPC N1-3 Passes 33-48
EPC S1-1 Passes 33-48
EPC S1-2 Passes 33-48
EPC S1-3 Passes 33-48
Pressure (lbf/in.2)
Elapsed Time (s)

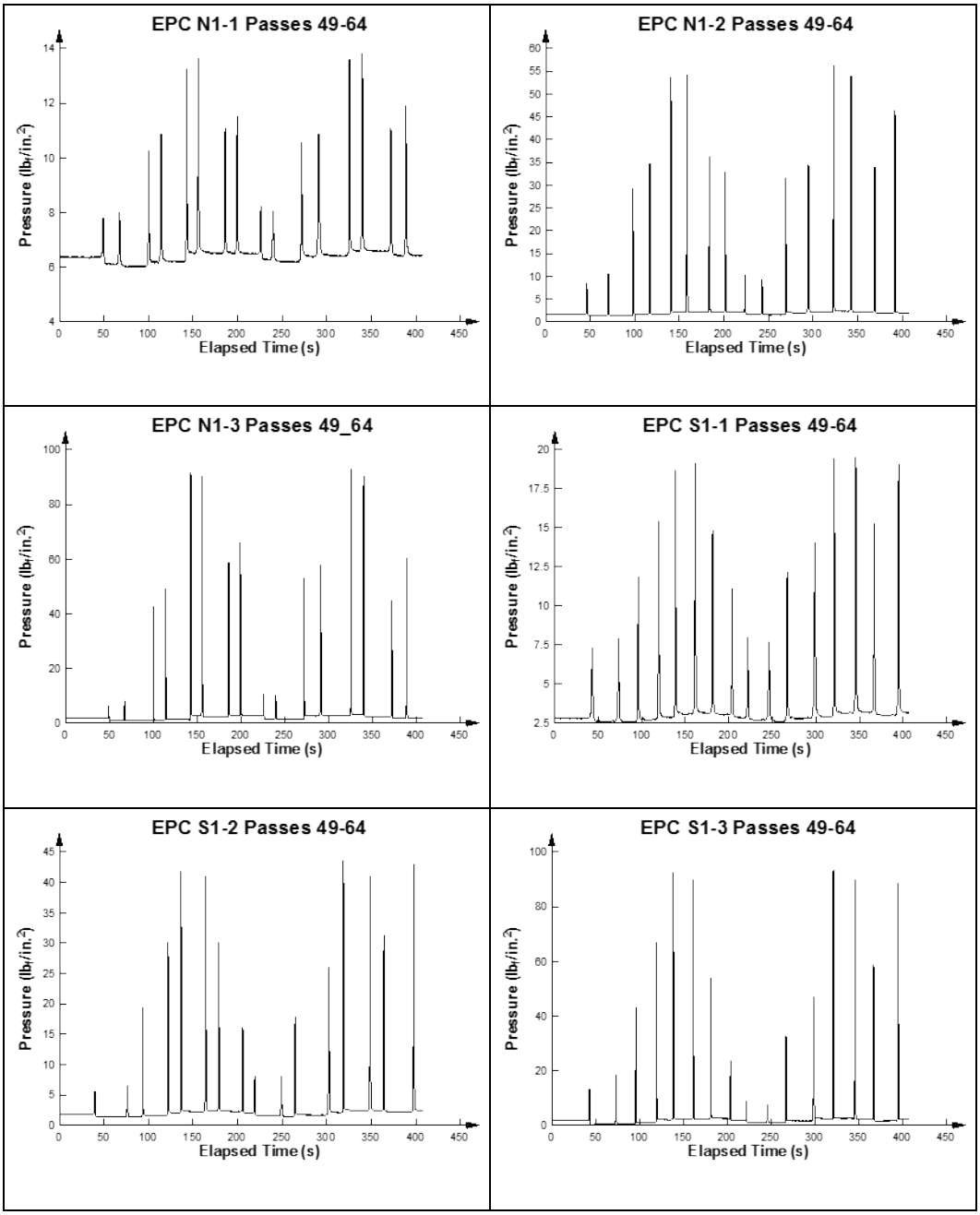
EPC N1-1 Passes 49-64
EPC N1-2 Passes 49-64
EPC N1-3 Passes 49_64
EPC S1-1 Passes 49-64
EPC S1-2 Passes 49-64
EPC S1-3 Passes 49-64
Pressure (lbf/in.2)
Elapsed Time (s)

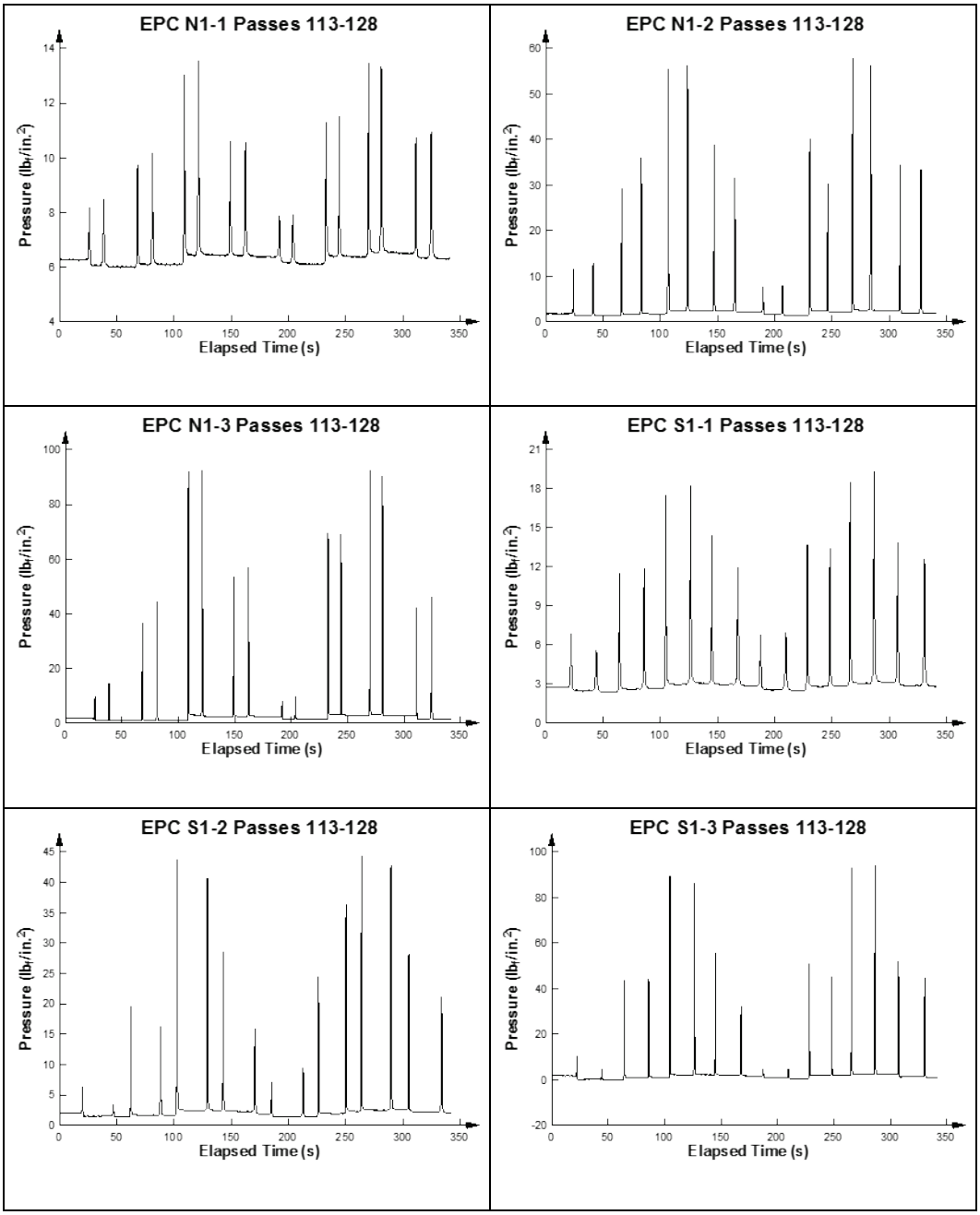
EPC N1-1 Passes 113-128
Pressure (lbf/in.2)
Elapsed Time (s)
EPC N1-2 Passes 113-128
Pressure (lbf/in.2)
Elapsed Time (s)
EPC N1-3 Passes 113-128
Pressure (lbf/in.2)
Elapsed Time (s)
EPC S1-1 Passes 113-128
Pressure (lbf/in.2)
Elapsed Time (s)
EPC S1-2 Passes 113-128
Pressure (lbf/in.2)
Elapsed Time (s)
EPC S1-3 Passes 113-128
Pressure (lbf/in.2)
Elapsed Time (s)

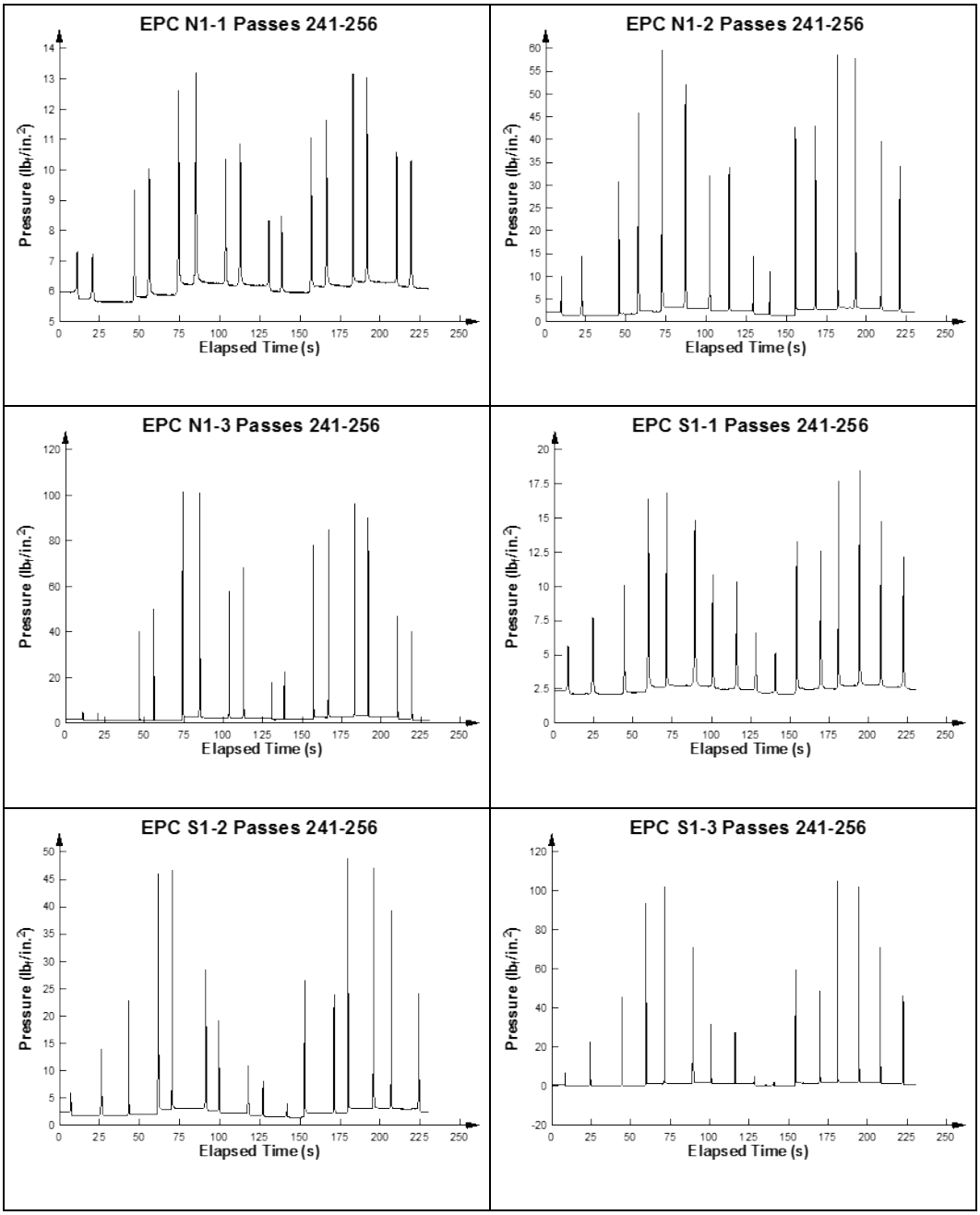
EPC N1-1 Passes 241-256
Pressure (lbf/in.2)
Elapsed Time (s)
EPC N1-2 Passes 241-256
Pressure (lbf/in.2)
Elapsed Time (s)
EPC N1-3 Passes 241-256
Pressure (lbf/in.2)
Elapsed Time (s)
EPC S1-1 Passes 241-256
Pressure (lbf/in.2)
Elapsed Time (s)
EPC S1-2 Passes 241-256
Pressure (lbf/in.2)
Elapsed Time (s)
EPC S1-3 Passes 241-256
Pressure (lbf/in.2)
Elapsed Time (s)

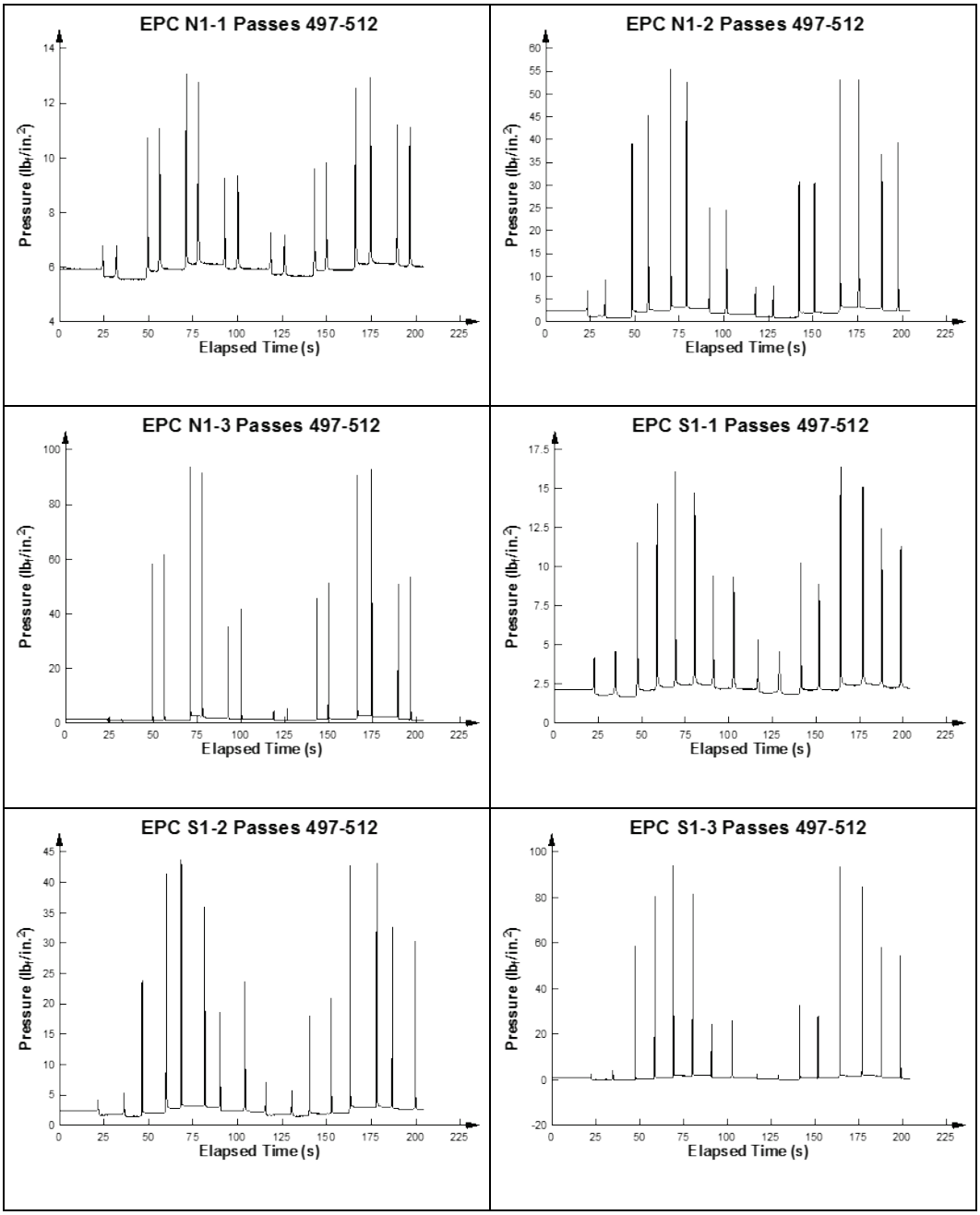
EPC N1-1 Passes 497-512
Pressure (lbf/in.2)
Elapsed Time (s)
EPC N1-2 Passes 497-512
Pressure (lbf/in.2)
Elapsed Time (s)
EPC N1-3 Passes 497-512
Pressure (lbf/in.2)
Elapsed Time (s)
EPC S1-1 Passes 497-512
Pressure (lbf/in.2)
Elapsed Time (s)
EPC S1-2 Passes 497-512
Pressure (lbf/in.2)
Elapsed Time (s)
EPC S1-3 Passes 497-512
Pressure (lbf/in.2)
Elapsed Time (s)

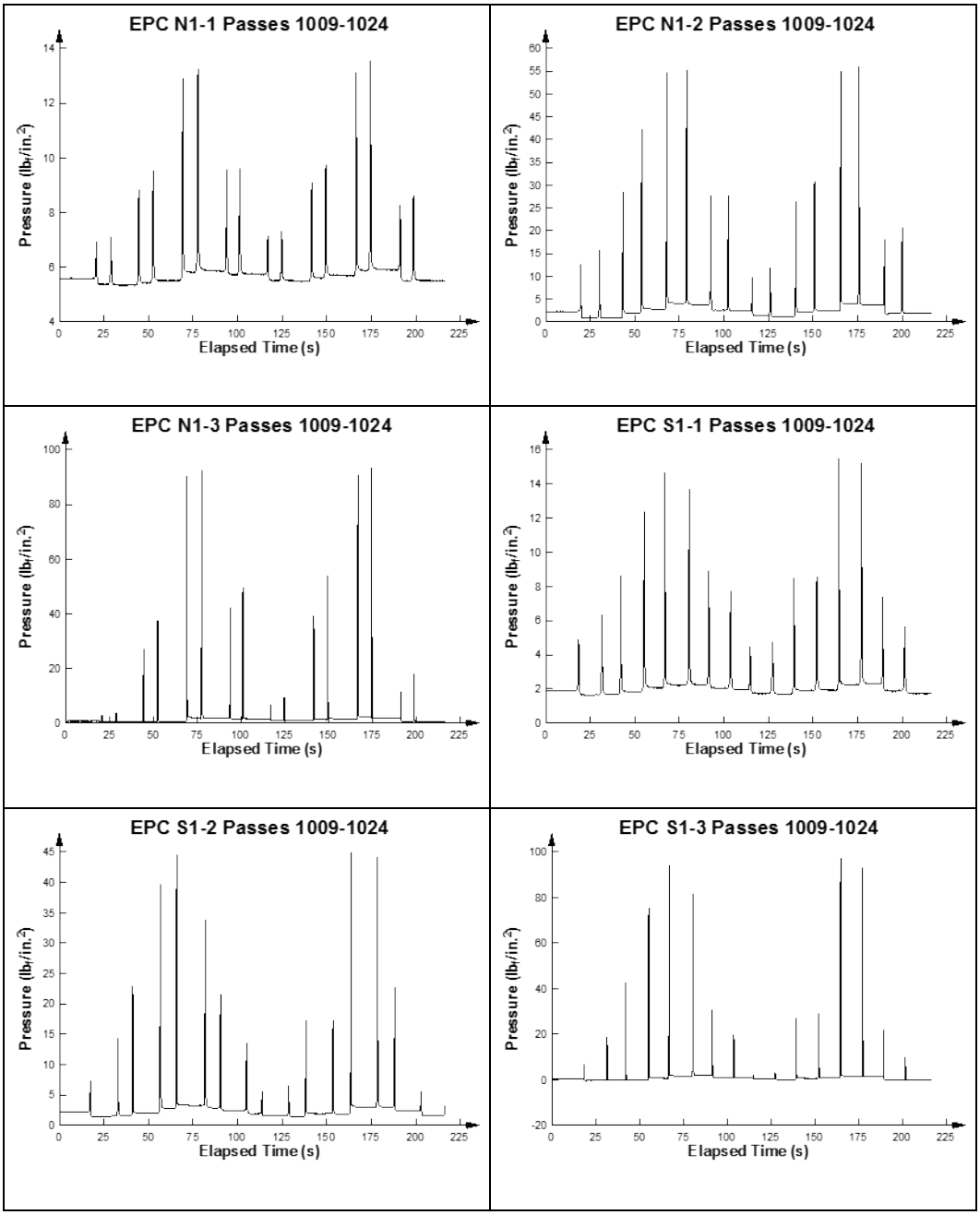
EPC N1-1 Passes 1009-1024
Pressure (lbf/in.2)
Elapsed Time (s)
EPC N1-2 Passes 1009-1024
Pressure (lbf/in.2)
Elapsed Time (s)
EPC N1-3 Passes 1009-1024
Pressure (lbf/in.2)
Elapsed Time (s)
EPC S1-1 Passes 1009-1024
Pressure (lbf/in.2)
Elapsed Time (s)
EPC S1-2 Passes 1009-1024
Pressure (lbf/in.2)
Elapsed Time (s)
EPC S1-3 Passes 1009-1024
Pressure (lbf/in.2)
Elapsed Time (s)

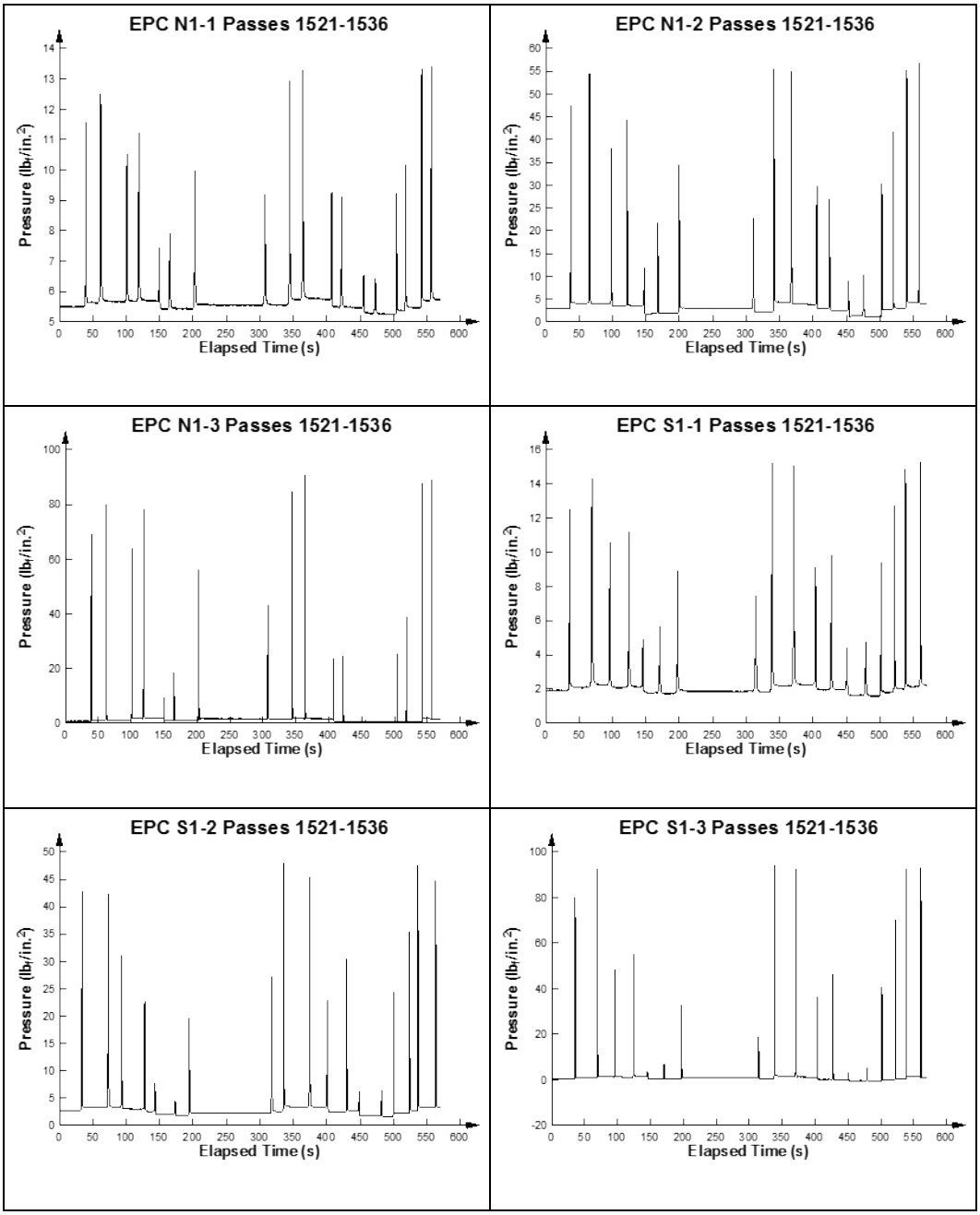
EPC N1-1 Passes 1521-1536
Pressure (lbf/in.2)
Elapsed Time (s)
EPC N1-2 Passes 1521-1536
Pressure (lbf/in.2)
Elapsed Time (s)
EPC N1-3 Passes 1521-1536
Pressure (lbf/in.2)
Elapsed Time (s)
EPC S1-1 Passes 1521-1536
Pressure (lbf/in.2)
Elapsed Time (s)
EPC S1-2 Passes 1521-1536
Pressure (lbf/in.2)
Elapsed Time (s)
EPC S1-3 Passes 1521-1536
Pressure (lbf/in.2)
Elapsed Time (s)

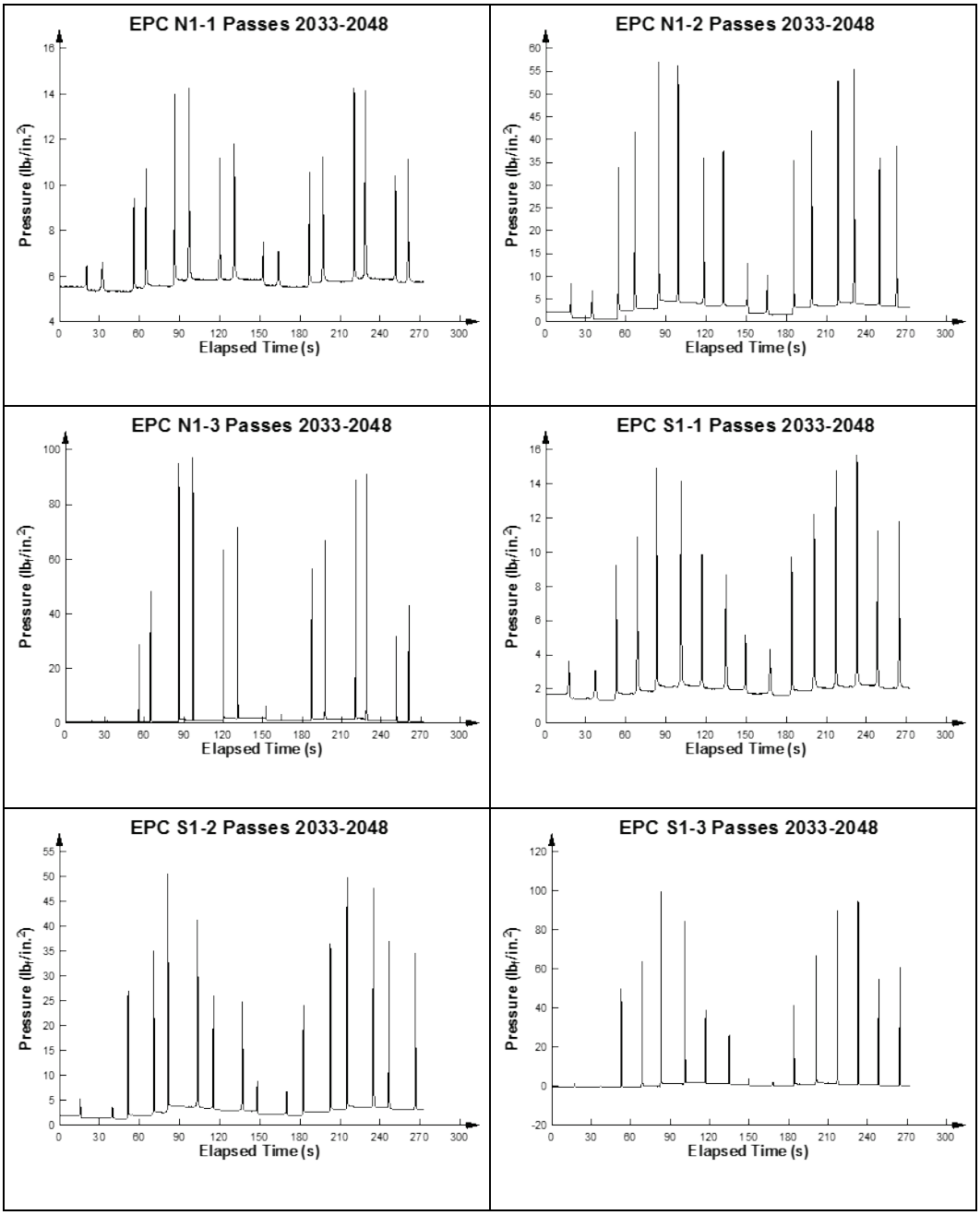
EPC N1-1 Passes 2033-2048
EPC N1-2 Passes 2033-2048
EPC N1-3 Passes 2033-2048
EPC S1-1 Passes 2033-2048
EPC S1-2 Passes 2033-2048
EPC S1-3 Passes 2033-2048
Pressure (lbf/in.2)
Elapsed Time (s)

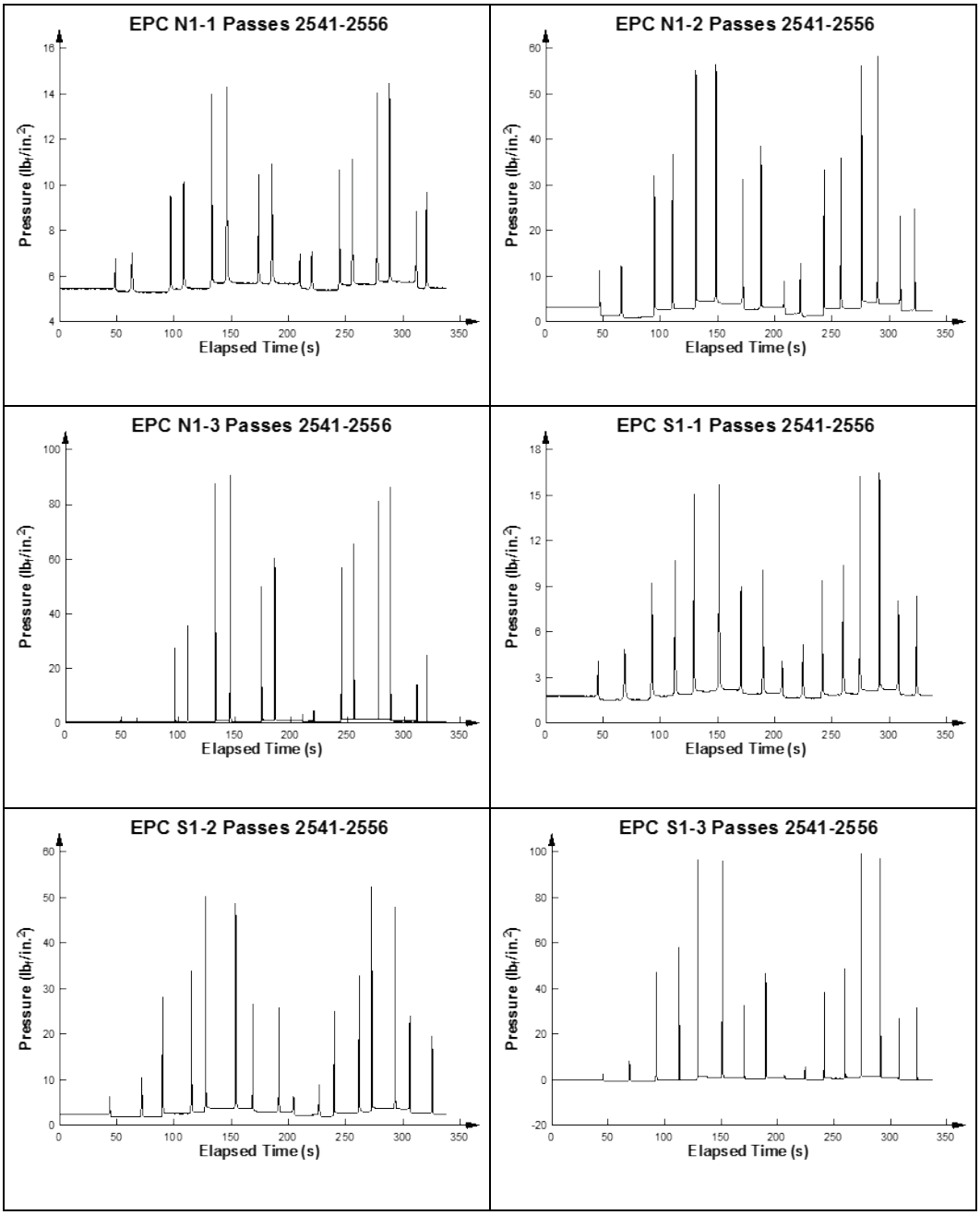
EPC N1-1 Passes 2541-2556
Pressure (lbf/in.2)
Elapsed Time (s)
EPC N1-2 Passes 2541-2556
Pressure (lbf/in.2)
Elapsed Time (s)
EPC N1-3 Passes 2541-2556
Pressure (lbf/in.2)
Elapsed Time (s)
EPC S1-1 Passes 2541-2556
Pressure (lbf/in.2)
Elapsed Time (s)
EPC S1-2 Passes 2541-2556
Pressure (lbf/in.2)
Elapsed Time (s)
EPC S1-3 Passes 2541-2556
Pressure (lbf/in.2)
Elapsed Time (s)

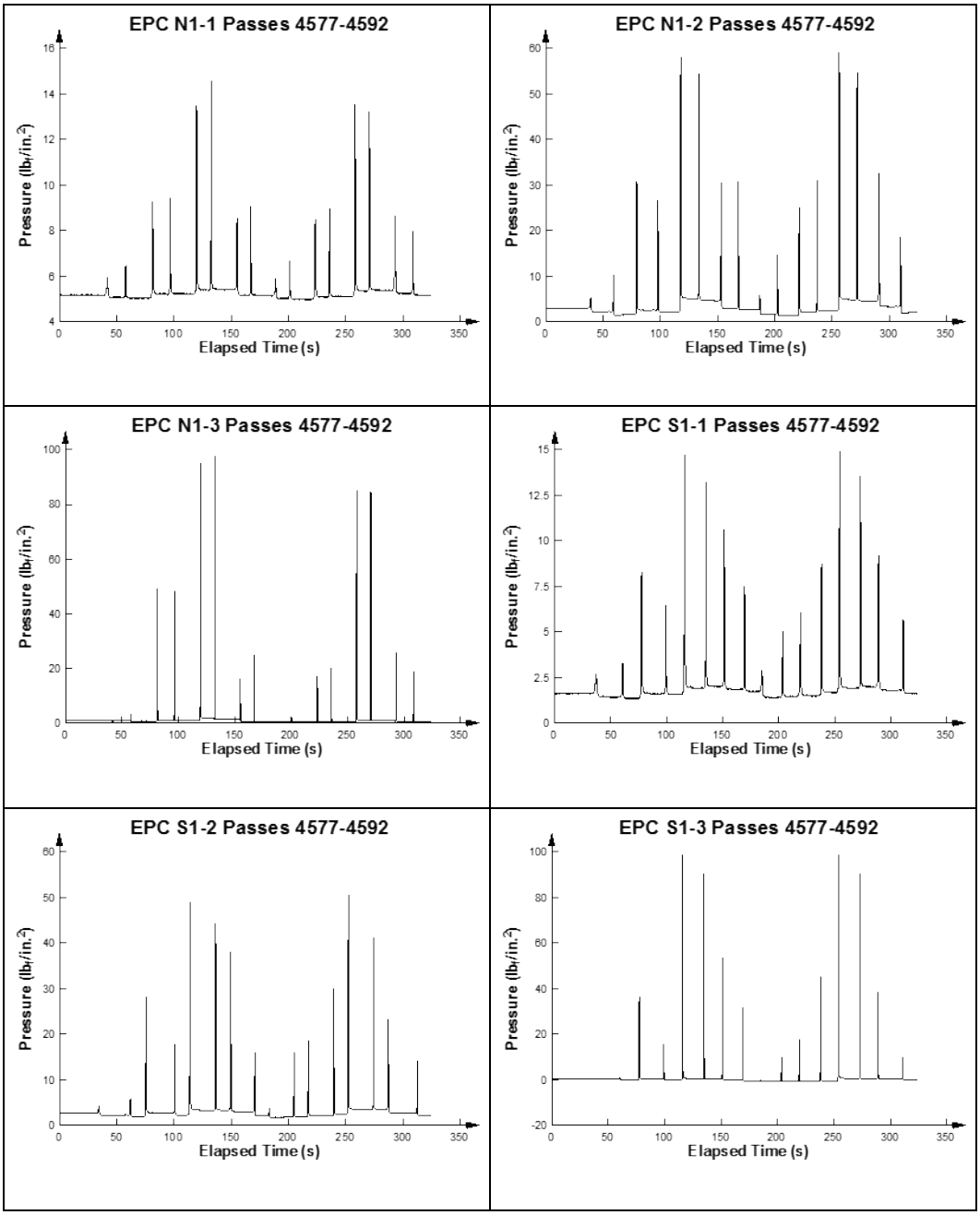
EPC N1-1 Passes 4577-4592
Pressure (lbf/in.2)
Elapsed Time (s)
EPC N1-2 Passes 4577-4592
Pressure (lbf/in.2)
Elapsed Time (s)
EPC N1-3 Passes 4577-4592
Pressure (lbf/in.2)
Elapsed Time (s)
EPC S1-1 Passes 4577-4592
Pressure (lbf/in.2)
Elapsed Time (s)
EPC S1-2 Passes 4577-4592
Pressure (lbf/in.2)
Elapsed Time (s)
EPC S1-3 Passes 4577-4592
Pressure (lbf/in.2)
Elapsed Time (s)

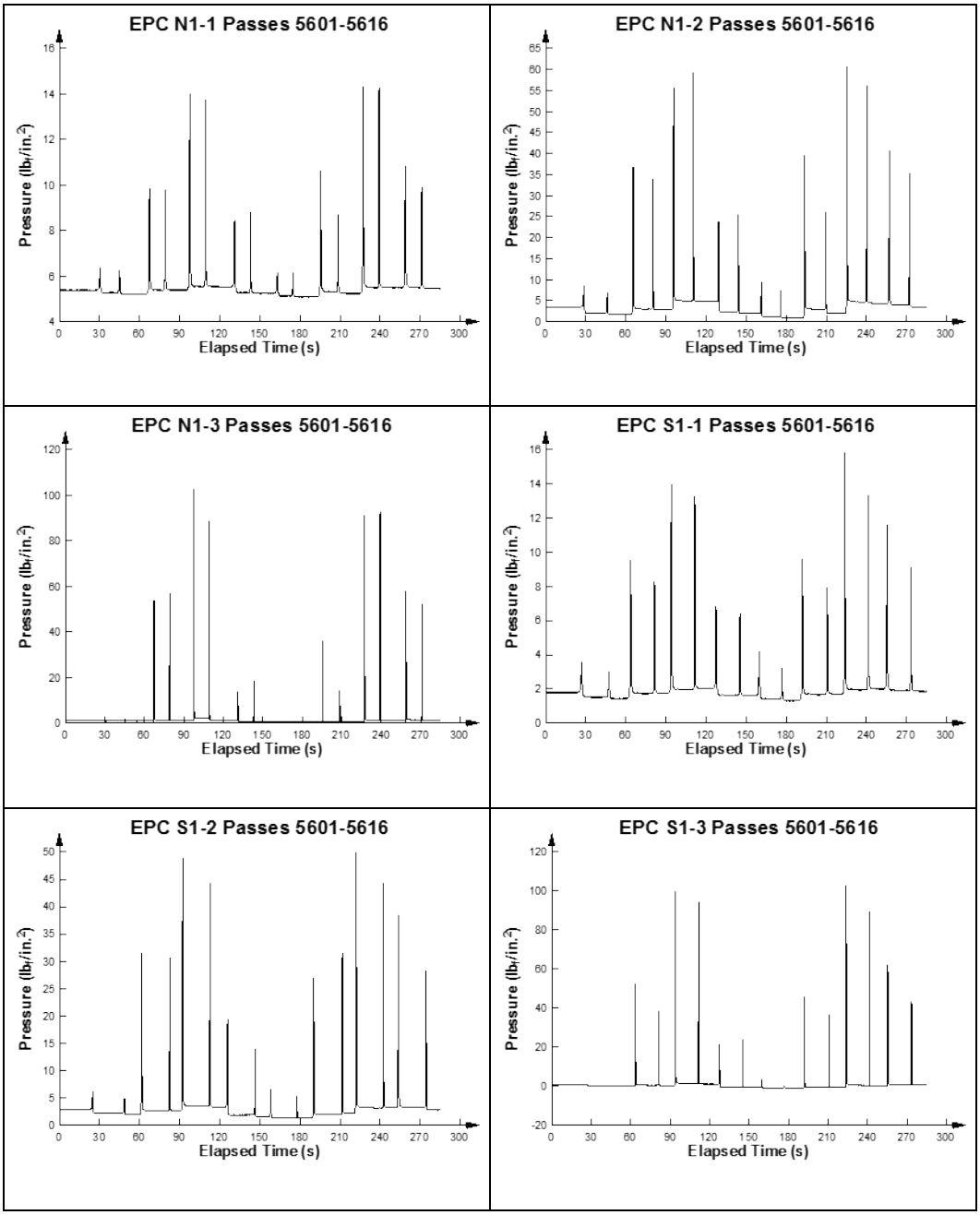
EPC N1-1 Passes 5601-5616
Pressure (lbf/in.2)
Elapsed Time (s)
EPC N1-2 Passes 5601-5616
Pressure (lbf/in.2)
Elapsed Time (s)
EPC N1-3 Passes 5601-5616
Pressure (lbf/in.2)
Elapsed Time (s)
EPC S1-1 Passes 5601-5616
Pressure (lbf/in.2)
Elapsed Time (s)
EPC S1-2 Passes 5601-5616
Pressure (lbf/in.2)
Elapsed Time (s)
EPC S1-3 Passes 5601-5616
Pressure (lbf/in.2)
Elapsed Time (s)

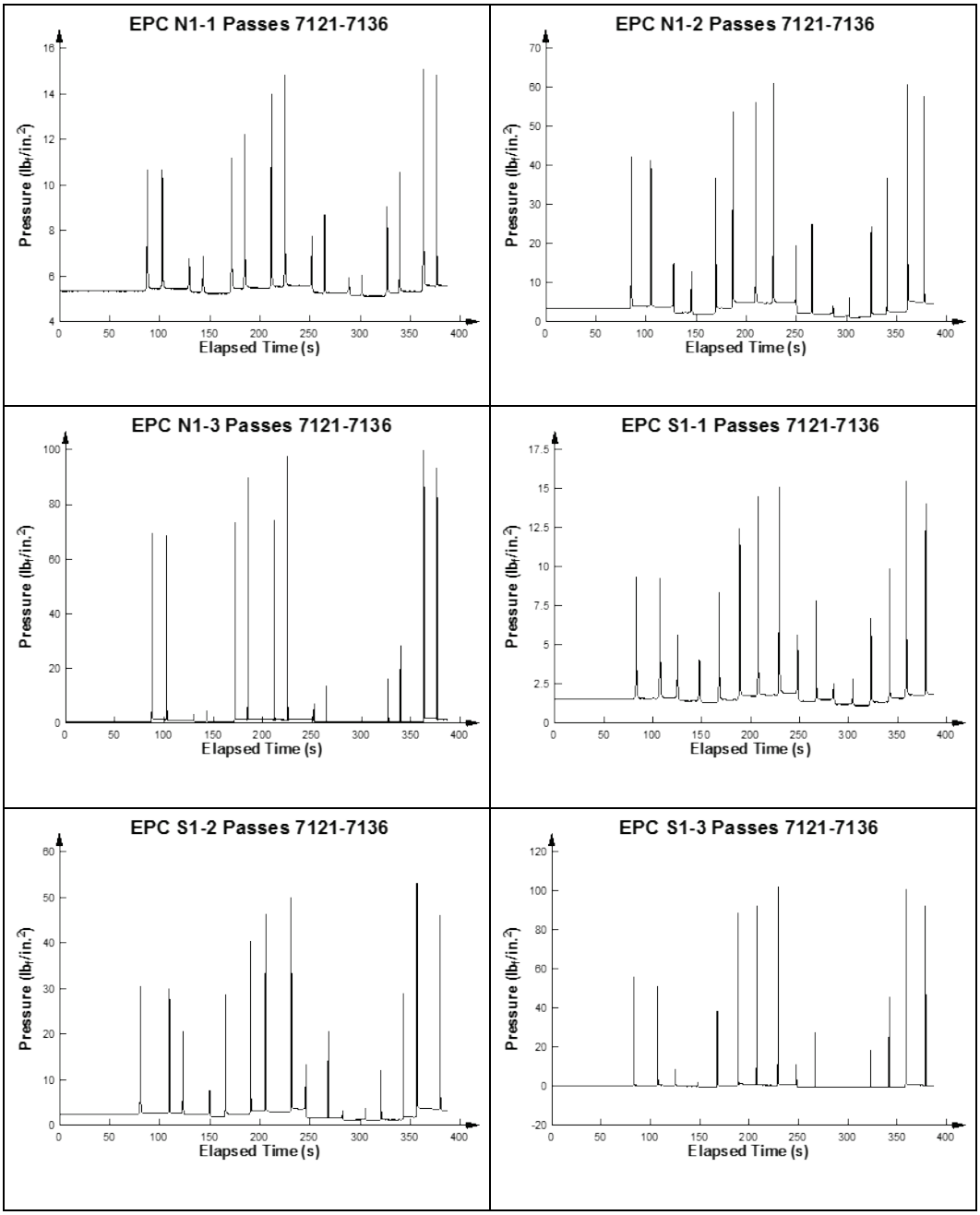
EPC N1-1 Passes 7121-7136
Pressure (lbf/in.2)
Elapsed Time (s)
EPC N1-2 Passes 7121-7136
Pressure (lbf/in.2)
Elapsed Time (s)
EPC N1-3 Passes 7121-7136
Pressure (lbf/in.2)
Elapsed Time (s)
EPC S1-1 Passes 7121-7136
Pressure (lbf/in.2)
Elapsed Time (s)
EPC S1-2 Passes 7121-7136
Pressure (lbf/in.2)
Elapsed Time (s)
EPC S1-3 Passes 7121-7136
Pressure (lbf/in.2)
Elapsed Time (s)

Appendix B: Earth Pressure Cell Data for the C-17 Test Item

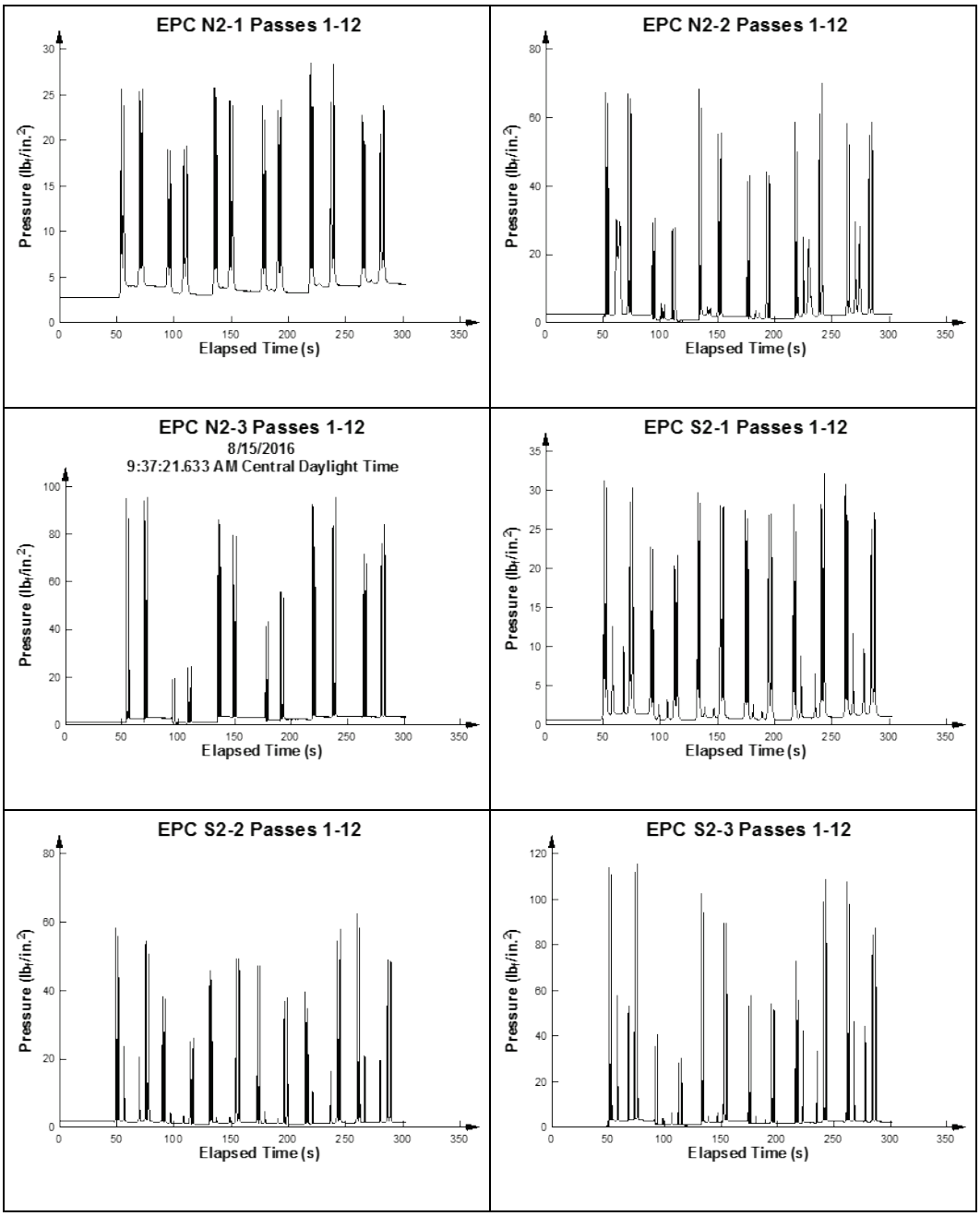

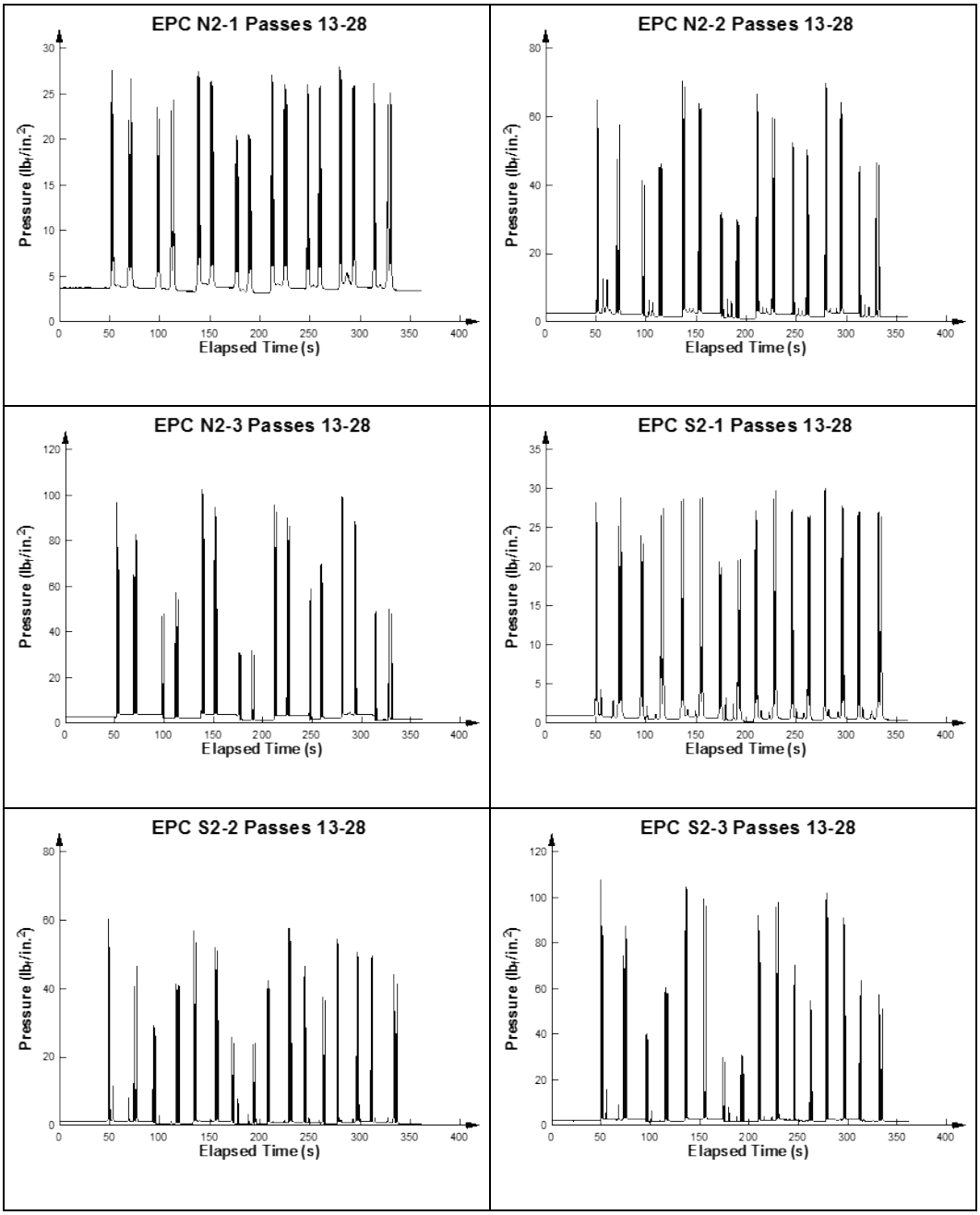
EPC N2-1 Passes 13-28
EPC N2-2 Passes 13-28
EPC N2-3 Passes 13-28
EPC S2-1 Passes 13-28
EPC S2-2 Passes 13-28
EPC S2-3 Passes 13-28
Pressure (lbf/in.2)
Elapsed Time (s)

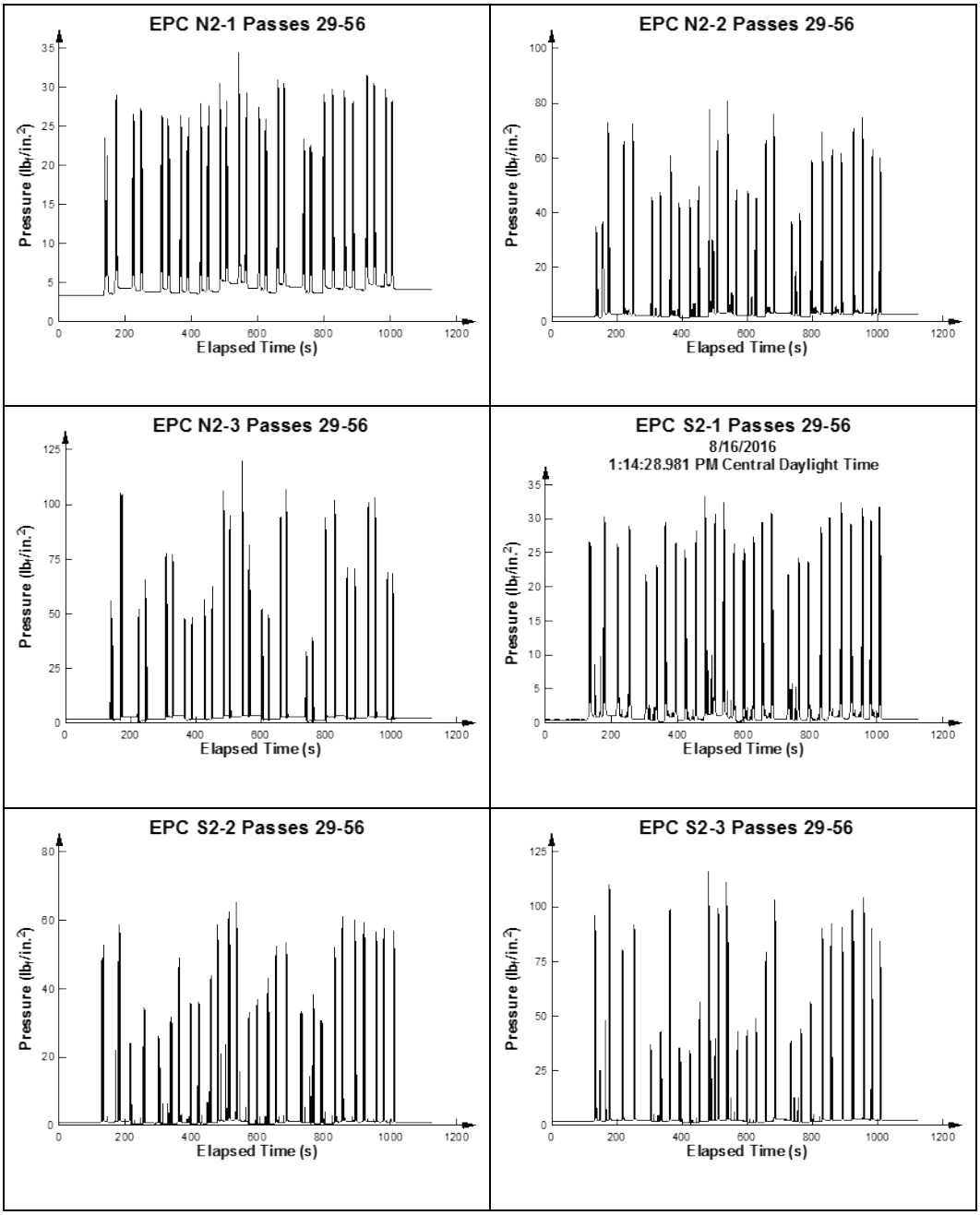
EPC N2-1 Passes 29-56
Pressure (lbf/in.2)
Elapsed Time (s)
EPC N2-2 Passes 29-56
Pressure (lbf/in.2)
Elapsed Time (s)
EPC N2-3 Passes 29-56
Pressure (lbf/in.2)
Elapsed Time (s)
EPC S2-1 Passes 29-56
8/16/2016
1:14:28.981 PM Central Daylight Time
Pressure (lbf/in.2)
Elapsed Time (s)
EPC S2-2 Passes 29-56
Pressure (lbf/in.2)
Elapsed Time (s)
EPC S2-3 Passes 29-56
Pressure (lbf/in.2)
Elapsed Time (s)

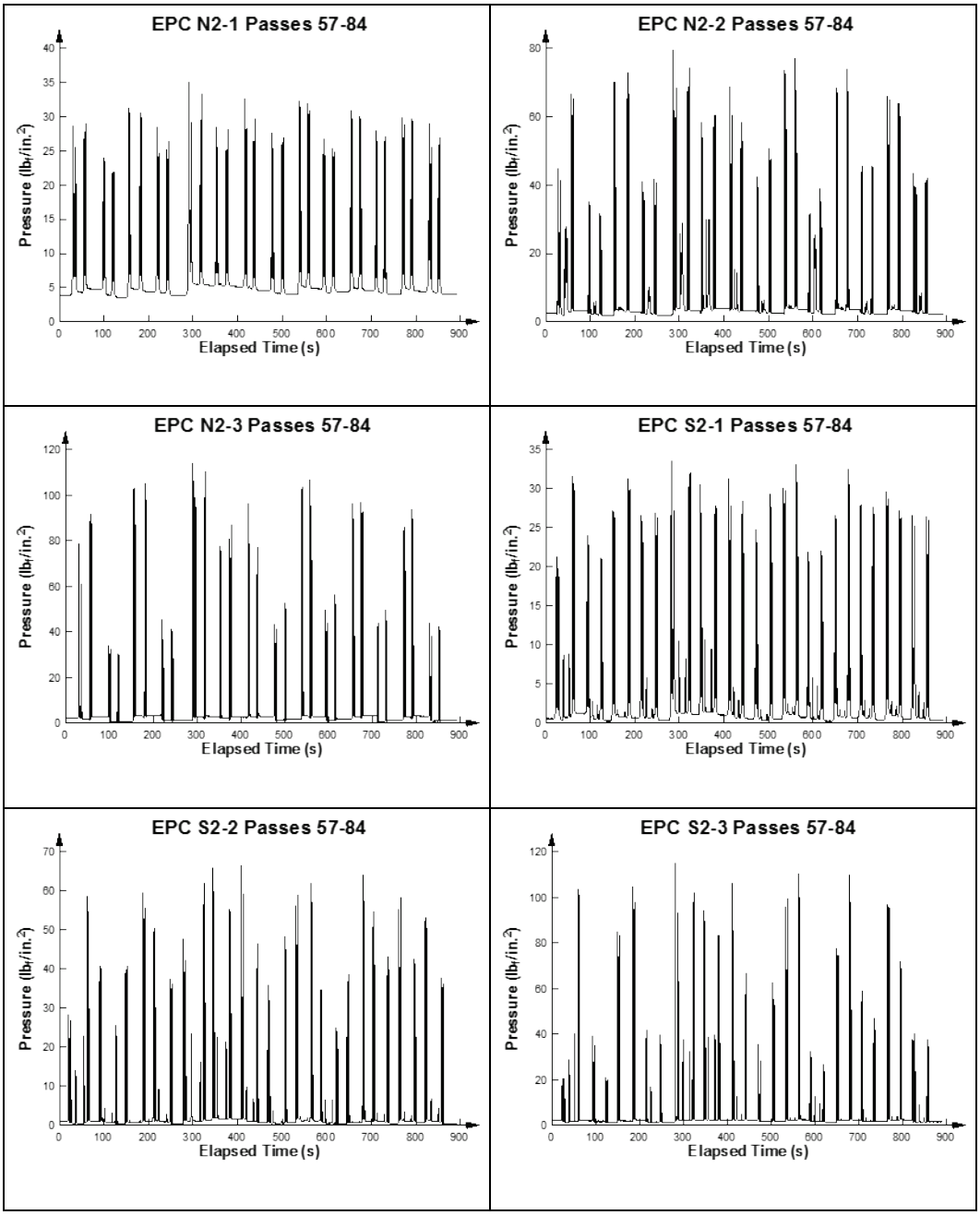
EPC N2-1 Passes 57-84
Pressure (lbf/in.2)
Elapsed Time (s)
EPC N2-2 Passes 57-84
Pressure (lbf/in.2)
Elapsed Time (s)
EPC N2-3 Passes 57-84
Pressure (lbf/in.2)
Elapsed Time (s)
EPC S2-1 Passes 57-84
Pressure (lbf/in.2)
Elapsed Time (s)
EPC S2-2 Passes 57-84
Pressure (lbf/in.2)
Elapsed Time (s)
EPC S2-3 Passes 57-84
Pressure (lbf/in.2)
Elapsed Time (s)

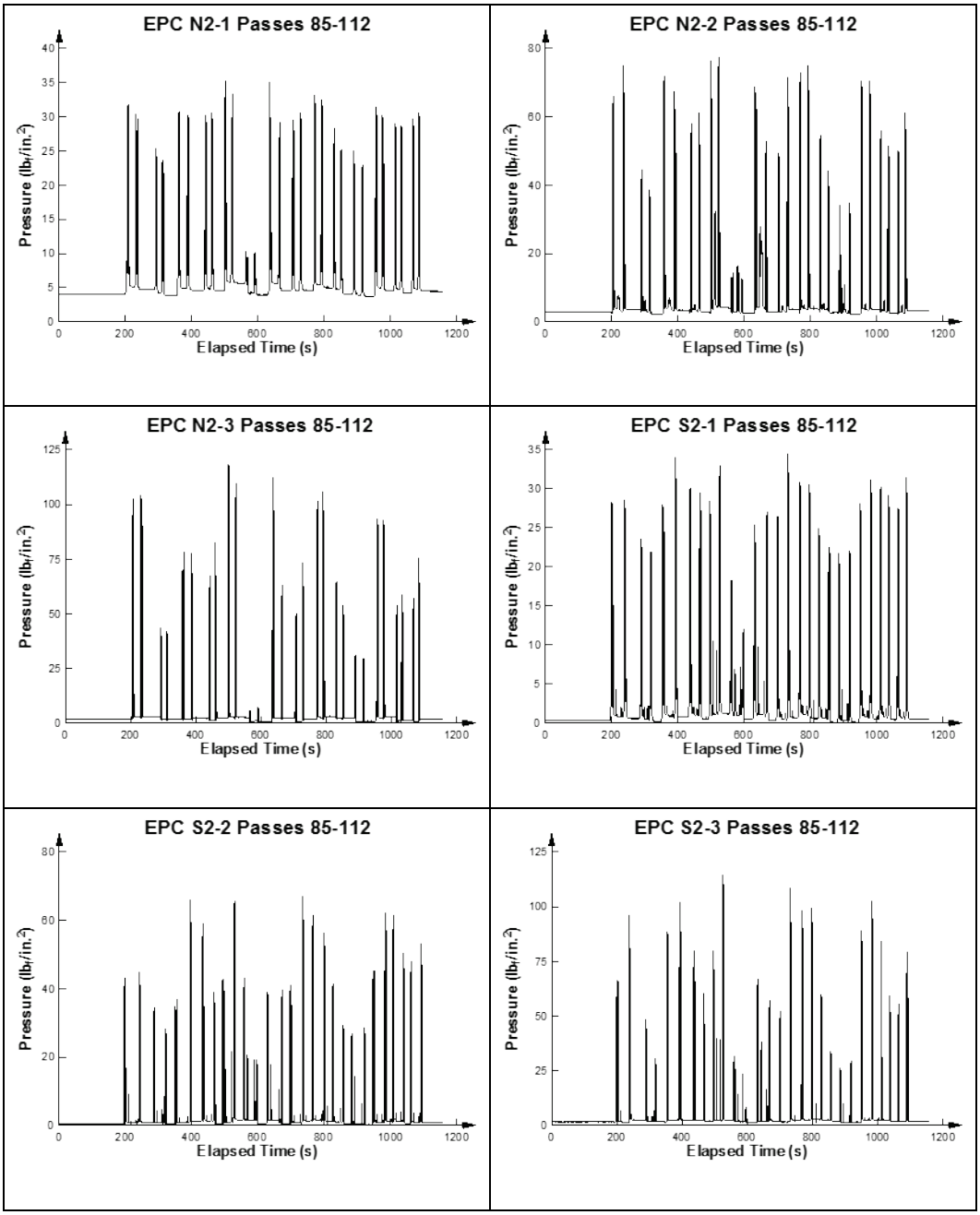
EPC N2-1 Passes 85-112
Pressure (lbf/in.2)
Elapsed Time (s)
EPC N2-2 Passes 85-112
Pressure (lbf/in.2)
Elapsed Time (s)
EPC N2-3 Passes 85-112
Pressure (lbf/in.2)
Elapsed Time (s)
EPC S2-1 Passes 85-112
Pressure (lbf/in.2)
Elapsed Time (s)
EPC S2-2 Passes 85-112
Pressure (lbf/in.2)
Elapsed Time (s)
EPC S2-3 Passes 85-112
Pressure (lbf/in.2)
Elapsed Time (s)

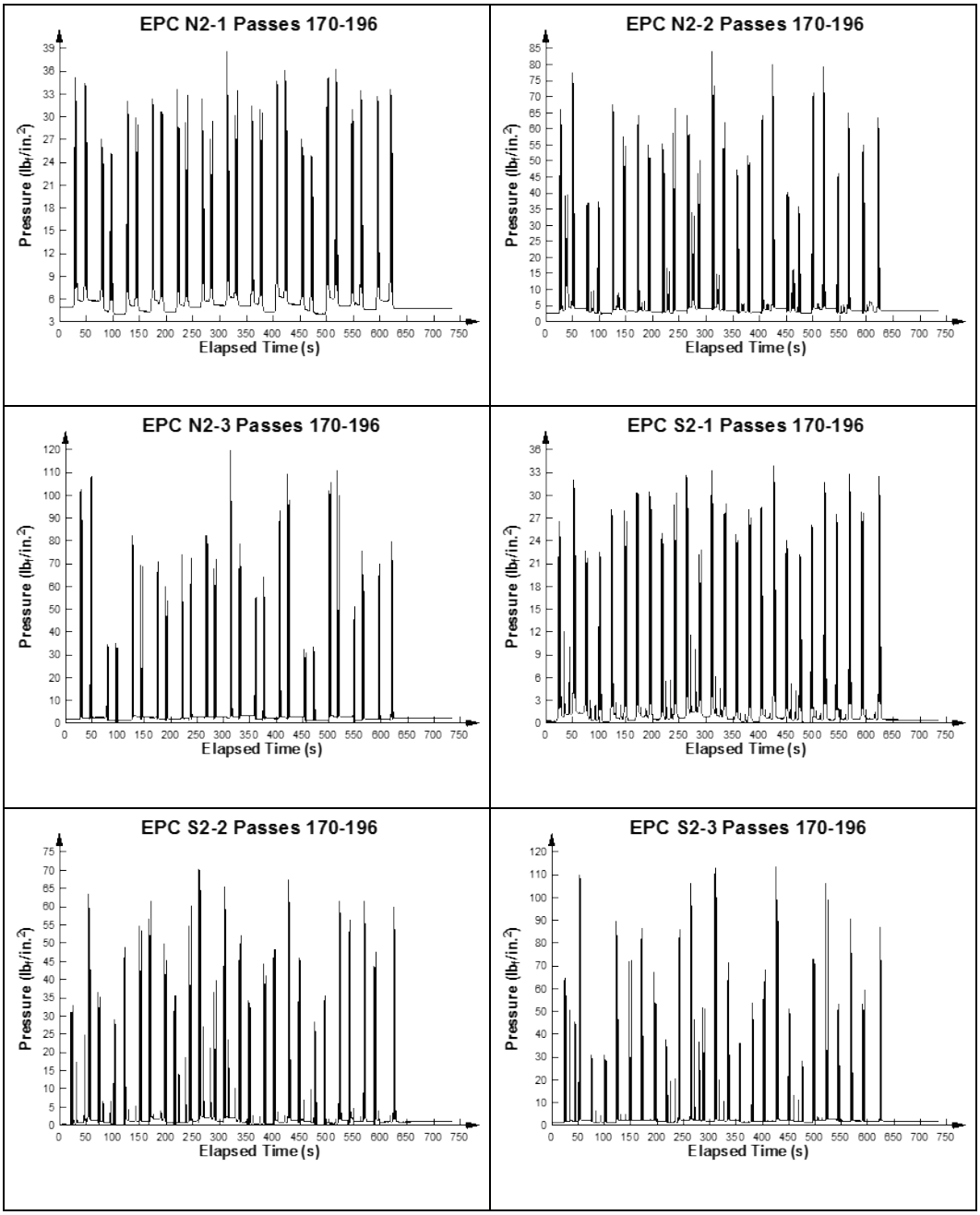
EPC N2-1 Passes 170-196
Pressure (lbf/in.2)
Elapsed Time (s)
EPC N2-2 Passes 170-196
Pressure (lbf/in.2)
Elapsed Time (s)
EPC N2-3 Passes 170-196
Pressure (lbf/in.2)
Elapsed Time (s)
EPC S2-1 Passes 170-196
Pressure (lbf/in.2)
Elapsed Time (s)
EPC S2-2 Passes 170-196
Pressure (lbf/in.2)
Elapsed Time (s)
EPC S2-3 Passes 170-196
Pressure (lbf/in.2)
Elapsed Time (s)

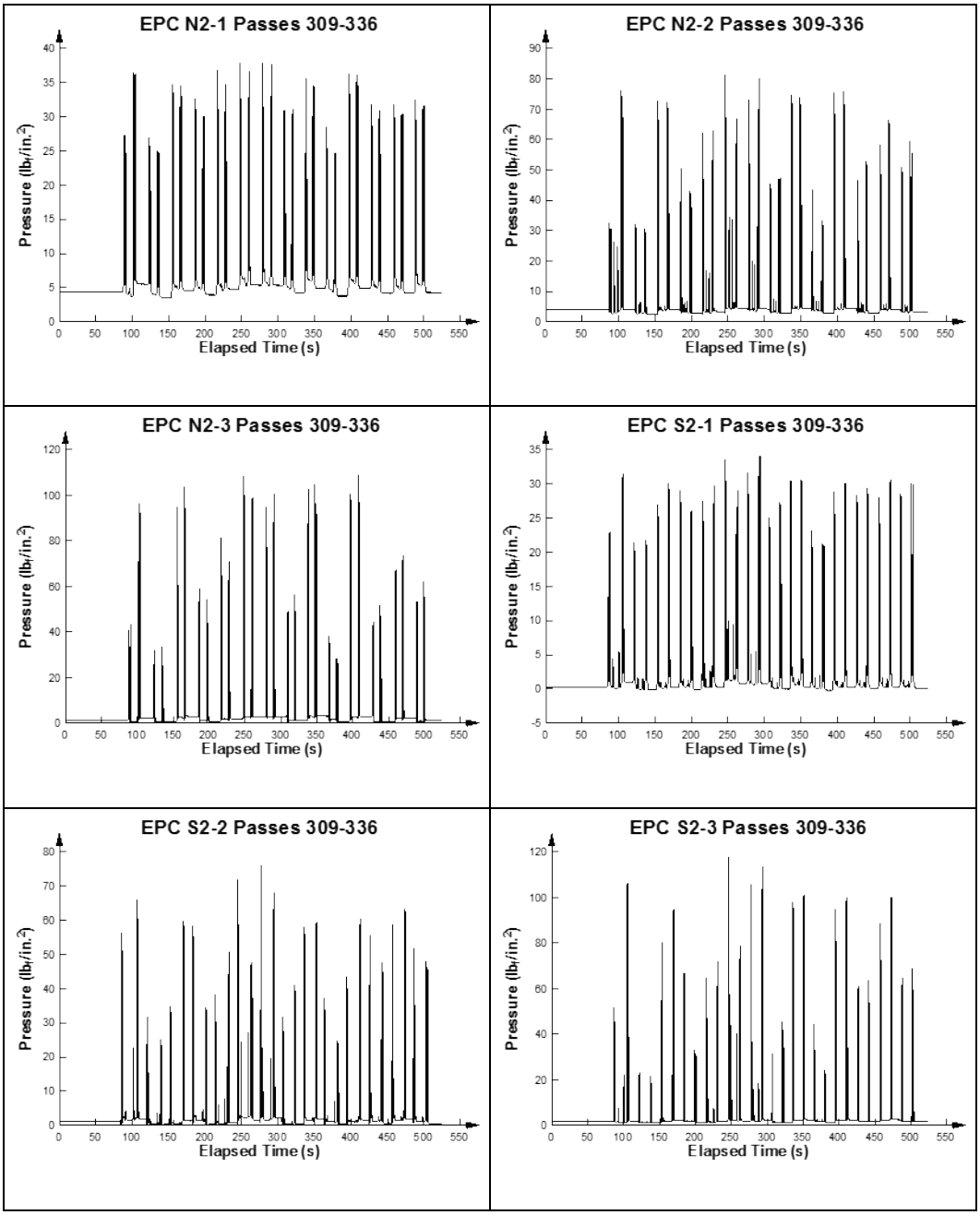
EPC N2-1 Passes 309-336
Pressure (lbf/in.2)
Elapsed Time (s)
EPC N2-2 Passes 309-336
Pressure (lbf/in.2)
Elapsed Time (s)
EPC N2-3 Passes 309-336
Pressure (lbf/in.2)
Elapsed Time (s)
EPC S2-1 Passes 309-336
Pressure (lbf/in.2)
Elapsed Time (s)
EPC S2-2 Passes 309-336
Pressure (lbf/in.2)
Elapsed Time (s)
EPC S2-3 Passes 309-336
Pressure (lbf/in.2)
Elapsed Time (s)

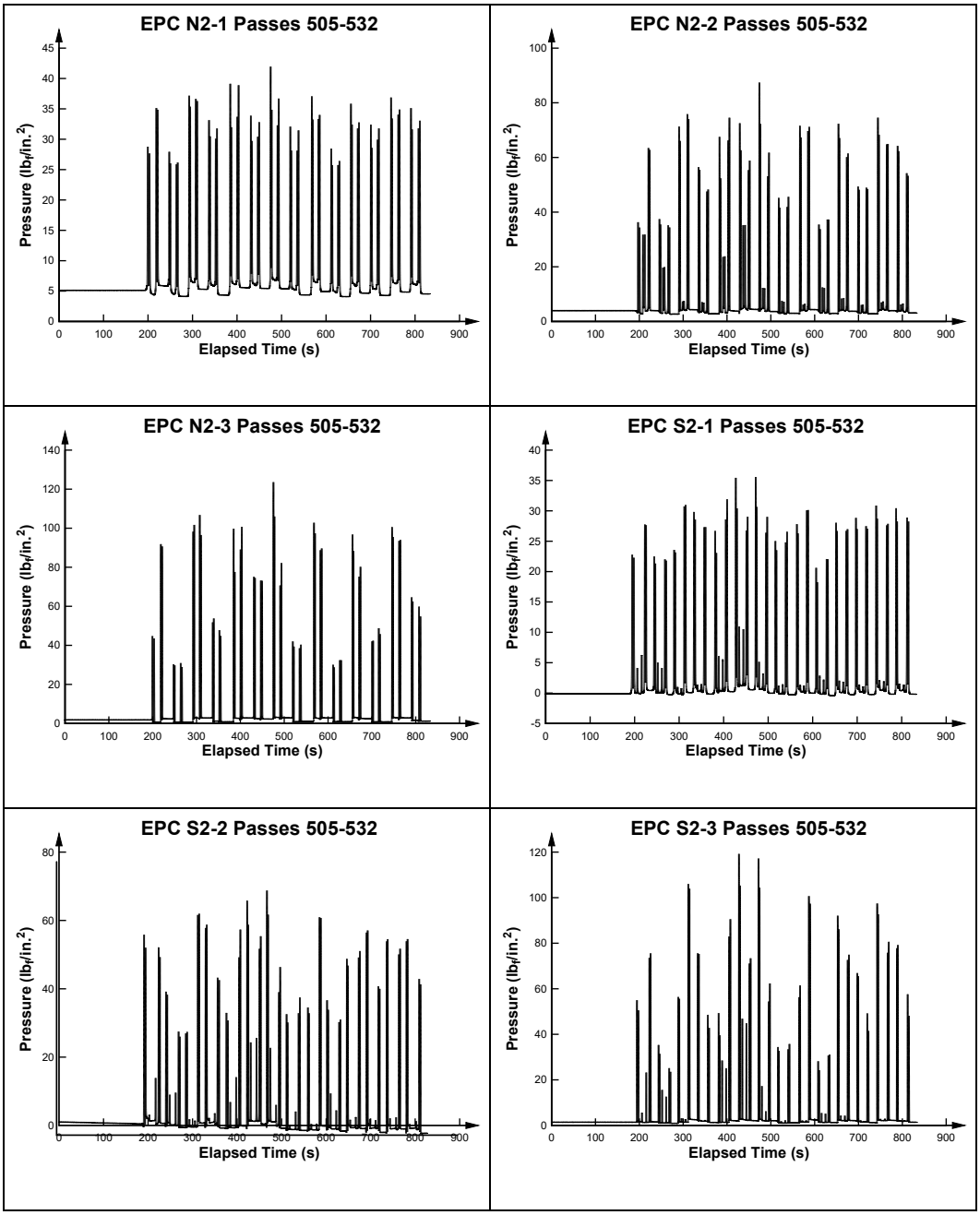
EPC N2-1 Passes 505-532
Pressure (lbf/in.2)
Elapsed Time (s)
EPC N2-2 Passes 505-532
Pressure (lbf/in.2)
Elapsed Time (s)
EPC N2-3 Passes 505-532
Pressure (lbf/in.2)
Elapsed Time (s)
EPC S2-1 Passes 505-532
Pressure (lbf/in.2)
Elapsed Time (s)
EPC S2-2 Passes 505-532
Pressure (lbf/in.2)
Elapsed Time (s)
EPC S2-3 Passes 505-532
Pressure (lbf/in.2)
Elapsed Time (s)

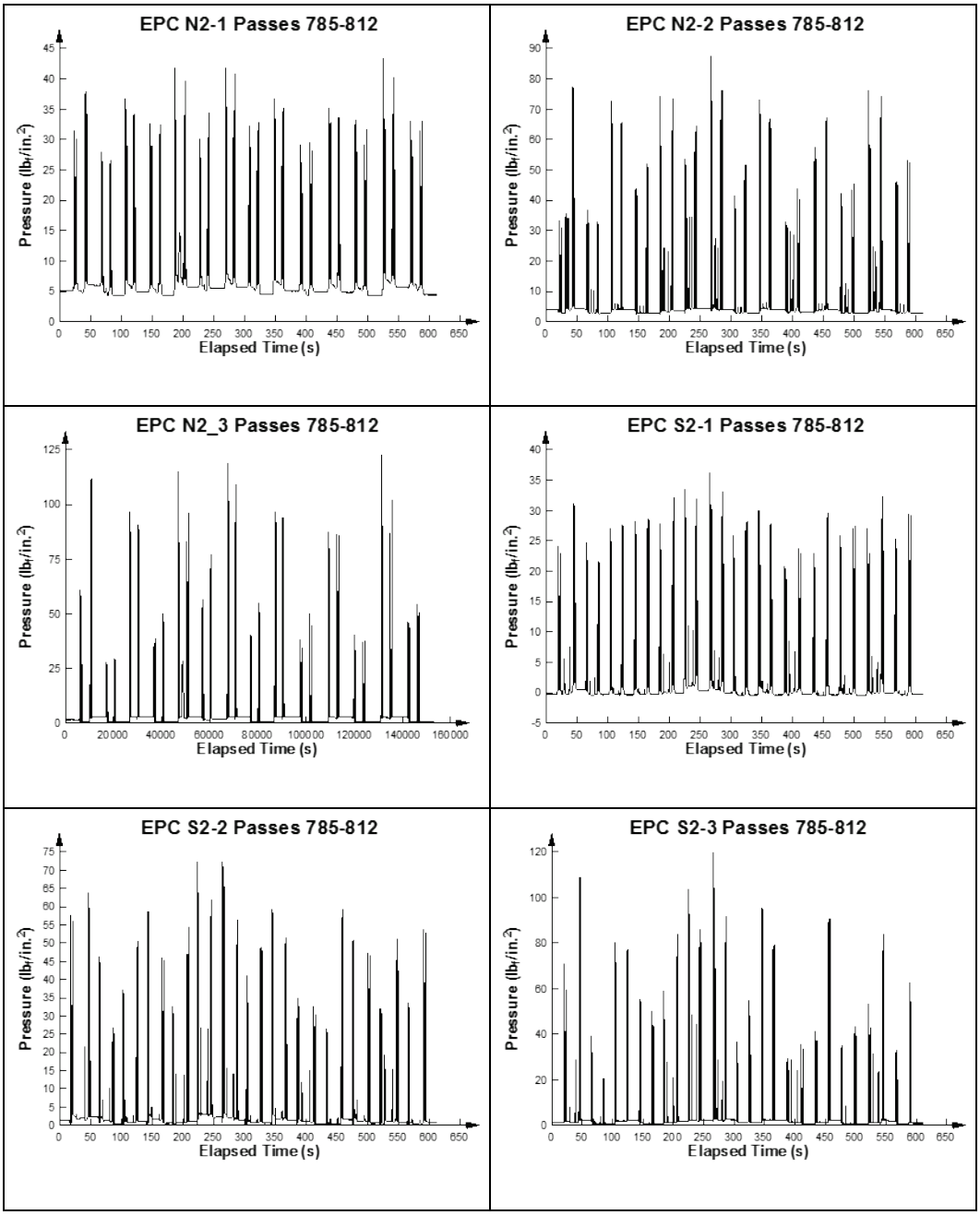
EPC N2-1 Passes 785-812
Pressure (lbf/in.2)
Elapsed Time (s)
EPC N2-2 Passes 785-812
Pressure (lbf/in.2)
Elapsed Time (s)
EPC N2_3 Passes 785-812
Pressure (lbf/in.2)
Elapsed Time (s)
EPC S2-1 Passes 785-812
Pressure (lbf/in.2)
Elapsed Time (s)
EPC S2-2 Passes 785-812
Pressure (lbf/in.2)
Elapsed Time (s)
EPC S2-3 Passes 785-812
Pressure (lbf/in.2)
Elapsed Time (s)

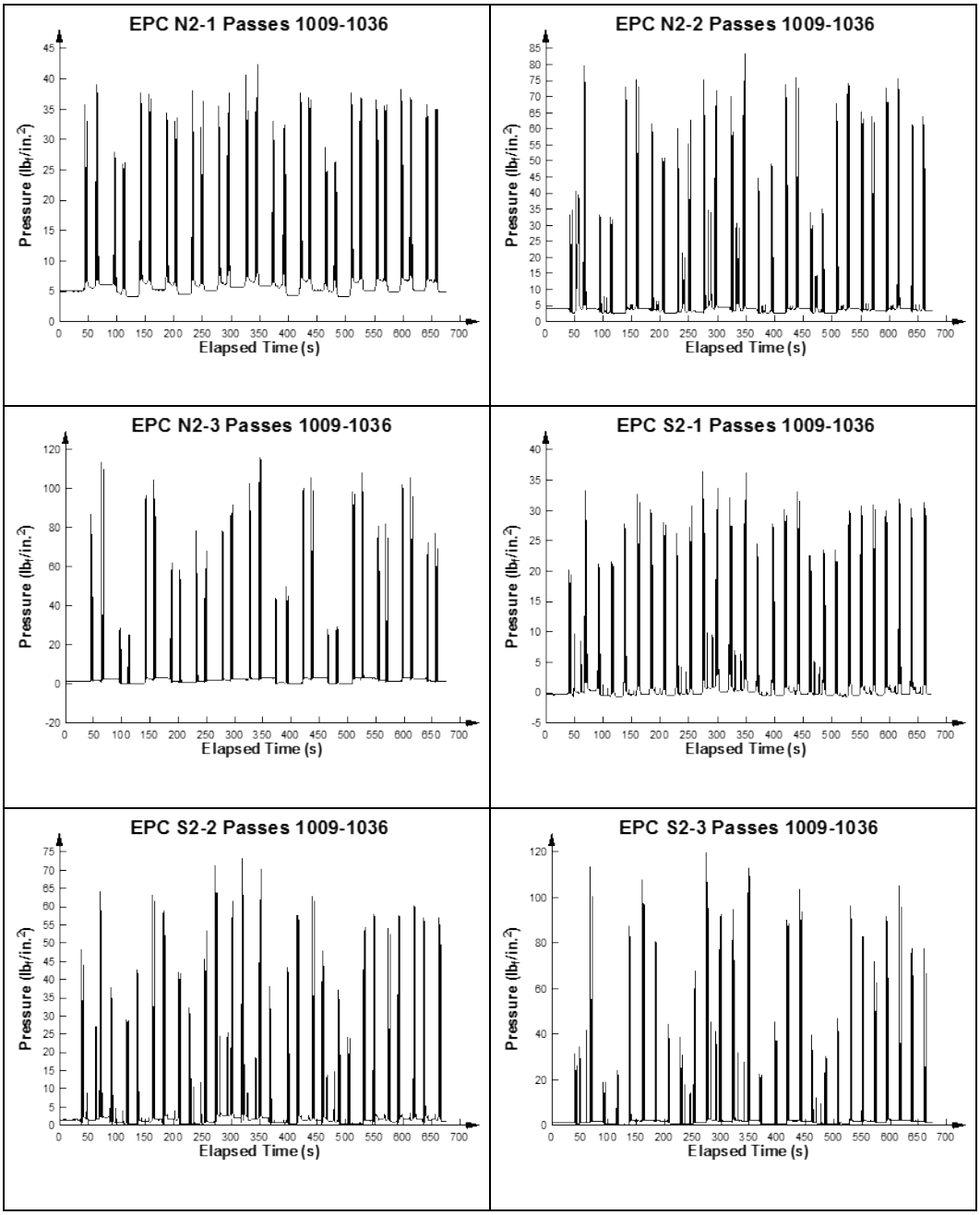
EPC N2-1 Passes 1009-1036
Pressure (lbf/in.2)
Elapsed Time (s)
EPC N2-2 Passes 1009-1036
Pressure (lbf/in.2)
Elapsed Time (s)
EPC N2-3 Passes 1009-1036
Pressure (lbf/in.2)
Elapsed Time (s)
EPC S2-1 Passes 1009-1036
Pressure (lbf/in.2)
Elapsed Time (s)
EPC S2-2 Passes 1009-1036
Pressure (lbf/in.2)
Elapsed Time (s)
EPC S2-3 Passes 1009-1036
Pressure (lbf/in.2)
Elapsed Time (s)

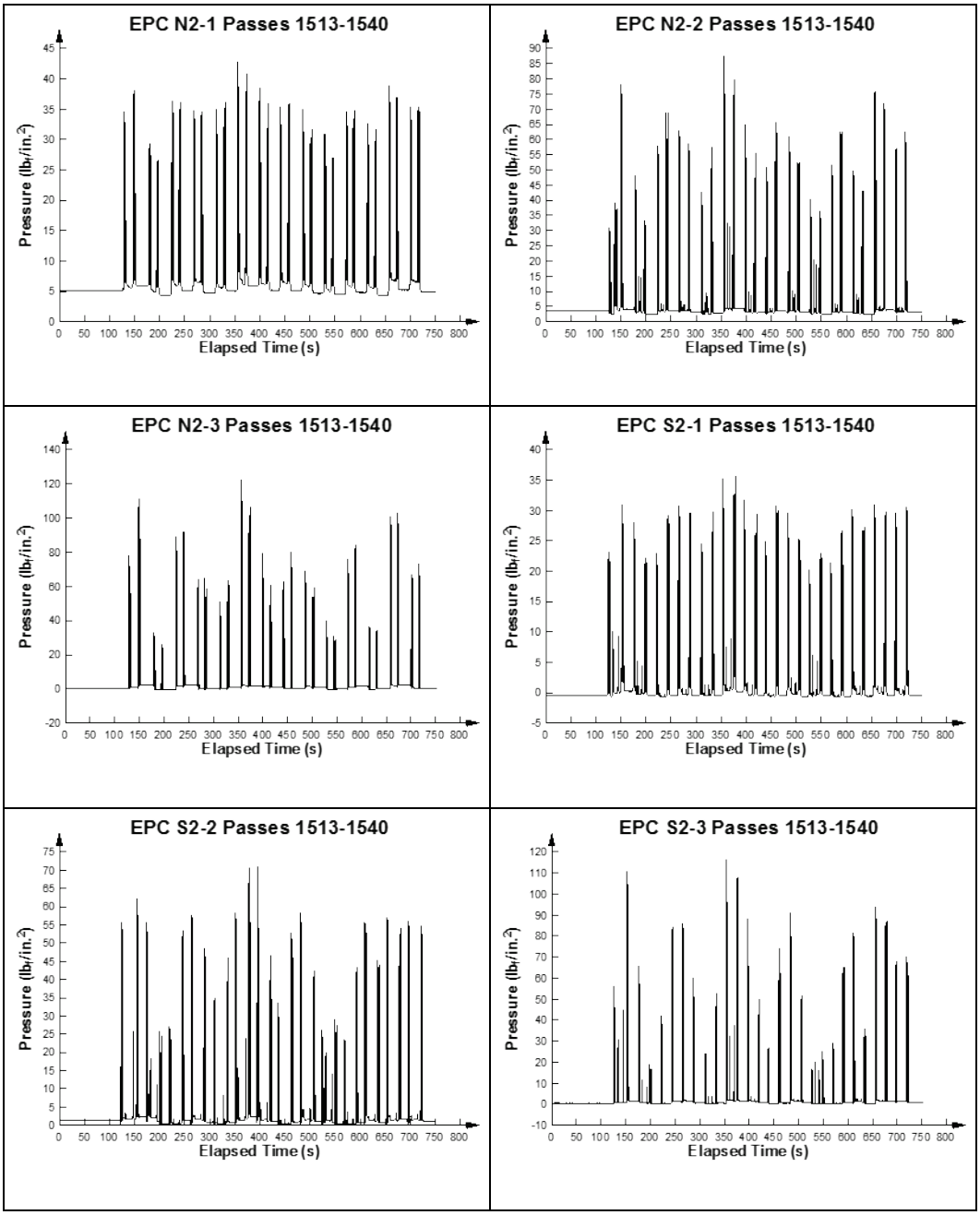
EPC N2-1 Passes 1513-1540
Pressure (lbf/in.2)
Elapsed Time (s)
EPC N2-2 Passes 1513-1540
Pressure (lbf/in.2)
Elapsed Time (s)
EPC N2-3 Passes 1513-1540
Pressure (lbf/in.2)
Elapsed Time (s)
EPC S2-1 Passes 1513-1540
Pressure (lbf/in.2)
Elapsed Time (s)
EPC S2-2 Passes 1513-1540
Pressure (lbf/in.2)
Elapsed Time (s)
EPC S2-3 Passes 1513-1540
Pressure (lbf/in.2)
Elapsed Time (s)

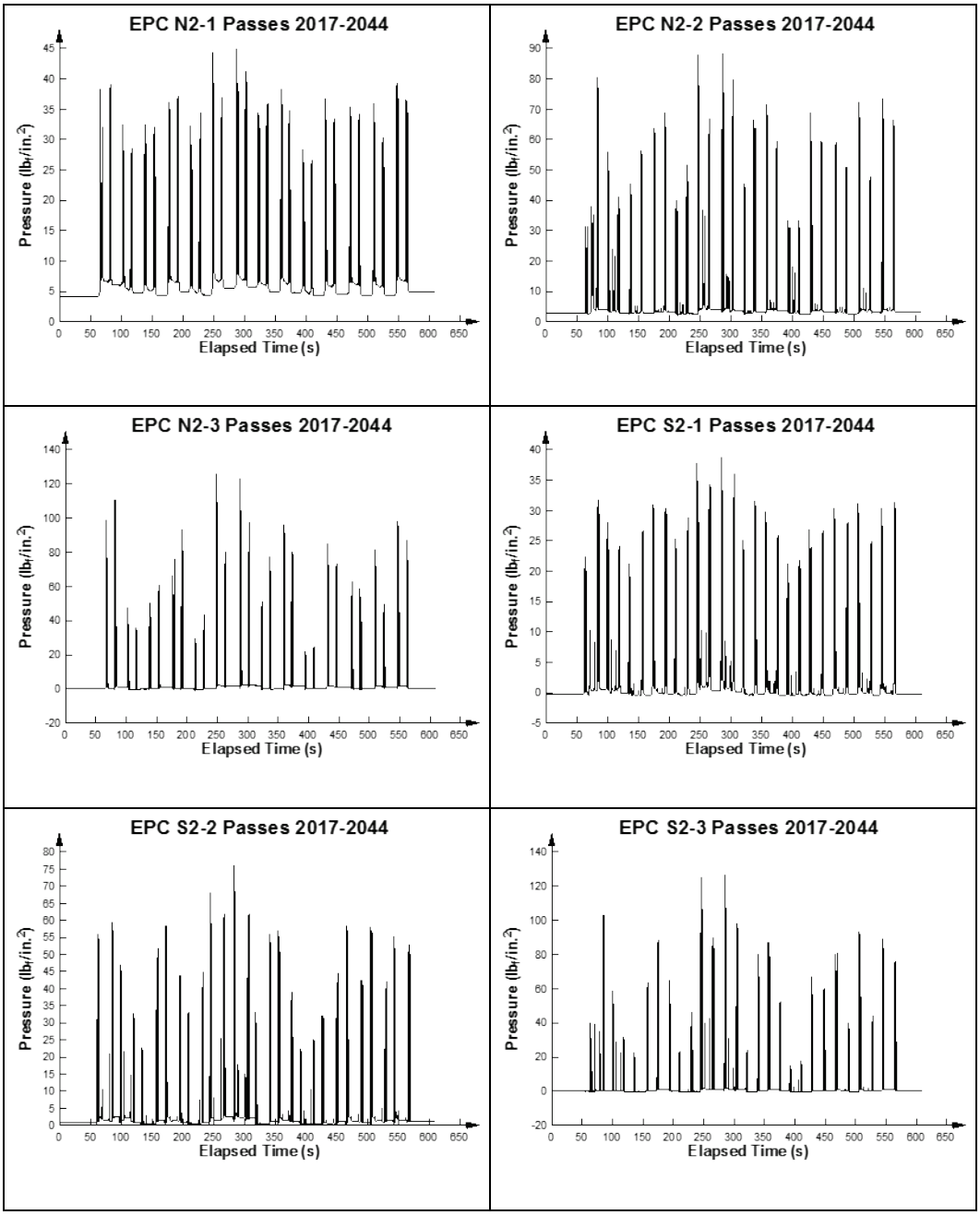
EPC N2-1 Passes 2017-2044
Pressure (lbf/in.2)
Elapsed Time (s)
EPC N2-2 Passes 2017-2044
Pressure (lbf/in.2)
Elapsed Time (s)
EPC N2-3 Passes 2017-2044
Pressure (lbf/in.2)
Elapsed Time (s)
EPC S2-1 Passes 2017-2044
Pressure (lbf/in.2)
Elapsed Time (s)
EPC S2-2 Passes 2017-2044
Pressure (lbf/in.2)
Elapsed Time (s)
EPC S2-3 Passes 2017-2044
Pressure (lbf/in.2)
Elapsed Time (s)

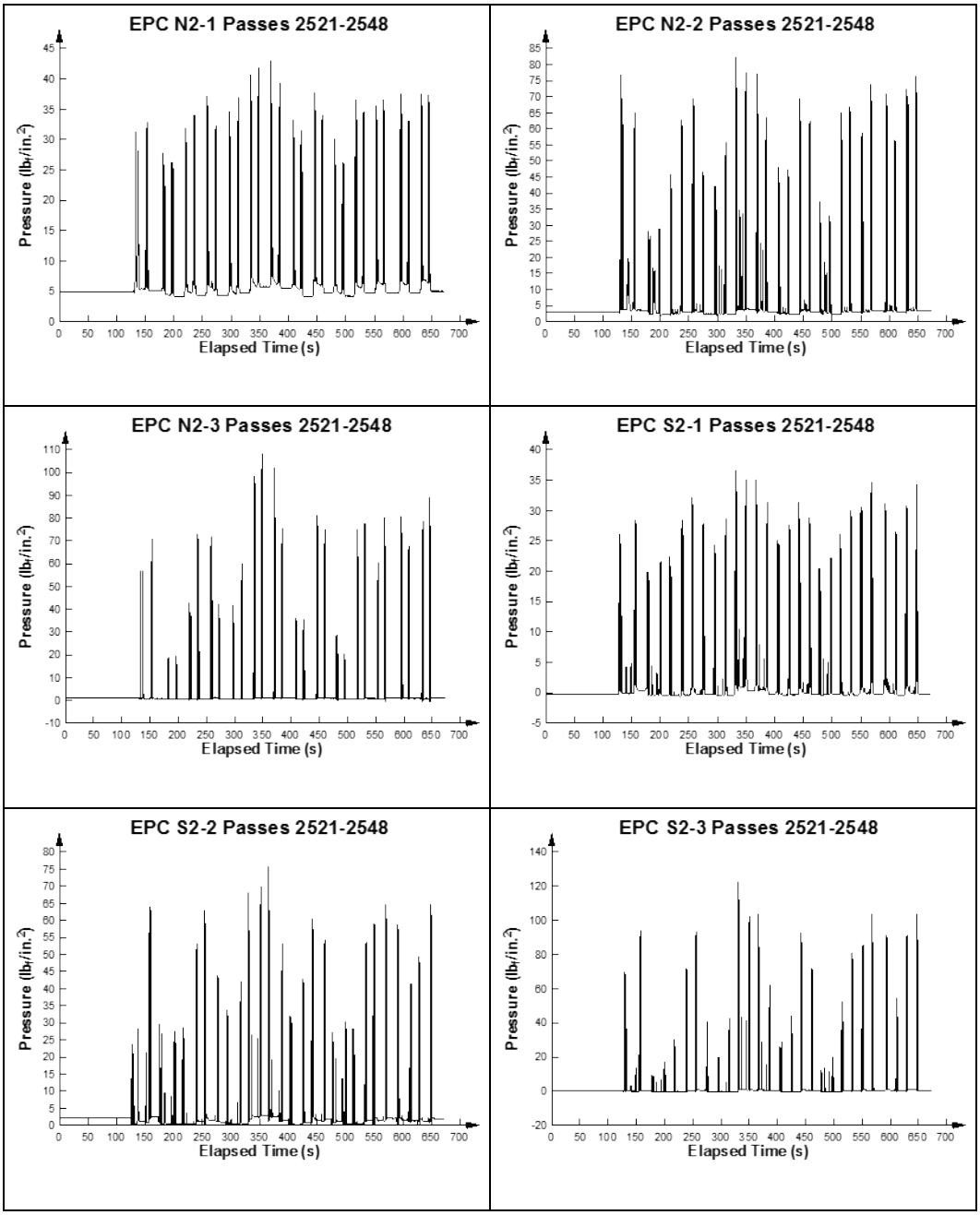
EPC N2-1 Passes 2521-2548
Pressure (lbf/in.2)
Elapsed Time (s)
EPC N2-2 Passes 2521-2548
Pressure (lbf/in.2)
Elapsed Time (s)
EPC N2-3 Passes 2521-2548
Pressure (lbf/in.2)
Elapsed Time (s)
EPC S2-1 Passes 2521-2548
Pressure (lbf/in.2)
Elapsed Time (s)
EPC S2-2 Passes 2521-2548
Pressure (lbf/in.2)
Elapsed Time (s)
EPC S2-3 Passes 2521-2548
Pressure (lbf/in.2)
Elapsed Time (s)

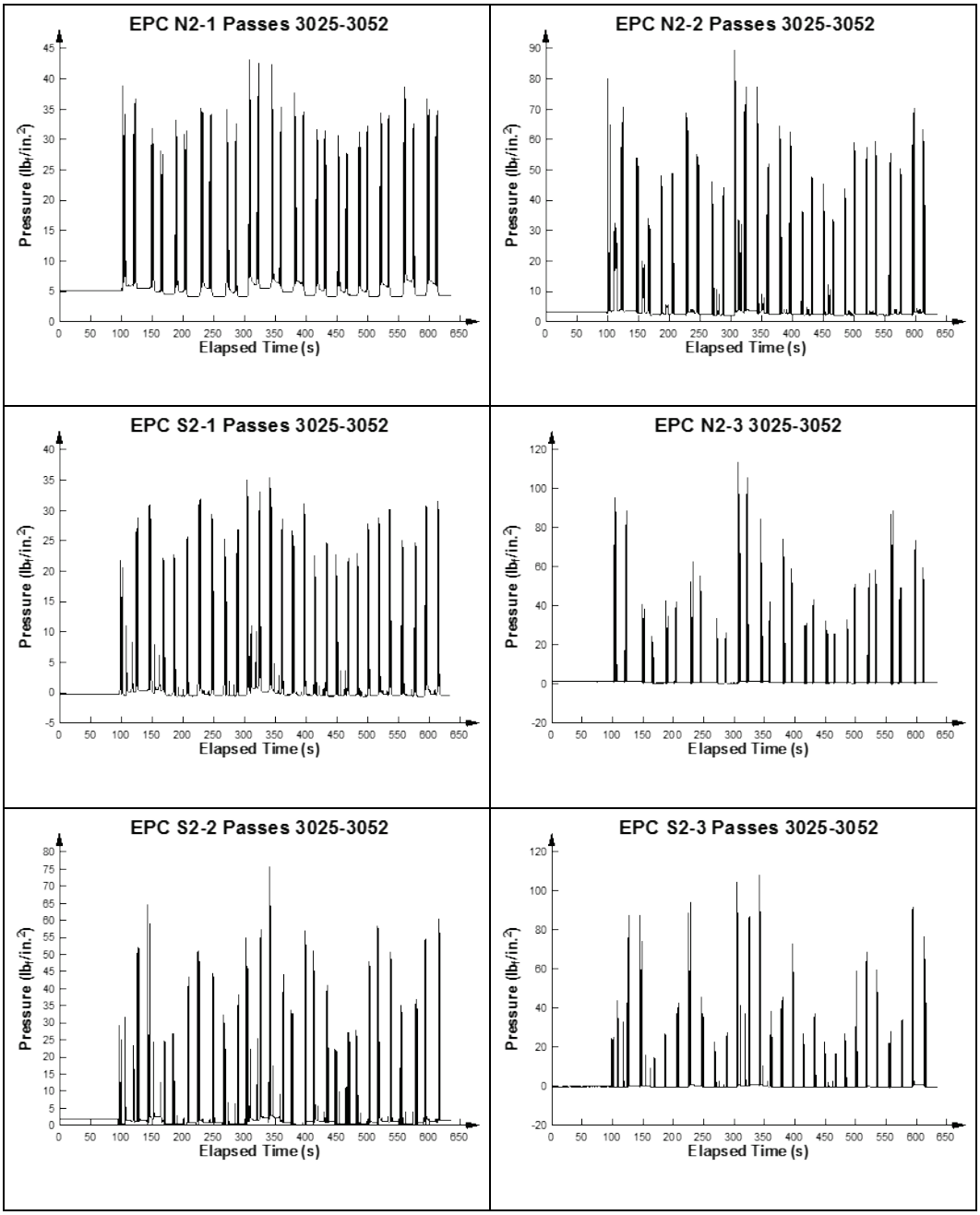
EPC N2-1 Passes 3025-3052
Pressure (lbf/in.2)
Elapsed Time (s)
EPC N2-2 Passes 3025-3052
Pressure (lbf/in.2)
Elapsed Time (s)
EPC S2-1 Passes 3025-3052
Pressure (lbf/in.2)
Elapsed Time (s)
EPC N2-3 3025-3052
Pressure (lbf/in.2)
Elapsed Time (s)
EPC S2-2 Passes 3025-3052
Pressure (lbf/in.2)
Elapsed Time (s)
EPC S2-3 Passes 3025-3052
Pressure (lbf/in.2)
Elapsed Time (s)

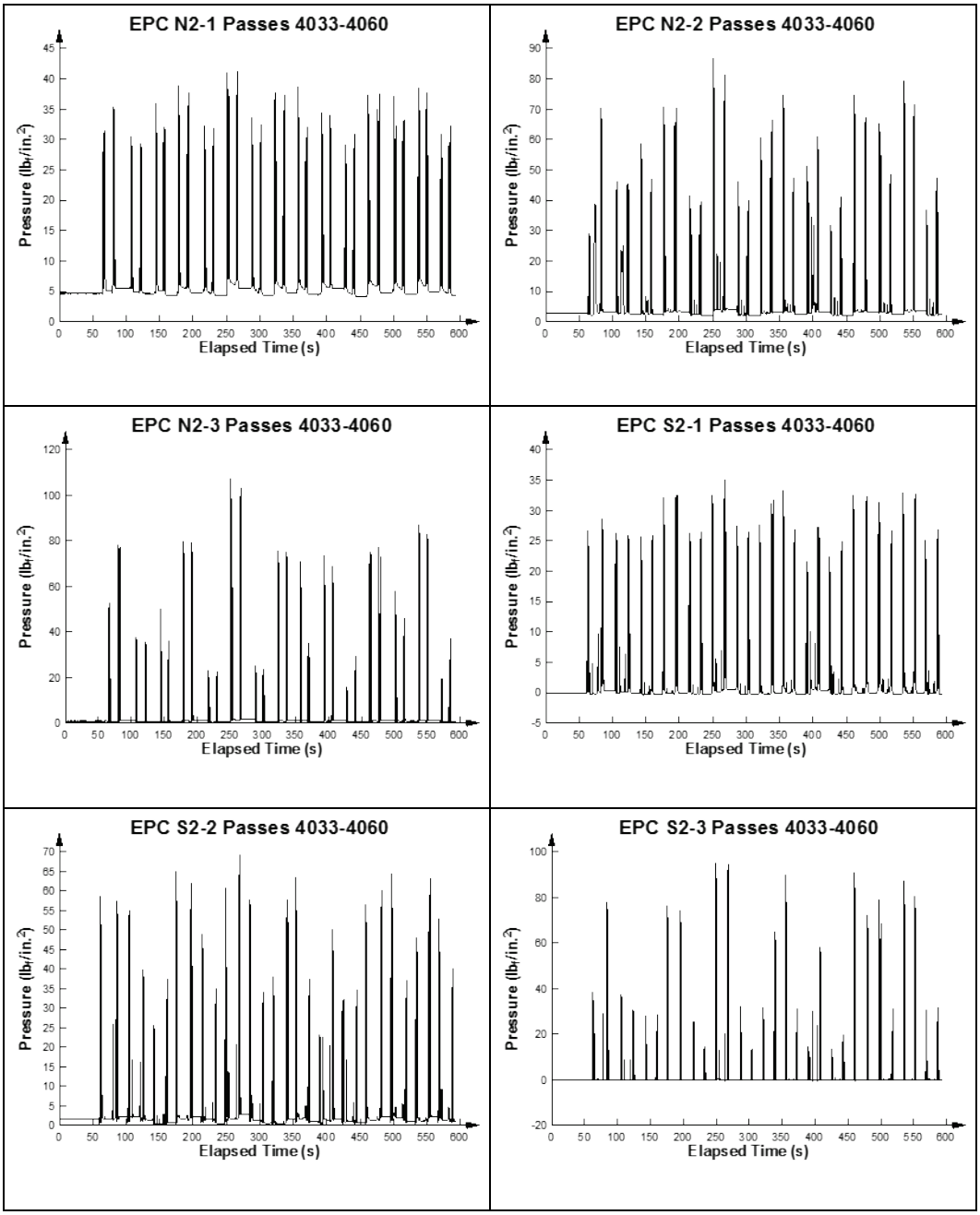
EPC N2-1 Passes 4033-4060
Pressure (lbf/in.2)
Elapsed Time (s)
EPC N2-2 Passes 4033-4060
Pressure (lbf/in.2)
Elapsed Time (s)
EPC N2-3 Passes 4033-4060
Pressure (lbf/in.2)
Elapsed Time (s)
EPC S2-1 Passes 4033-4060
Pressure (lbf/in.2)
Elapsed Time (s)
EPC S2-2 Passes 4033-4060
Pressure (lbf/in.2)
Elapsed Time (s)
EPC S2-3 Passes 4033-4060
Pressure (lbf/in.2)
Elapsed Time (s)

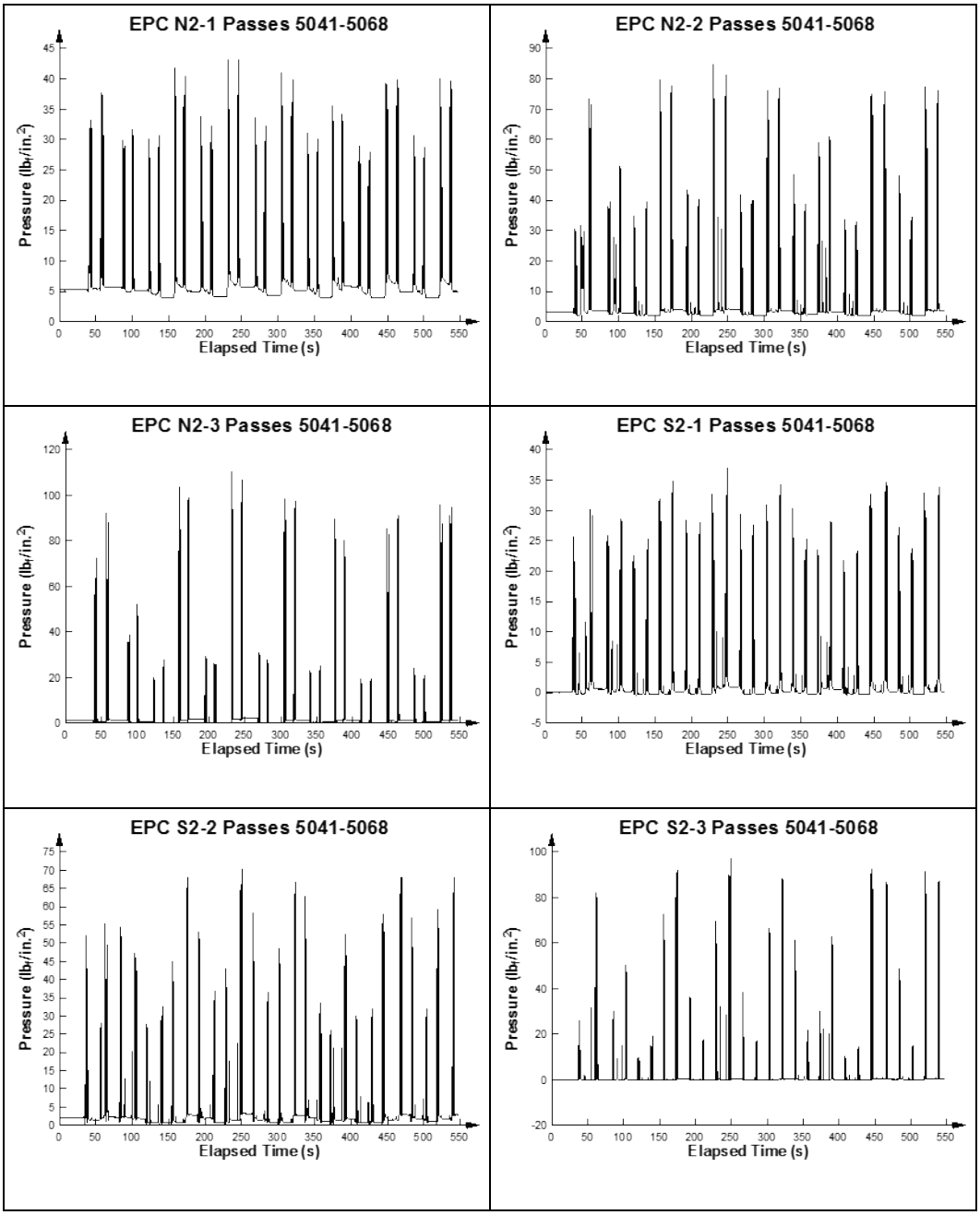
EPC N2-1 Passes 5041-5068
Pressure (lbf/in.2)
Elapsed Time (s)
EPC N2-2 Passes 5041-5068
Pressure (lbf/in.2)
Elapsed Time (s)
EPC N2-3 Passes 5041-5068
Pressure (lbf/in.2)
Elapsed Time (s)
EPC S2-1 Passes 5041-5068
Pressure (lbf/in.2)
Elapsed Time (s)
EPC S2-2 Passes 5041-5068
Pressure (lbf/in.2)
Elapsed Time (s)
EPC S2-3 Passes 5041-5068
Pressure (lbf/in.2)
Elapsed Time (s)

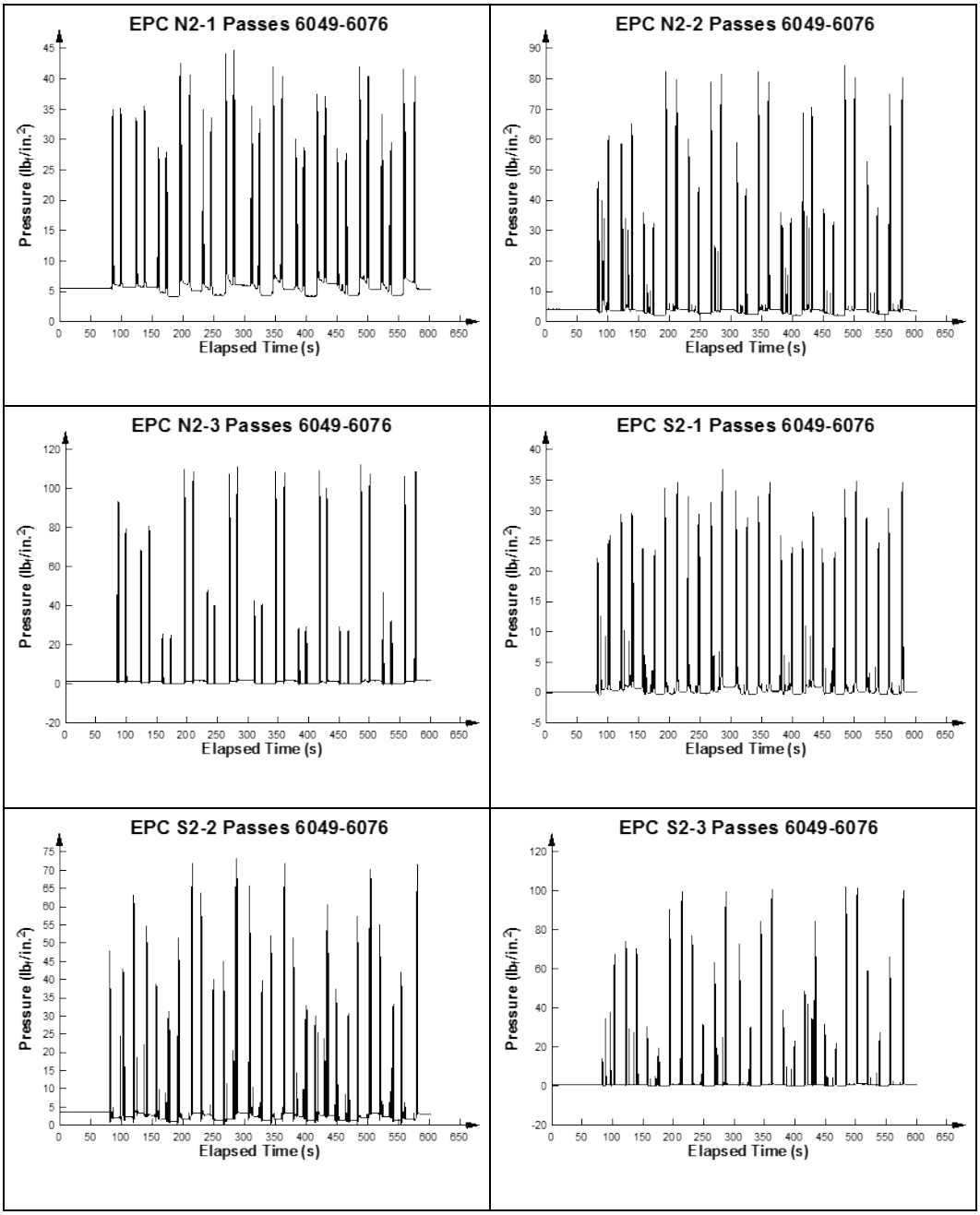
EPC N2-1 Passes 6049-6076
Pressure (lbf/in.2)
Elapsed Time (s)
EPC N2-2 Passes 6049-6076
Pressure (lbf/in.2)
Elapsed Time (s)
EPC N2-3 Passes 6049-6076
Pressure (lbf/in.2)
Elapsed Time (s)
EPC S2-1 Passes 6049-6076
Pressure (lbf/in.2)
Elapsed Time (s)
EPC S2-2 Passes 6049-6076
Pressure (lbf/in.2)
Elapsed Time (s)
EPC S2-3 Passes 6049-6076
Pressure (lbf/in.2)
Elapsed Time (s)

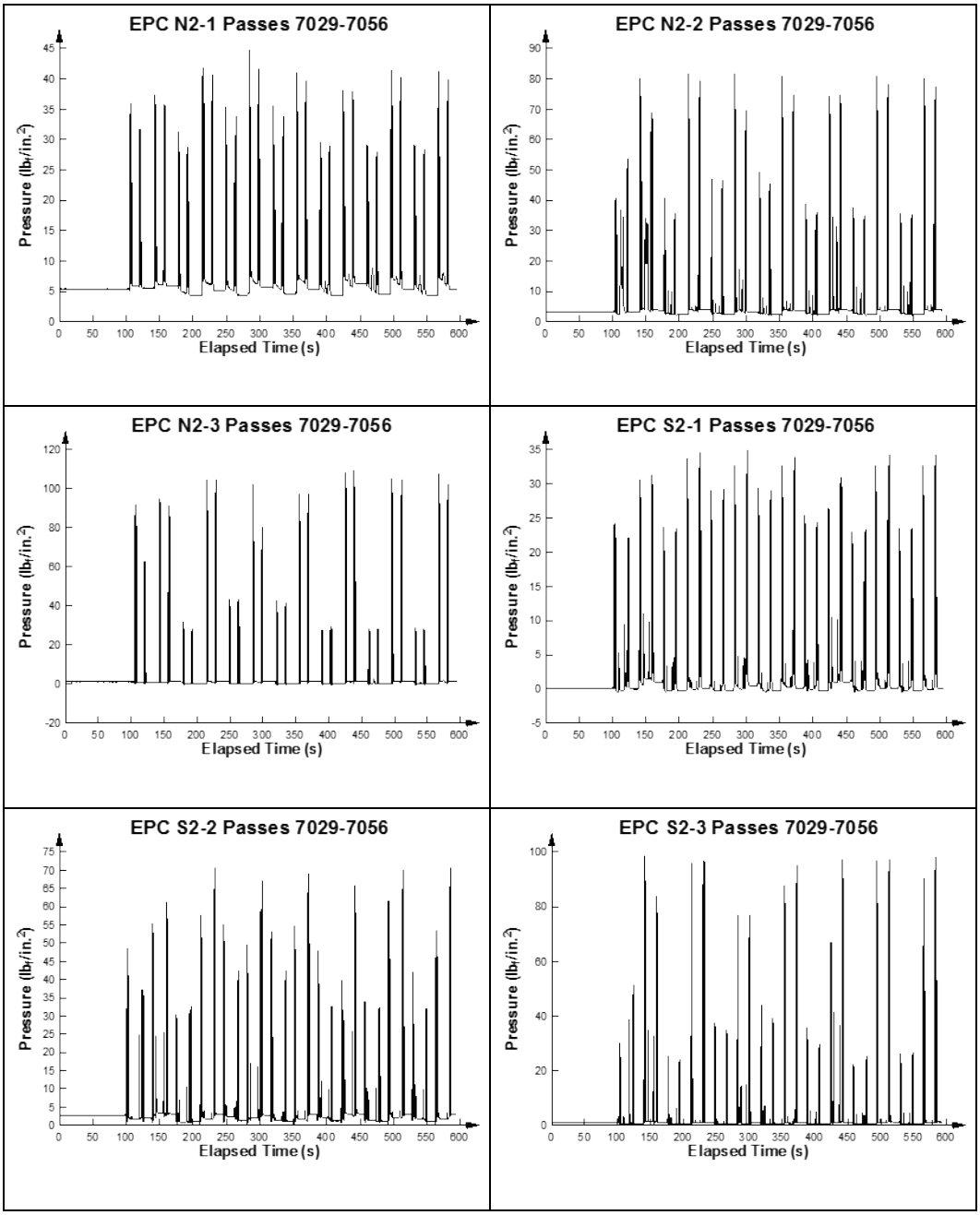
EPC N2-1 Passes 7029-7056
Pressure (lbf/in.2)
Elapsed Time (s)
EPC N2-2 Passes 7029-7056
Pressure (lbf/in.2)
Elapsed Time (s)
EPC N2-3 Passes 7029-7056
Pressure (lbf/in.2)
Elapsed Time (s)
EPC S2-1 Passes 7029-7056
Pressure (lbf/in.2)
Elapsed Time (s)
EPC S2-2 Passes 7029-7056
Pressure (lbf/in.2)
Elapsed Time (s)
EPC S2-3 Passes 7029-7056
Pressure (lbf/in.2)
Elapsed Time (s)

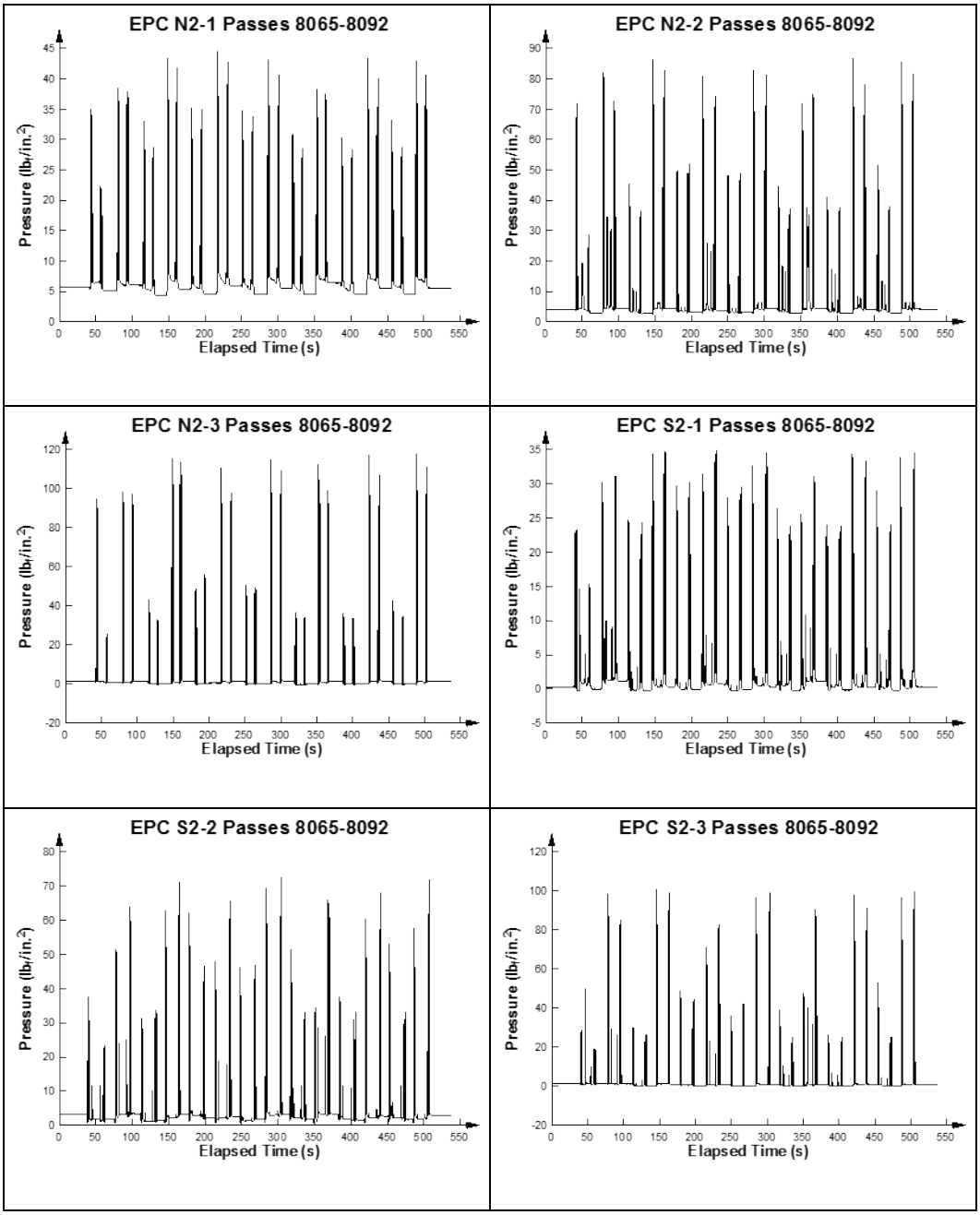
EPC N2-1 Passes 8065-8092
Pressure (lbf/in.2)
Elapsed Time (s)
EPC N2-2 Passes 8065-8092
Pressure (lbf/in.2)
Elapsed Time (s)
EPC N2-3 Passes 8065-8092
Pressure (lbf/in.2)
Elapsed Time (s)
EPC S2-1 Passes 8065-8092
Pressure (lbf/in.2)
Elapsed Time (s)
EPC S2-2 Passes 8065-8092
Pressure (lbf/in.2)
Elapsed Time (s)
EPC S2-3 Passes 8065-8092
Pressure (lbf/in.2)
Elapsed Time (s)

Appendix C: Strain Gauge Data for the F-15E Test Item

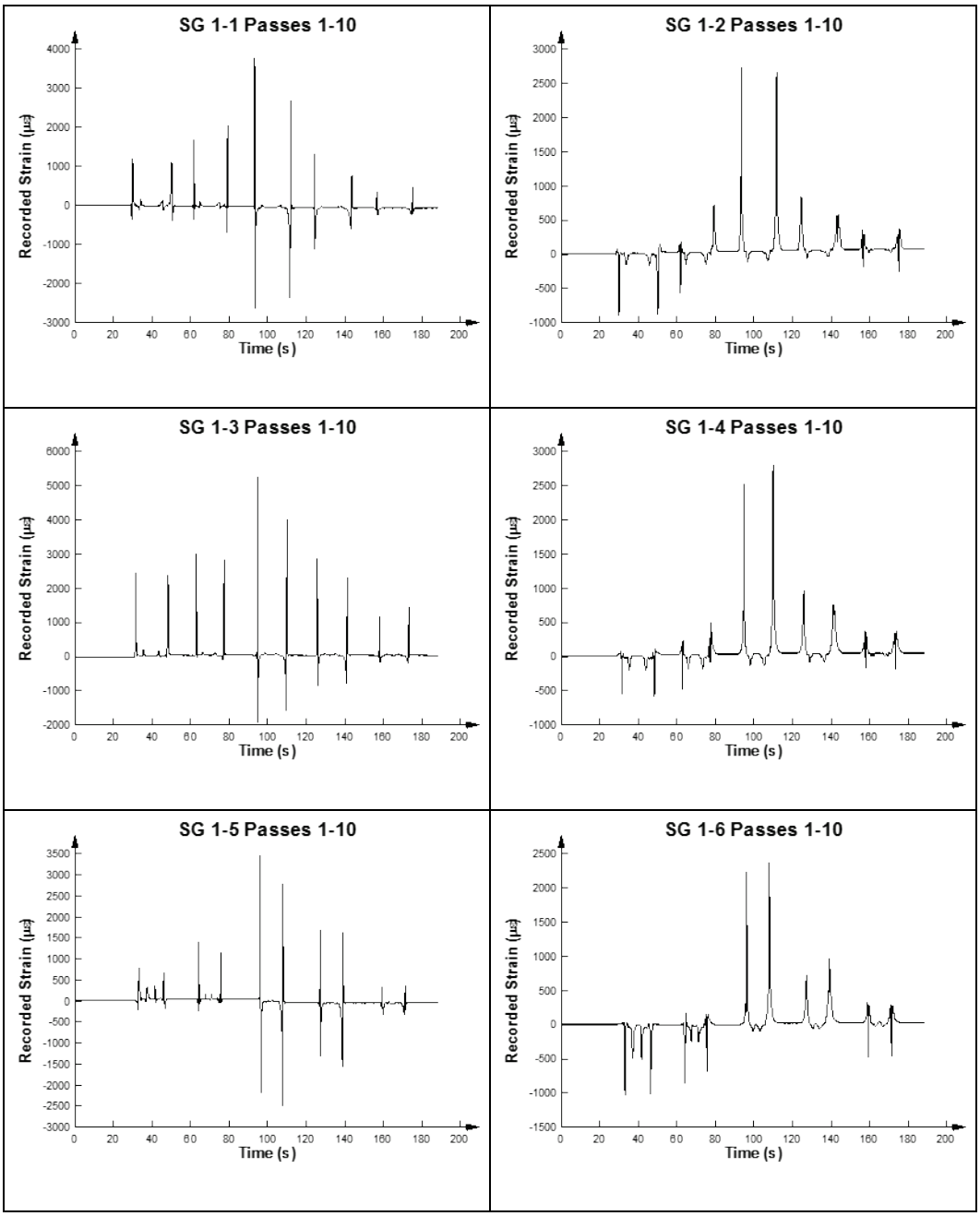

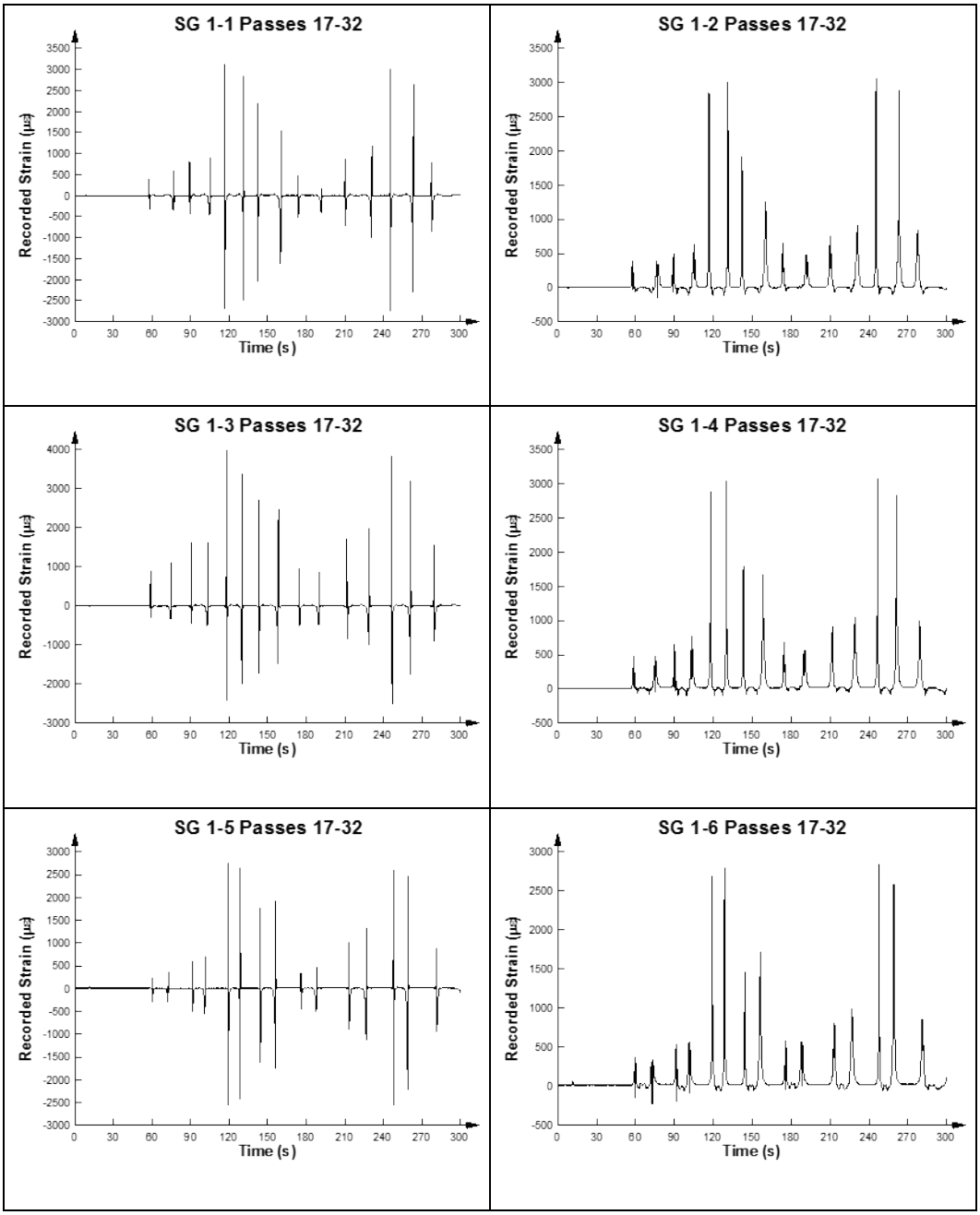
SG 1-1 Passes 17-32
SG 1-2 Passes 17-32
SG 1-3 Passes 17-32
SG 1-4 Passes 17-32
SG 1-5 Passes 17-32
SG 1-6 Passes 17-32
Recorded Strain (με)
Time (s)

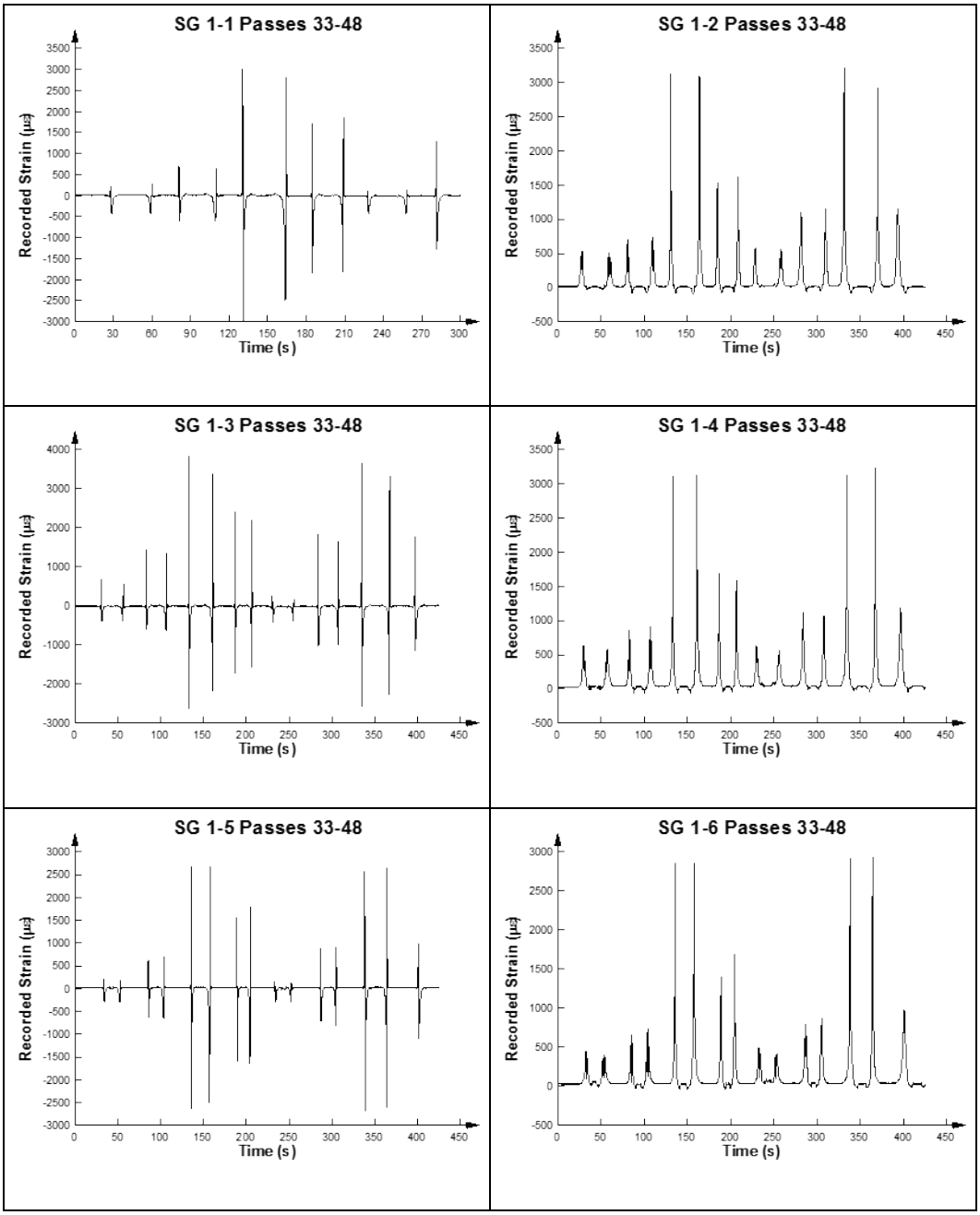
SG 1-1 Passes 33-48
Recorded Strain (με)
Time (s)
SG 1-2 Passes 33-48
Recorded Strain (με)
Time (s)
SG 1-3 Passes 33-48
Recorded Strain (με)
Time (s)
SG 1-4 Passes 33-48
Recorded Strain (με)
Time (s)
SG 1-5 Passes 33-48
Recorded Strain (με)
Time (s)
SG 1-6 Passes 33-48
Recorded Strain (με)
Time (s)

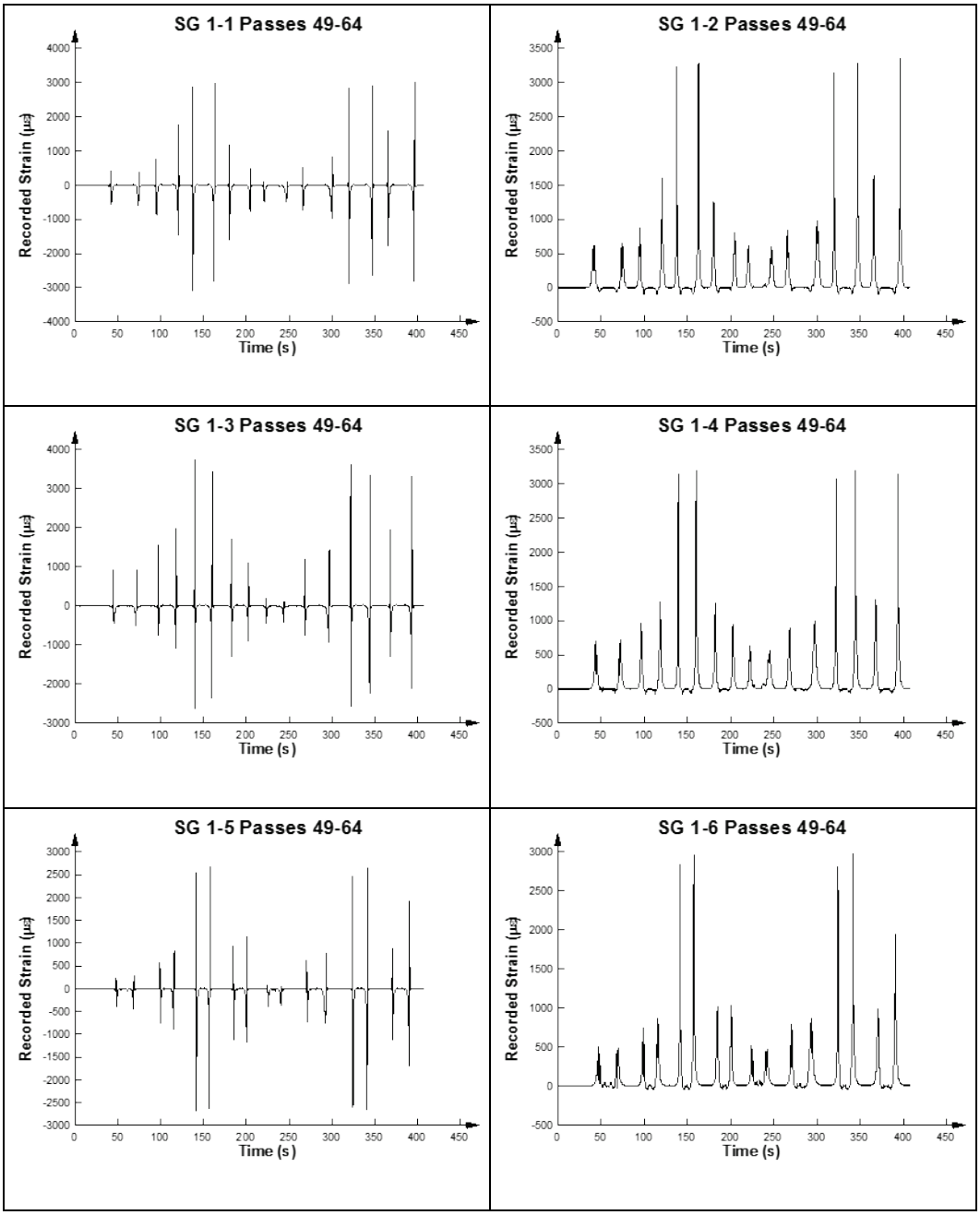
SG 1-1 Passes 49-64
Recorded Strain (με)
Time (s)
SG 1-2 Passes 49-64
Recorded Strain (με)
Time (s)
SG 1-3 Passes 49-64
Recorded Strain (με)
Time (s)
SG 1-4 Passes 49-64
Recorded Strain (με)
Time (s)
SG 1-5 Passes 49-64
Recorded Strain (με)
Time (s)
SG 1-6 Passes 49-64
Recorded Strain (με)
Time (s)

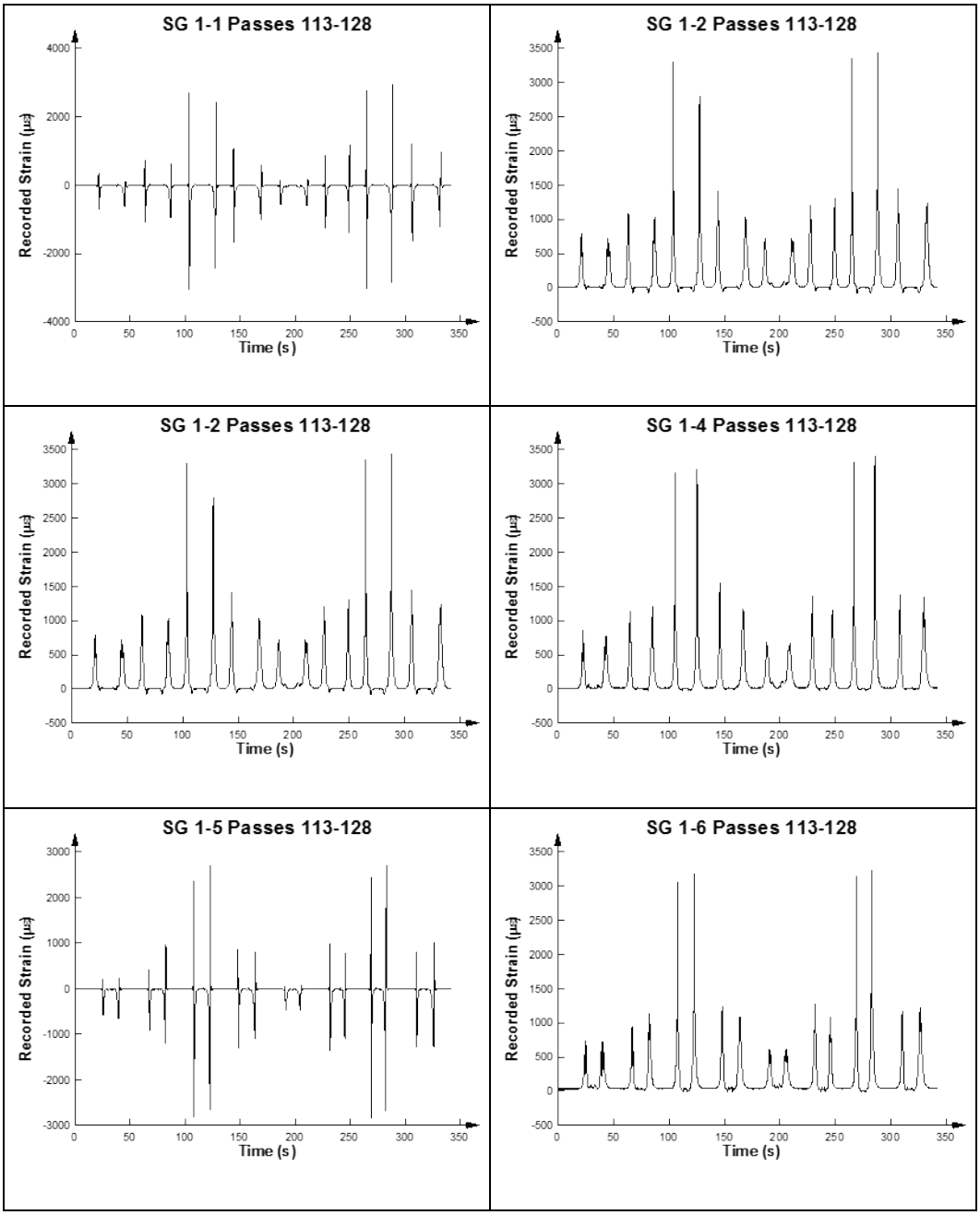
SG 1-1 Passes 113-128
Recorded Strain (με)
Time (s)
SG 1-2 Passes 113-128
Recorded Strain (με)
Time (s)
SG 1-2 Passes 113-128
Recorded Strain (με)
Time (s)
SG 1-4 Passes 113-128
Recorded Strain (με)
Time (s)
SG 1-5 Passes 113-128
Recorded Strain (με)
Time (s)
SG 1-6 Passes 113-128
Recorded Strain (με)
Time (s)

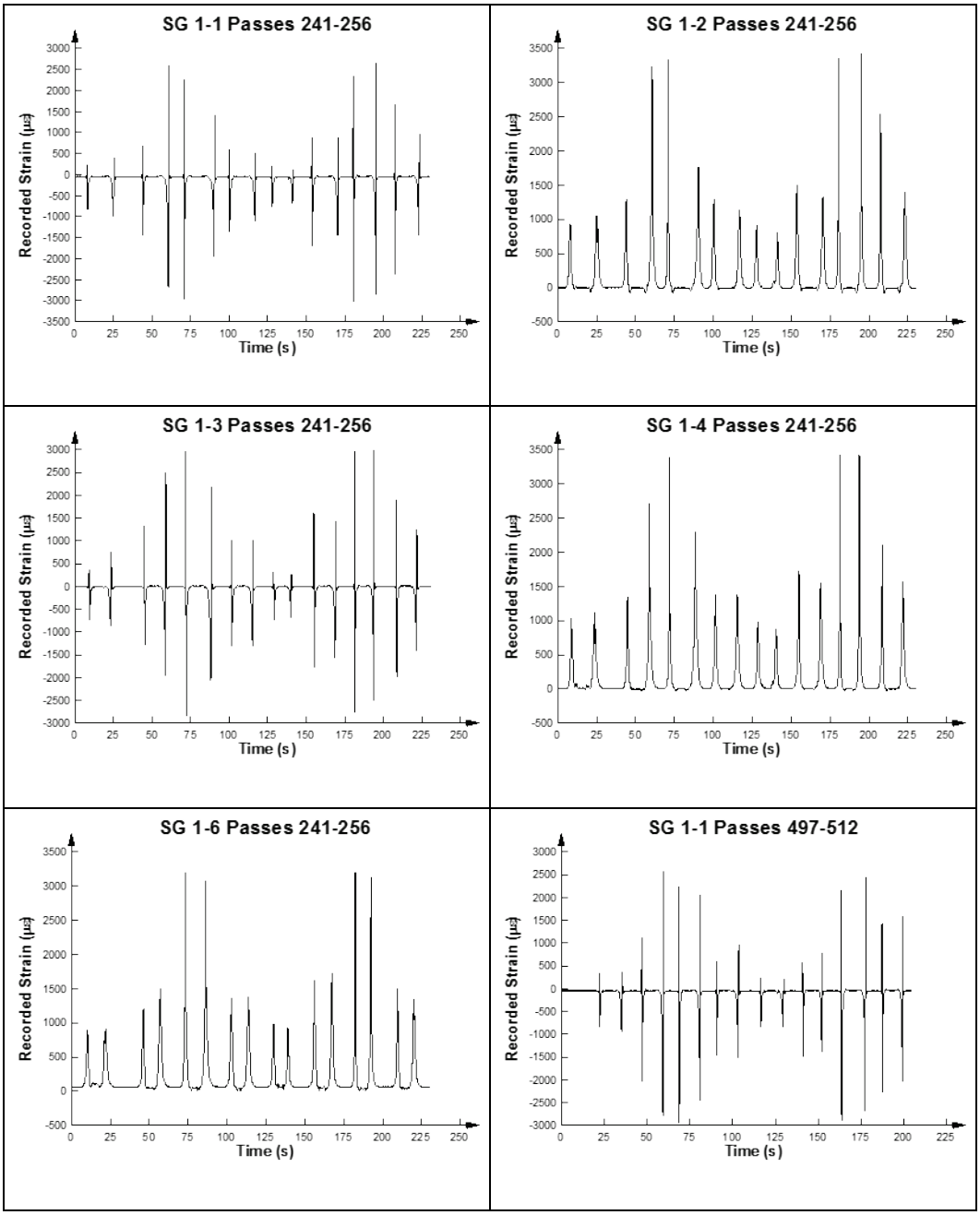
SG 1-1 Passes 241-256
SG 1-2 Passes 241-256
SG 1-3 Passes 241-256
SG 1-4 Passes 241-256
SG 1-6 Passes 241-256
SG 1-1 Passes 497-512
Recorded Strain (με)
Time (s)

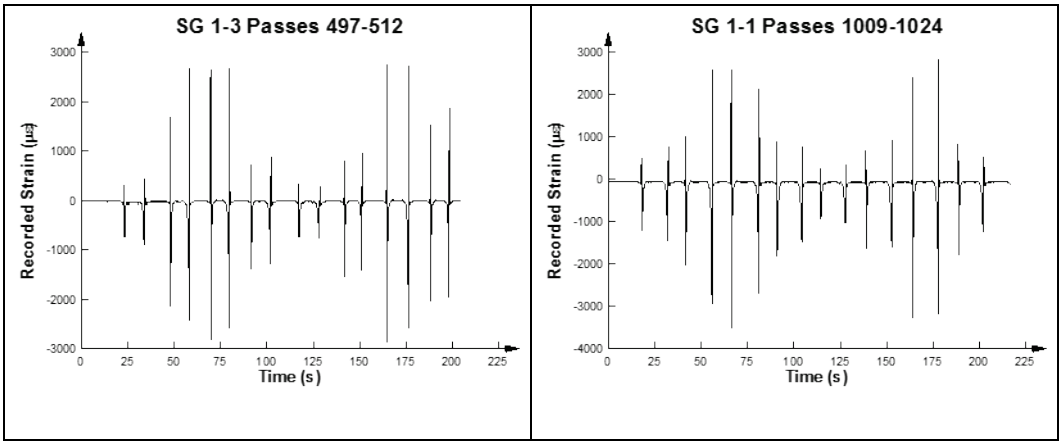
SG 1-3 Passes 497-512
Recorded Strain (με)
Time (s)
SG 1-1 Passes 1009-1024
Recorded Strain (με)
Time (s)

Appendix D: Strain Gauge Data for the C-17 Test Item

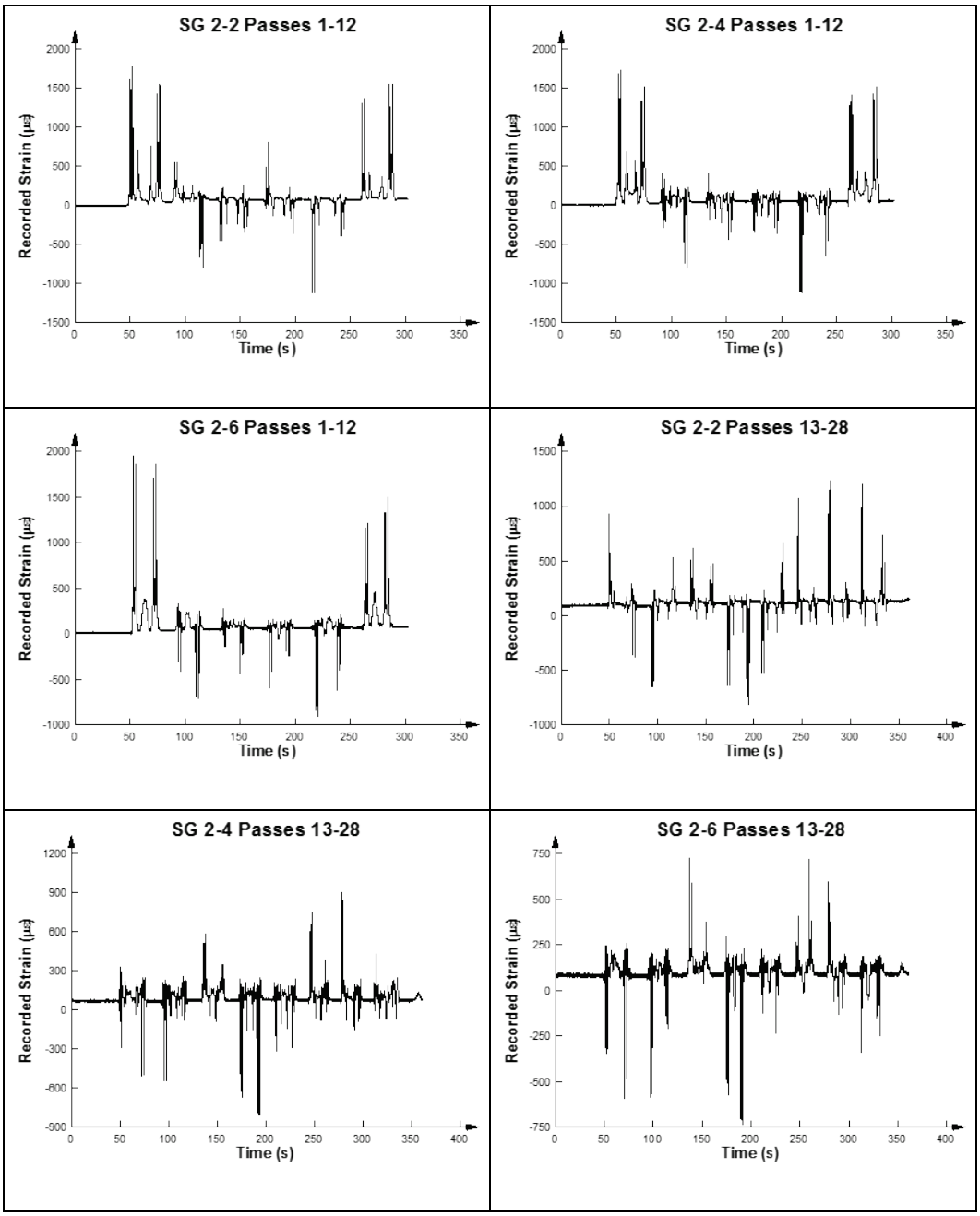

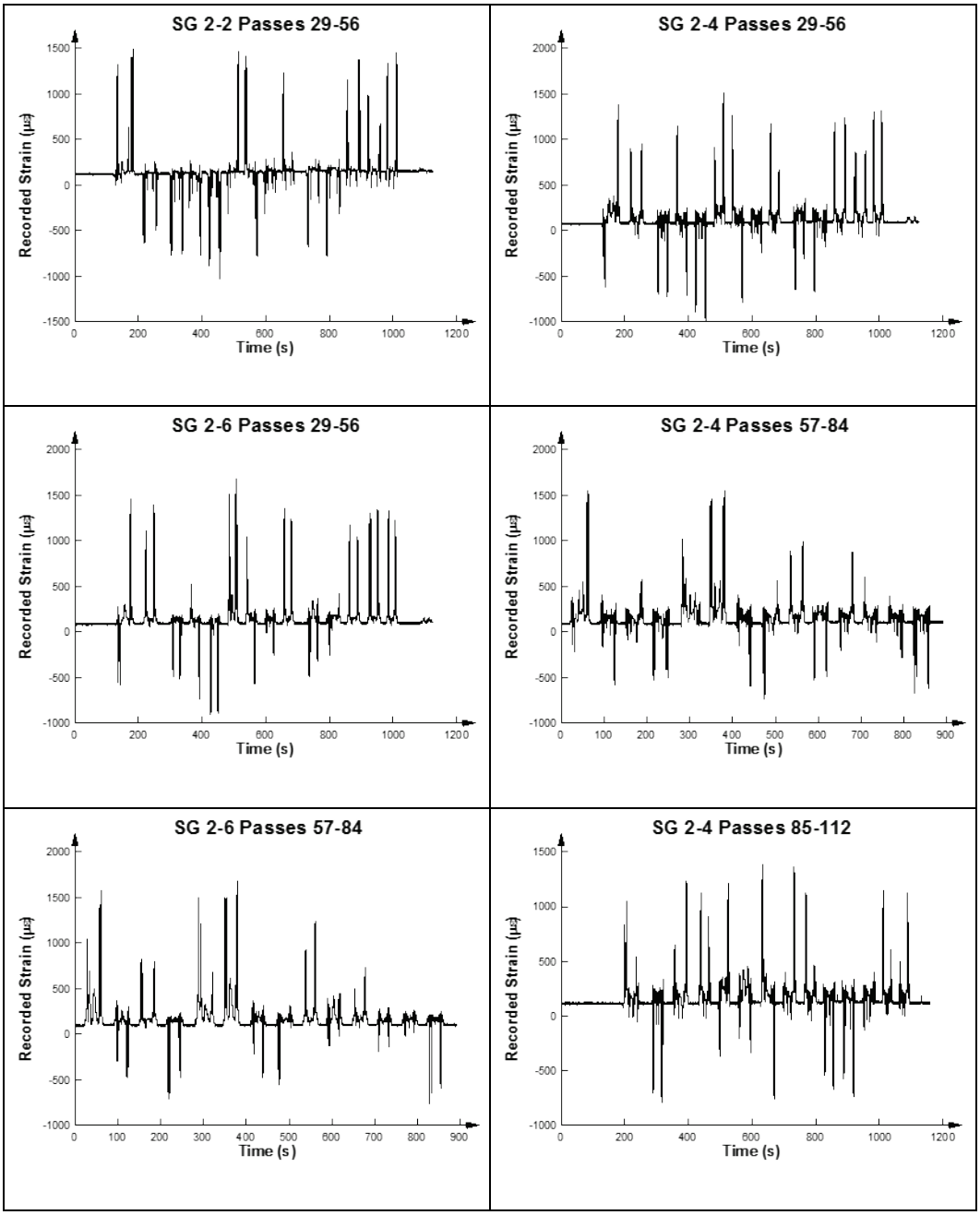
SG 2-2 Passes 29-56
SG 2-4 Passes 29-56
SG 2-6 Passes 29-56
SG 2-4 Passes 57-84
SG 2-6 Passes 57-84
SG 2-4 Passes 85-112
Recorded Strain (με)
Time (s)

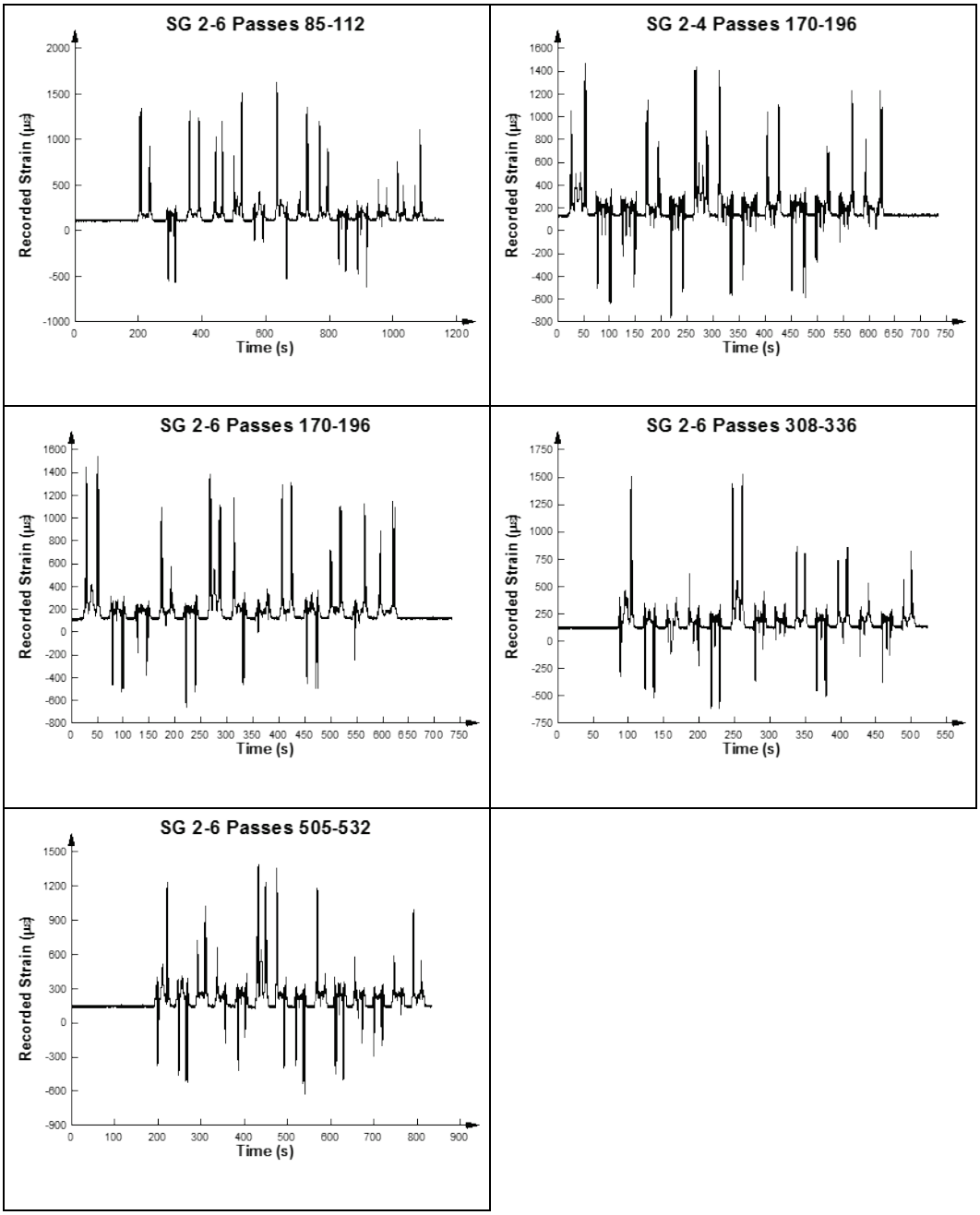
SG 2-6 Passes 85-112
Recorded Strain (με)
Time (s)
SG 2-4 Passes 170-196
Recorded Strain (με)
Time (s)
SG 2-6 Passes 170-196
Recorded Strain (με)
Time (s)
SG 2-6 Passes 308-336
Recorded Strain (με)
Time (s)
SG 2-6 Passes 505-532
Recorded Strain (με)
Time (s)

REPORT DOCUMENTATION PAGE

Form Approved
OMB No. 0704-0188

1. REPORT DATE *(DD-MM-YYYY)*	2. REPORT TYPE	3. DATES COVERED *(From - To)*
April 2018	Final	

4. TITLE AND SUBTITLE

Evaluation of AM2 2-1 Lay Pattern Over a 25 CBR Subgrade

5a. CONTRACT NUMBER

5b. GRANT NUMBER

5c. PROGRAM ELEMENT NUMBER

6. AUTHOR(S)

Nolan R. Hoffman, Lyan Garcia, and Timothy W. Rushing

5d. PROJECT NUMBER
470802

5e. TASK NUMBER

5f. WORK UNIT NUMBER

7. PERFORMING ORGANIZATION NAME(S) AND ADDRESS(ES)

Geotechnical and Structures Laboratory
U.S. Army Engineer Research and Development Center
3909 Halls Ferry Road
Vicksburg, MS 39180-6199

8. PERFORMING ORGANIZATION REPORT NUMBER

ERDC/GSL TR-18-7

9. SPONSORING / MONITORING AGENCY NAME(S) AND ADDRESS(ES)

Headquarters, Air Force Civil Engineer Center
Tyndall Air Force Base, FL 32403-5319

10. SPONSOR/MONITOR'S ACRONYM(S)

TARDEC
HQ-USACE

11. SPONSOR/MONITOR'S REPORT NUMBER(S)

12. DISTRIBUTION / AVAILABILITY STATEMENT

Approved for public release; distribution is unlimited.

13. SUPPLEMENTARY NOTES

14. ABSTRACT

AM2 matting has a long history of successful performance as an expeditionary airfield surfacing system. Previous evaluations determined the number of passes to failure of AM2 when installed in a brickwork pattern over a wide range of soil strengths and alternate 2-1 and 3-4 lay patterns installed over soft soils. To determine the reliability of AM2 when installed in alternate patterns over stronger soils, the U.S. Air Force Civil Engineer Center (AFCEC) sponsored the evaluation of AM2 over a soil with a CBR of 25 installed in a 2-1 lay pattern. A CBR of 25 is considered by the U.S. Navy Naval Air Systems Command (NAVAIR EAF) to be the minimum threshold at which no subgrade maintenance is required during expeditionary operations. Recent investigations showed that the 2-1 configuration significantly reduces the operating life of AM2 over subgrades with a CBR of 6. In contrast, the results of the 25 CBR, 2-1 lay evaluation showed that both F-15E traffic and C-17 traffic surpassed the 1,500 pass requirement. The evaluation validated the NAVAIR EAF requirement for a minimum CBR of 25 to minimize maintenance requirements for F-15E and C-17 operations.

15. SUBJECT TERMS

Runways (Aeronautics) – Evaluation
Runways (Aeronautics) – Maintenance and repair
Airfield matting
AM2
Expedient
Runway
Aluminum
Landing mats
Soils – strength

16. SECURITY CLASSIFICATION OF:			17. LIMITATION OF ABSTRACT	18. NUMBER OF PAGES	19a. NAME OF RESPONSIBLE PERSON
a. REPORT	b. ABSTRACT	c. THIS PAGE			19b. TELEPHONE NUMBER *(include area code)*
Unclassified	Unclassified	Unclassified		115	